Orientation and location dependency of the mechanical properties of an AlSi10Mg part produced using direct metal laser sintering (DMLS)

-

a microsample approach

André Diogo Roberto de Sousa

Master thesis

UMBC advisor:

Dr. Marc Zupan

UMBC co-advisor:

Dr. Richard Everett

FEUP advisor:

Dr. Abel Santos

Integrated Master in Mechanical Engineering

Porto, 15 of October 2017

To my parents and family.

Abstract

Additive manufacturing (AM) has the potential to revolutionize the way the industry and government agencies design, manufacture, inventory, and deliver countless currently and future parts utilized in engineering systems. While the rapid evolution of AM has promoted numerous innovative processes and machines, AM has grown with minimal understanding of the impact of processing parameters on global part properties making it difficult for industry and the department of defense to take full advantage of the technology. To realize the full potential of AM, each AM part must demonstrate a set of minimum performance characteristics. These characteristics are generally assured by qualifying manufacturing processes and certifying said processes were followed by competent operators. Currently there is a gap/disconnect between material processing and part performance that precludes AM parts insertion.

The layer-by-layer approach used by almost all AM machines to build these novel parts has direct definite ramifications for the microstructures and mechanical properties of these parts. Layers introduce a build direction anisotropy and synthesis parameter variability, and create opportunities for defects (e.g., voids) adding complexity to materials microstructures which, in turn, influence the mechanical properties. Despite the recent interest in additive manufacturing, the property variations in an AM build are still not known or understood. This is because conventional mechanical characterization techniques usually measure an average property and cannot resolve the important variations tied to specific microstructural and defect features present in the sample. This work uses microtensile testing to reveal how the mechanical properties of the AM structure vary with orientation, possible defects and location in the build.

In this work microtensile testing, with specimens having a footprint of 1 x 3 mm and a gage section of ≈250 x 250 μm, has been successfully applied to additively manufactured materials to determine location- and orientation-specific mechanical properties. A microsample approach was used to explore and characterize the inhomogeneous performance of an AlSi10Mg aluminum alloy part produced using direct metal laser sintering (DMLS). The part was produced using standard EOS process parameters and microsamples were extracted along the part and oriented along three different directions: two directions parallel to the powder deposition plane (x and y directions, perpendicular to each other) and one direction parallel to the build direction (z direction). Microsamples were afterwards prepared for tensile testing and tested using a microsample tensile testing system. Engineering and true stress-strain responses

were obtained and Young's modulus, yield strength and ultimate tensile strength (UTS) values were determined.

Mechanical properties values showed variability along the part and higher for different orientations, including along two different orientations parallel to the powder deposition plane, in contradiction to what is reported in literature. For a given orientation, the Young's modulus variability along the part suggests the different prevalence of grains with a specific crystallographic orientation for each microsample.

Higher values of yield strength were obtained on the y direction, followed by the x and z directions, respectively. Similarly, UTS values showed to be higher for the z direction, followed by the y and x direction respectively. The small size of microsamples allowed to explore the material inhomogeneities, which is not achievable using large size standard samples as in literature, since they are usually only capable of measuring an average property.

A fractographic analysis to the fracture surface of the tested microsamples using scanning electron microscopy (SEM) showed that the AM manufactured materials have a mixed mode deformation, which is in accordance with the observed strains to failure. Necking was not evident. The SEM images also showed the presence of processing defects, suggesting localized lack of overlap between melt pools, which is an indicative that an as-fabricated material has wide spread defects. By working to eliminate the processing defects and improving melt pool boundary strength, these materials show potential to have increased toughness.

Dependência das propriedades mecânicas com a orientação e a localização numa peça de liga de alumínio AlSi10Mg produzida por sinterização direta de metais por laser (DMLS) – uma abordagem usando microprovetes

Resumo

Os processos de fabrico aditivo (do inglês, *additive manufacturing*) têm o potencial para revolucionar a forma como a indústria e as agências governamentais projetam, produzem e disponibilizam inúmeros componentes utilizados em sistemas de engenharia. Ainda que a rápida evolução do fabrico aditivo tenha proporcionado o aparecimento de vários processos e máquinas inovadores, tal foi conseguido com um conhecimento e compreensão mínimos da influência dos parâmetros dos processos nas propriedades globais dos materiais produzidos, dificultando a possibilidade de beneficiar por completo do potencial desta tecnologia. Para tirar o maior partido dos processos de fabrico aditivo, cada componente produzido deve apresentar um conjunto mínimo de requisitos a nível de desempenho. Estes requisitos são geralmente assegurados com a qualificação dos processos de fabrico e com a certificação da aptidão dos operadores. Atualmente existe uma falta de conhecimento da relação processamento do componente – características do componente que impede a inserção de componentes fabricados por fabrico aditivo.

O fabrico de peças por sobreposição de camadas, usado pela maior parte das máquinas de fabrico aditivo, tem uma influência direta na microestrutura e, por consequência, nas propriedades mecânicas dos materiais produzidos. A sobreposição de camadas introduz anisotropia ao longo da direção de construção e variabilidade de parâmetros, proporcionando ainda o aparecimento de defeitos, que contribuem para a complexidade da microestrutura dos materiais obtidos. Apesar do atual interesse nos processos de fabrico aditivo, as variações das propriedades num material produzido desta forma ainda não são perfeitamente conhecidas ou compreendidas. Isto deve-se essencialmente ao facto de que as técnicas convencionais usadas para caracterizar o comportamento mecânico dos materiais apenas medem uma propriedade média, não possuindo capacidade para explorar as variações importantes associadas às particularidades microestruturais e de presença de defeitos. Neste trabalho recorre-se ao uso de microprovetes para explorar e para melhor compreender como as propriedades mecânicas de

um material produzido por um processo de fabrico aditivo variam com a orientação, localização e presença de possíveis defeitos numa peça.

Neste trabalho, testes de tração a microprovetes com dimensões de 1 x 3 mm e uma secção de teste com ≈250 x 250 μm foram realizados com sucesso para estudar a dependência das propriedades mecânicas com a orientação e a localização numa peça produzida por fabrico aditivo. A abordagem que consiste no uso destes microprovetes foi usada para explorar e caracterizar a heterogeneidade de uma peça de liga de alumínio AlSi10Mg, produzida por sinterização direta de metais por laser (DMLS). A peça foi produzida usando parâmetros de processo padrão de uma máquina EOS e os microprovetes foram extraídos ao longo desta e para três diferentes orientações: duas direções paralelas ao plano de deposição dos pós metálicos (direções x e y, perpendiculares entre si) e uma direção paralela à direção de construção (direção z). Posteriormente, os microprovetes foram preparados para poderem ser testados à tração e foram tracionados usando uma máquina especialmente concebida para este efeito. Como resultado dos testes de tração, as curvas de tração de engenharia e reais foram obtidas e os valores do módulo de Young, tensão limite de elasticidade e tensão de rotura foram determinados.

Os valores das propriedades mecânicas demonstraram variabilidade ao longo da peça e para diferentes orientações, tendo sido mais alta no segundo caso. Foram ainda verificadas diferenças entre as propriedades mecânicas relativas às duas orientações paralelas ao plano de deposição dos pós metálicos, ao contrário do reportado na literatura. Para uma dada orientação, a variabilidade do módulo de Young ao longo da peça sugere uma diferente prevalência de grãos com uma dada orientação da estrutura cristalina para cada microprovete.

Valores superiores de tensão limite de elasticidade foram obtidos para a direção y, seguido das direções x e z, respetivamente. De uma forma semelhante, valores de tensão de rotura superiores foram observados para a direção z, seguido das direções y e x, respetivamente. A pequena escala dos microprovetes permitiu explorar a heterogeneidade do material, o que de outra forma não é possível com o uso de provetes *standard* de maiores dimensões, tal como reportado na literatura. Provetes *standard* de maiores dimensões são geralmente apenas capazes de medir uma propriedade média do material.

Uma análise às superfícies dos microprovetes após a rotura foi realizada usando microscopia eletrónica de varrimento (SEM) e permitiu concluir que os materiais produzidos por fabrico aditivo possuem um modo misto de deformação, o que está de acordo com os valores de

extensão após rotura obtidos. Estricção dos microprovetes não foi visível. Foi ainda possível observar a presença de defeitos resultantes do fabrico, relacionados com falhas localizadas na ligação e/ou sobreposição entre cordões de fusão dos pós metálicos. Trabalhando no sentido de eliminar a presença de defeitos decorrentes do fabrico e melhorando a resistência na ligação entre cordões de fusão, estes materiais demonstram potencial para possuir valores superiores de tenacidade.

Acknowledgments

I want to first thank my parents Fátima and Toni for all the support they gave me throughout my life, including in my academic career. It was thanks to an enormous effort from them in every way that I could conduct research for my thesis at the University of Maryland, Baltimore County, in the USA. Moreover, it allowed me to realize my long childhood dream of going to the US. Thank you for cheering me up in my worst moments, for being so patient with me and my crazy ideas, and for being always by my side. Thank you for being who you are.

I would also like to thank all my family and friends for all the support and understanding over the years. Not referring any name intending to not leave anyone apart, each one of them will know who I am speaking of. Thank you both for the understanding and for always being there when I need you the most. Love you all.

Thank you to my UMBC advisor, Dr. Marc Zupan. I have learned a lot from and thanks to you. Thank you for your guidance, patience and great energy. Also, thank you to my UMBC co-advisor, Dr. Richard Everett, for all your support and all you have taught me. Thank you both for reviewing my thesis and for all the suggestions given. Finally, thank you to my advisor at the Faculty of Engineering of the University of Porto (FEUP), Dr. Abel Santos for all the ideas, understanding and support given.

I also want to thank my lab mates Duffy, Keith and João, from the Micromaterials Laboratory at UMBC, for all the knowledge and support given which was indispensable for the realization of this thesis. Particularly Keith, thank you for being the person you are and I wish you the best of luck in this new step of your life.

The opportunity and possibility to conduct research at UMBC to develop my thesis was possible thanks to my parents and to the MOBILE + project scholarship, coordinated by the University of Porto, to which I owe my gratitude.

This research was funded by the Johns Hopkins Applied Physics Lab contract number 140391, Dr. Steven Storck program manager, and the UMBC-TRIPOS Global Engineering Partnership to which I also owe my thankfulness.

I would finally like to thank Dr. Lucas da Silva and Ms. Mónica Faria for the understanding and support, without whom this would not be possible.

Table of Contents

List of Acronyms

AM – Additive manufacturing

ASTM – American Society for Testing and Materials

CAD – Computer-aided drafting

CCD – Charge-coupled device

CNC – Computer numerical control

DED – Direct energy deposition

DIC – Digital image correlation

DMLS – Direct metal laser sintering

EDM – Electric discharge machining

EVA – Extra Vehicular Activities

FCC – Face-centered cubic

FEF – Freeze-form extrusion fabrication

FEUP – Faculty of Engineering of the University of Porto

FGM – Functionally graded materials

FSW – Friction stir welding

ISDG – Interferometric strain/displacement gage

MML – Micromaterials Laboratory

PBF – Powder bed fusion

SEM – Scanning Electron Microscopy

STL – Stereolithography

UMBC – University of Maryland, Baltimore County

UTS – Ultimate tensile strength

YS – Yield strength

List of Figures

List of Tables

1 Motivation

1.1 Motivation

Objects and devices all around are subject to some sort of manufacturing process in order to be obtained. Fabrication processes date as far back as 8000 – 3000 B.C. (Groover 2007) and have been evolving since then. New technologies have emerged, allowing for more complex geometries, lighter structures and stronger materials to be developed. Manufacturing provides the necessary and most wanted goods for society and it represents an important technological, economical and historical activity (Jorge Rodrigues 2005).

The strategic development and utilization of materials has enabled the technological advance of mankind, but given the warming climate and the need to lift millions out of poverty, the world spends too much energy, carbon, time, and resources on making materials. Globally humans consume roughly 10 billion metric tons of engineering materials per year, an average of 1.5 metric tons per person. Making materials consumes about 21% of global energy and is responsible for about the same fraction of carbon emitted to the atmosphere. For example, in 2012 the total global energy consumed was estimated to be about $5x10^{20}$ Joules/year and it is, of course, rising (Ashby 2015).

A significant fraction of this energy is used inefficiently for transportation and simple melting. Bauxite (the principle ore for aluminum) is routinely transported to Iceland, from locations as far away as Australia, because the low cost of geothermal energy there makes such a laborious path economical. Once turned into metal, it gets sent around the globe again to be made into objects, which will travel the world yet again to eventually end up in landfills (Ashby 2015). This work will take a proactive posture to address key high-energy demands needed to manufacture materials, while providing improved material performance.

The fabrication of a product up to its ready-to-use state usually requires several successive intermediate operations or manufacturing processes. The amount of processes necessary to create a product directly influences the energy, time and costs involved (Jorge Rodrigues 2005). In addition to that, the product design is limited by the processing capabilities of the manufacturing processes available.

On the contrary, additive manufacturing enables to create a product in a single processing operation, possibly only requiring little final machining or surface finishing treatment. It

consists in the addition of layers of material along the intended geometry of the final part defined by a 3D CAD model, as seen in Figure 1, reason why minimal waste is produced. Moreover, it allows for complex and optimized shaped structures to be produced, with little or no design restrictions. Therefore, high strength and light-weight structures can be produced. The advantages associated to this manufacturing process makes it very desired and needed in the industry.

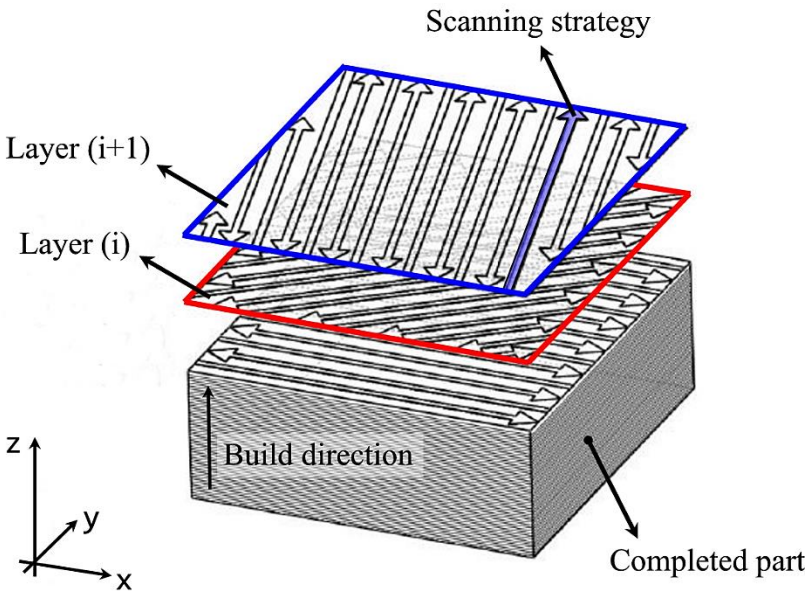

Figure 1 – Schematic representation of the typical building strategy used to fabricate a part by means of additive manufacturing technologies (Diego Manfredi 2013).

Additive manufacturing first emerged as rapid prototyping, developed in the 1980s (Hernandez 2012). This technology was primarily used to produce prototypes and models for applications such as product design evaluation and validation and medicine purposes. It has recently begun to be used as an important commercial manufacturing technology. However, it is still a very young technology subject to and in the need of plenty of research. AM has grown with minimal understanding of the impact of processing parameters on resultant defects and global part properties making it difficult for industry and government agencies to take full advantage of the technology.

The part fabrication using additive manufacturing processes involves local complex thermal evolutions of the material, which influence its microstructure and consequently its mechanical

behavior. The layer-by-layer approach of AM technologies, Figure 1, results in microstructural anisotropies and inhomogeneities of the produced material. Layers introduce a build direction anisotropy and synthesis parameter variability, and create opportunities for defects (e.g., voids) adding complexity to materials microstructures which, in turn, influence the mechanical properties. It is thus important to understand and characterize how the AM process parameters affects materials behaviors.

Despite the recent interest in additive manufacturing, the property variations in an additive manufactured part are still not known or understood. Efforts to characterize additive manufactured materials mechanical behaviors have essentially turned to the use of standard large size samples for tensile testing (Diego Manfredi 2013). However, tensile tests at this length scale will average across the inhomogeneities of the material and cannot resolve the important variations tied to specific microstructural and defect features present in the sample, making this an ineffective method to fully characterize an AM material. Therefore, a novel approach consisting in microsample tensile testing is used in this work. Studies using this technique on parts produced using additive manufacturing are still very limited.

Microsample testing consists in carrying out tensile tests to samples whose gage section is 1.78 mm long with a square shaped cross-section of 250 μm x 250 μm, with a test region volume roughly 500,000 times smaller than a standard sample (D. A. LaVan and W. N. Sharpe 1999). Therefore, it allows to measure the local mechanical properties of a material. The use of microsample testing for an additive manufactured material will allow to explore and characterize its inhomogeneous performance. In this work, this technique will be used to examine the mechanical behavior of an AlSi10Mg aluminum alloy part produced using direct metal laser sintering (DMLS), along the AM part and along different orientations.

1.2 Thesis context and linkage to UMBC

The research that allowed to develop this thesis was conducted at the University of Maryland, Baltimore County, located in Baltimore, state of Maryland, United States of America, as one of the current research projects happening in the Micromaterials Laboratory.

Additive manufacturing technologies allow to obtain objects directly from 3D CAD models through the addition of consecutive layers of material along the intended geometry. This manufacturing process involves complex local material evolutions on the fabrication of the part, which influences its microstructure and thus its mechanical properties. Due to the knowledge gap existent in literature about the material characterization and the mechanical properties variation as a function of location and orientation on an additive manufactured part, the application of a novel technique consisting in microsample tensile testing thrives to answer these problems.

The Micromaterials Laboratory at UMBC has already a high practice in the area of microsample tensile testing, with several published works. It thus allowed to better apply this technique to fulfil the main purpose of this study. Moreover, the existent strong coalition between the different departments in this University was also important for the realization of this work, inasmuch the application of other techniques such as scanning electron microscopy (SEM) was possible.

1.3 Thesis overview

The purpose of this work consists in using microsample testing to investigate and explore the orientation and location dependency of the mechanical properties of an AlSi10Mg part, produced using direct metal laser sintering (DMLS).

Chapter 2 provides the reader an introduction and the state of the art on additive manufacturing with an overview, a description of the process and the process parameters influence on the material microstructure, together with the defect generation mechanisms. Posteriorly, a description of the specific AM process used to fabricate the part studied in this work, direct metal laser sintering (DMLS), is made. It also provides with information on the composition and mechanical properties reported in literature for the aluminum alloy used, AlSi10Mg. Finally, an introduction to scanning electron microscopy (SEM) is made, together with a description of its advantages to this work.

In chapter 3, the production of the material used in this work is described, including the process parameters used.

Chapter 4 presents an introduction to microsample testing and the details of its application for the present study. A description of how the microsamples were extracted from the fabricated part and afterwards prepared for tensile testing is made. An overview of the microsample tensile testing system and testing variables used is also referred. It also provides with an introduction to digital image correlation (DIC), used for strain measurement of microsamples, and the VIC-2D 6 software settings used.

Chapter 5 provides the results from microsample testing and a detailed analysis of their relationship to the additive manufacturing process. Also, a comparison to the mechanical properties values reported in literature is made. Afterwards, the statistical significance t-test carried out to determine the statistical significance of the difference between each of the mechanical properties for different orientations is reported. Finally, the fractographic analysis made to explain the measured mechanical response deformation and failure mechanisms is described.

Finally, the conclusions taken from this study are presented in chapter 6.

2 Literature Review

2.1 Additive Manufacturing

Additive manufacturing (AM) is, as defined by the American Society of Testing and Materials (ASTM), "The process of joining materials to make objects from 3D model data, usually layer upon layer, as opposed to subtractive manufacturing methodologies" (Flaviana Calignano 2017). It is also often referred as 3D printing, additive fabrication, additive process, additive techniques, additive layer manufacturing, layer manufacturing and freeform fabrication (Flaviana Calignano 2017, Herderick 2011).

Although it was developed in the 1980s, it was first used as rapid prototyping and only recently has begun to be used as an important commercial manufacturing technology in response to modern industry demands on costs and manufacturing times reduction and on the ability to produce complex and light-weight structures (Frazier 2014, Herderick 2011, Flaviana Calignano 2017, Nesma T. Aboulkhair 2014). However, the technology and its utilization is still very young and currently subject of plenty of research. Figure 2 to Figure 6 show examples of parts of different materials produced using varied AM technologies, specifically applied to medicine and in the industry.

Figure 2 – Biomedical hip stems implants in a mesh, hole and solid configurations of Ti6Al4V, fabricated using EBM (Nannan GUO 2013).

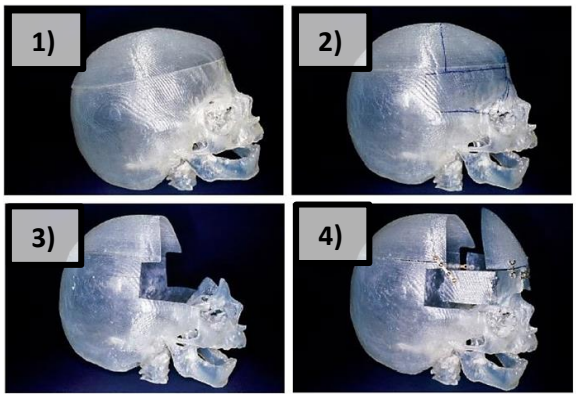

Figure 3 – Stereolithography model of a human cranium, used to effectively plan a surgical treatment, using a photosensitive resin (Gebhardt and Hötter 2016, Flaviana Calignano 2017).

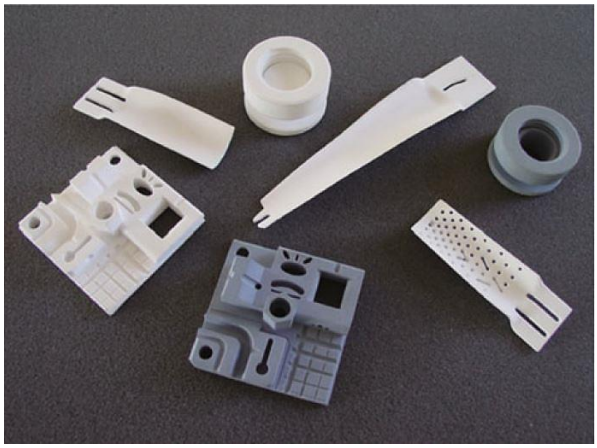

Figure 4 – Alumina and silica ceramic cores for investment casting of turbine blades, among others, produced using SLS (Nannan GUO 2013).

Figure 5 – Airbus A320 titanium nacelle hinge bracket with optimized topology made by using DMLS technology (EOS) (Nickels 2015).

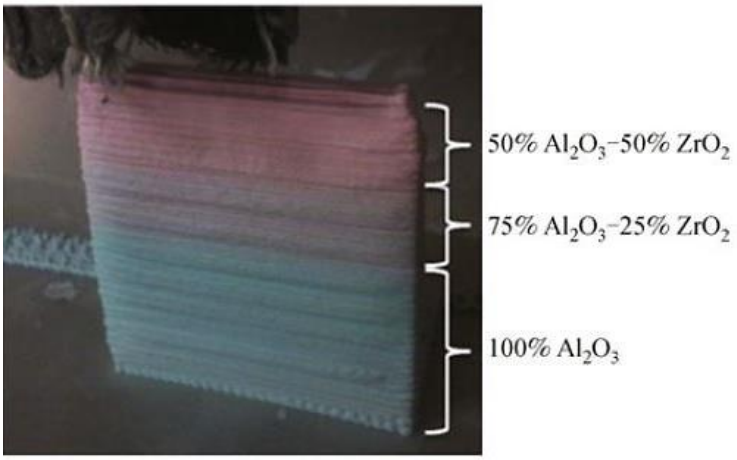

Figure 6 – Functionally graded material part produced using a triple-extruder freeze-form extrusion fabrication (FEF) process, with a gradient from 100 % Al_2O_3 to 50 % Al_2O_3 and 50% ZrO_2 (Nannan GUO 2013).

Additive manufacturing was first used in the production of polymer material objects (Figure 3) (M. Fera 2016) and the majority of its current global activity consists in using polymer-based systems (Herderick 2011). Currently, materials such as metals (Figure 2 and Figure 5), ceramics (Figure 4 and Figure 6), composites, biological systems (Figure 2) and functionally graded materials (FGM) (Figure 6) (Nannan GUO 2013) can also be used for this manufacturing process (Flaviana Calignano 2017, Frazier 2014). However, not all commonly used manufacturing materials are possible to be used in AM (Hernandez 2012).

Its first applications, as referred, were for rapid prototyping (Figure 3) and tooling (Flaviana Calignano 2017). However, the continuous development of additive manufacturing capabilities is making it possible for this manufacturing process to be increasingly used for the direct production of parts. It is well suited for a wide group of industries including marine, land and aerospace vehicles. Research is being made to improve its reliability and applicability, while being currently in use (Flaviana Calignano 2017, Hernandez 2012). It has also its applications in the medical sector such as enabling the production of rapid prototypes and models of damaged bones for analysis and high-quality bone transplants (Figure 2) (Hernandez 2012). Furthermore, it is also suitable for several other purposes such as the manufacturing of parts no longer being produced by its original manufacturers (Herderick 2011) and in the automotive industry (Hernandez 2012), radio-frequency field (Flaviana Calignano 2017), architectural modeling, fuel cell manufacturing and art (Hernandez 2012).

Additive manufacturing presents several advantages to conventional manufacturing techniques. It allows to quickly manufacture ready-to-use geometrically complex objects without the need of tooling through simplified manufacturing logistics at a low cost (Flaviana Calignano 2017). Usually, it requires little final machining or finishing (Lawrence E. Murr 2012). Unlike subtractive manufacturing processes such as machining, that removes up to 95% of material from the original as-bought bulk material, AM produces minimal waste since unmelted powder is recovered and in some cases can be recycled (Lawrence E. Murr 2012).

However, the influence on the microstructure and properties of the material of different AM technologies is currently not well characterized or understood (Bartłomiej Wysocki 2016). The intrinsic characteristics of this process, the layer by layer addition of material, may result in discontinuities in as-built materials which could and does develop mechanical anisotropies, dimensional inaccuracy and inacceptable finishing and structural state (Sofiane Guessasma 2015). The source of the materials anisotropy produced using AM is starting to receive additional attention by the AM community (Frazier 2014). Anisotropy can be reduced or at least managed by selecting an appropriate orientation of the part during its manufacturing (Sofiane Guessasma 2015) or by postprocessing the as-built part using a heat treatment, although it affects the cost-effectiveness of the process (Frazier 2014).

Although additive manufacturing global activity uses in its majority polymer-based systems, further attention and importance is being given to metallic part fabrication (Herderick 2011). The direct fabrication without the need for tooling or machining of net or near-net shaped (Herderick 2011), lightweight and extremely complex metallic parts allows for a wide range of

new design possibilities on numerous extremely critical and important applications. The possibility to fabricate high performance parts at a reduced overall cost has been of particular interest in the biomedical and aerospace industries (Figure 2 and Figure 5 respectively) (Herderick 2011).

Numerous metal additive manufacturing technologies are presently available, characterized by the heat source and on how the material is supplied (Seifi 2016). According to ASTM, additive manufacturing technologies of metal parts are classified into categories such as binder jetting, material jetting, direct energy deposition, sheet laminations, material extrusion, powder bed fusion and vat photo-polymerization (Flaviana Calignano 2017). Figure 7 shows two major categories from the ones referred previously, powder bed fusion (PBF) and direct energy deposition (DED), and the associated AM technologies and commercial machine supplier names.

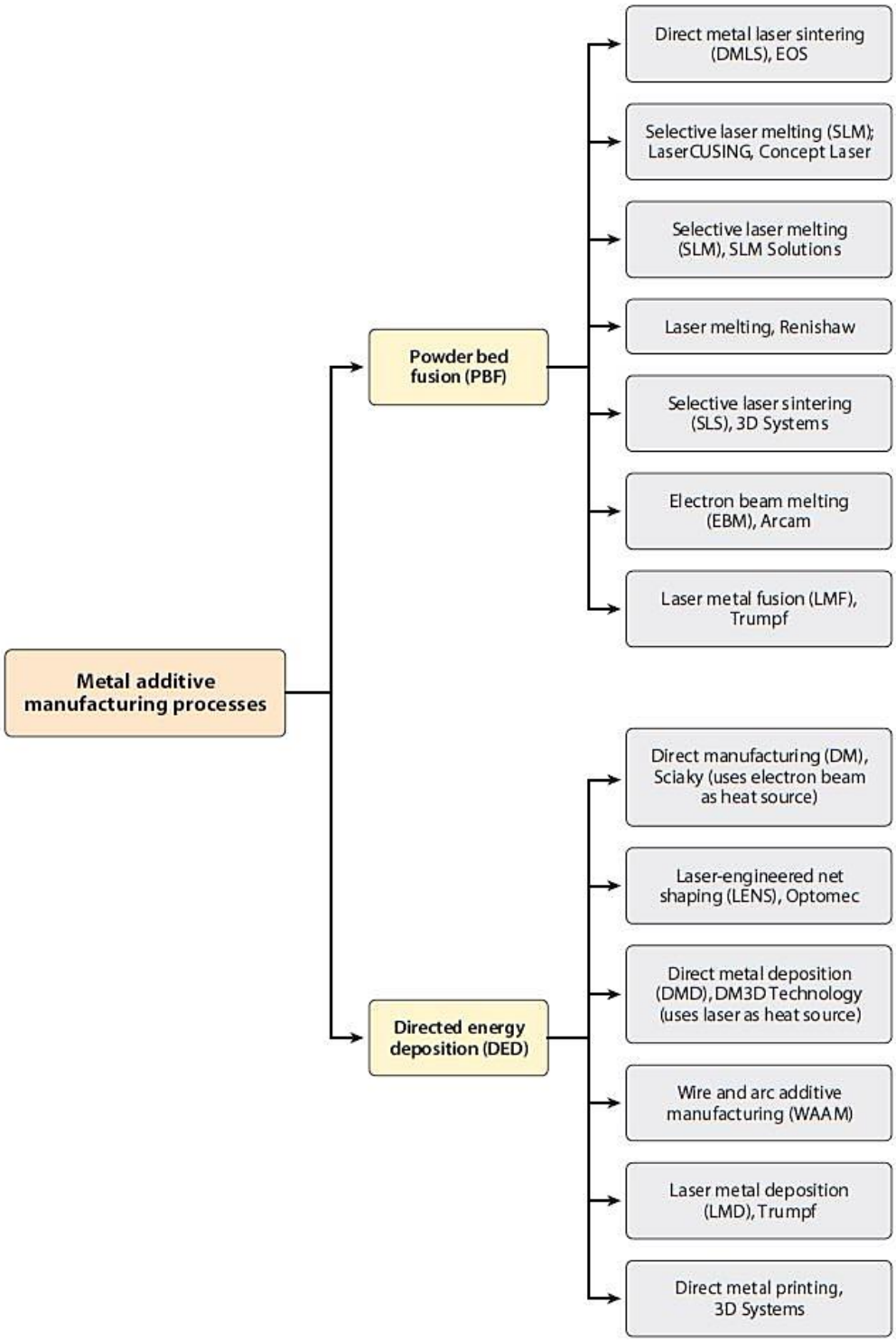

Figure 7 – Two major additive manufacturing categories and the associated AM technologies and commercial machine supplier names (Seifi 2016).

Typically, additive manufacturing takes the information from a computer-aided design (CAD) file and converts it to a stereolithography (STL) file that contains information of each layer to be printed. In the conversion process between the CAD file to a STL file, the continuous geometry of the drawing made in the CAD software is approximated through a series of small triangles and sliced (Hernandez 2012). Both approximations from the conversion process introduce inaccuracy on the intended part geometry, since the continuous contours are replaced by discrete ones. The smaller the triangles, the more accurate and closer to the intended design the final part will be (Hernandez 2012). Moreover, the creation of separate STL files and posterior combination of both may be done to reduce the inaccuracy introduced when the material is sliced (Hernandez 2012). A representation of the data flow in the STL file creation software is shown in Figure 8.

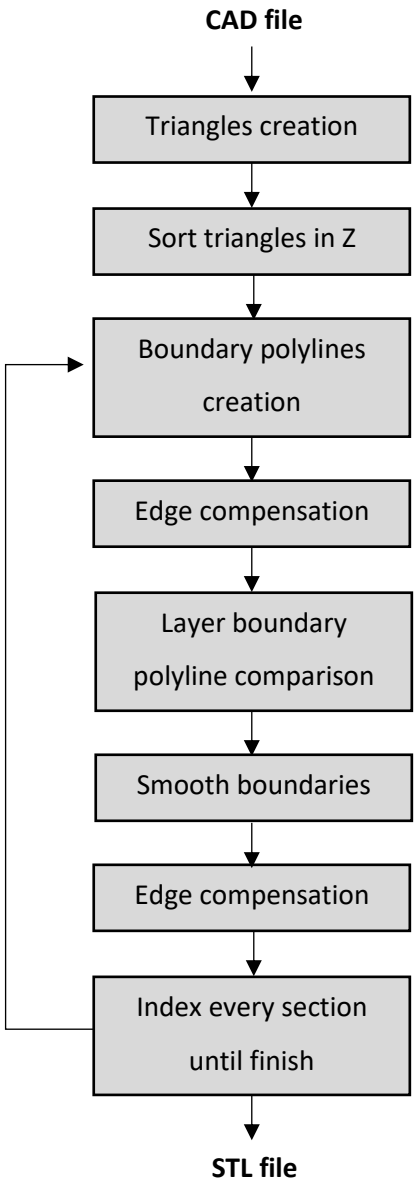

Figure 8 – Data flow representation in the STL file creation (Hernandez 2012).

It then uses a heat source such as electron beam, laser or arc to melt a material supplied via powder or wire feed, layer upon layer and over specific regions, to form the final object (Seifi 2016). A schematic representation of the typical additive manufacturing process steps is shown in Figure 9.

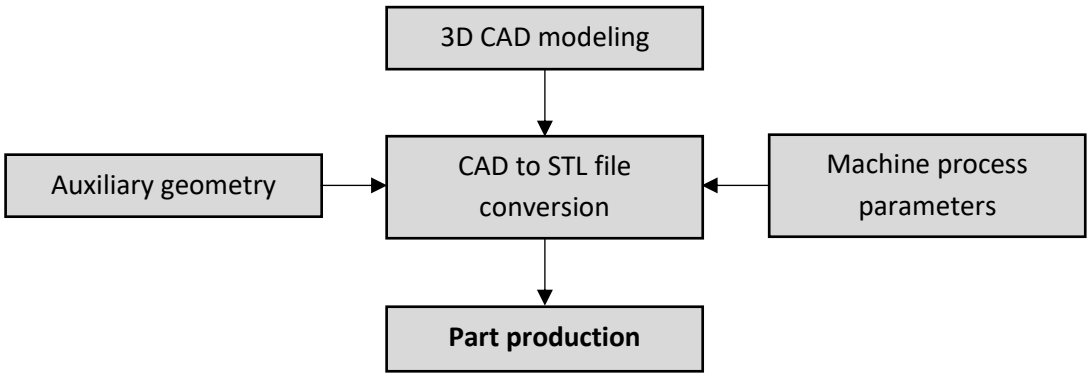

Figure 9 – Schematic representation of the steps involved in a part production through an additive manufacturing process.

Different combinations of absorbed power (P) and beam velocity (V) are used to melt the metal powder, which then solidifies. During this process, the material is subjected to cooling rates that depend on P-V combinations, hatching space (i.e. laser overlap) (D. Manfredi 2013) and on any preheating of the substrate, resulting in complex thermal cycles which accordingly affects the microstructure of the part (Seifi 2016).

As for the terminology used by most references in literature, the xy plane corresponds to the powder deposition plane and the z direction to the building direction, upon which subsequent layers are superimposed, as it can be observed in Figure 10.

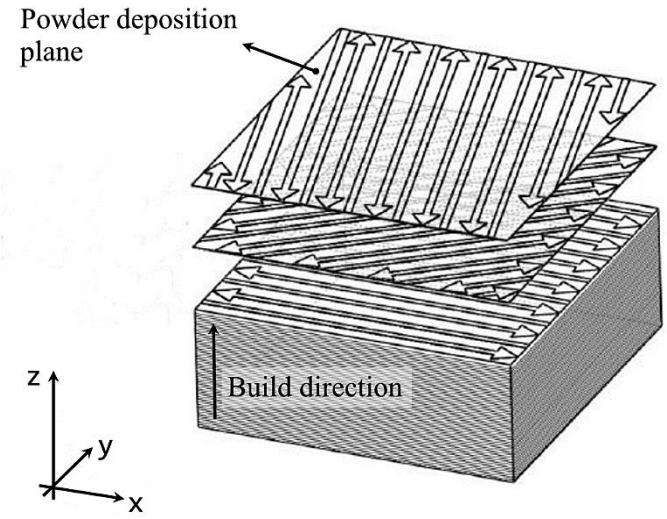

Figure 10 – Schematic representation of the powder deposition plane and build direction orientations, on the fabrication of a part through direct metal laser sintering (DMLS) (Diego Manfredi 2013).

An example on how the process parameters of an additive manufacturing technology and the resulting thermal cycles involved affect the microstructure of the part is shown in Figure 11 for an AlSi10Mg part produced using direct metal laser sintering (DMLS), in which it is evident the presence of melt pools and their geometry. It is also possible to observe that very fine microstructures are generated by the rapid and localized melting and cooling rates (Diego Manfredi 2013).

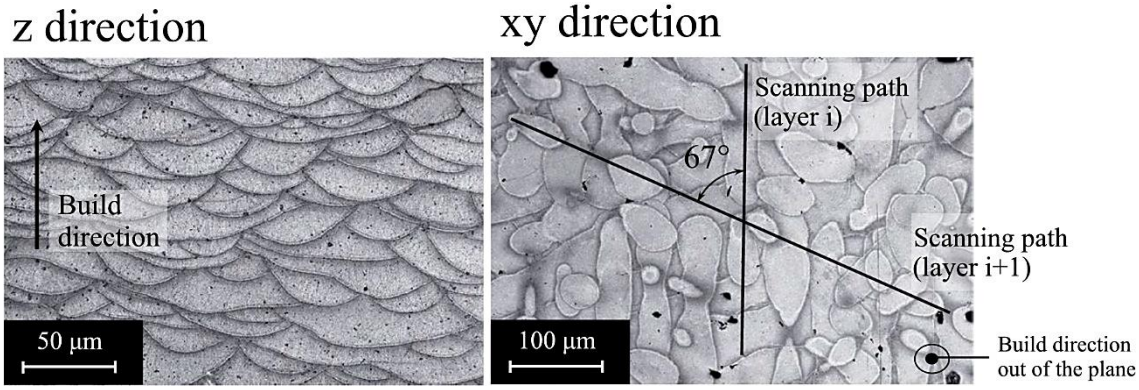

Figure 11 - Optical micrographs of vertical (z direction) and horizontal (xy direction) cross-sections of an AlSi10Mg part obtained through the direct metal laser sintering (DMLS) technology, showing the presence of melting pools and their geometry (D. Manfredi 2013).

For the z direction cross-section, the melt pools borders are all sequentially overlaid as a result of the superimposition of the different layers during the fabrication of the part (D. Manfredi 2013). As for the xy direction cross-section, the melt pool contour lines are shown as irregular geometric figures which could be attributed to the scanning rotation between consecutive layers and to the partial re-melting of the different layers, which are cross-sectioned at different heights and widths (D. Manfredi 2013). For this cross-section, two lines following the supposed scanning path for different layers were drawn. The angle between them was measured, corresponding to 67 degrees, as expected to this AM process. Parameters such as laser power, hatching distance and scanning strategy, corresponding essentially to the scan orientation, dictate the melt pools dimensions (D. Manfredi 2013).

For a more profound investigation on the influence of this thermal cycles on the microstructure of a part, higher magnifications are required such as in Figure 12 (D. Manfredi 2013).

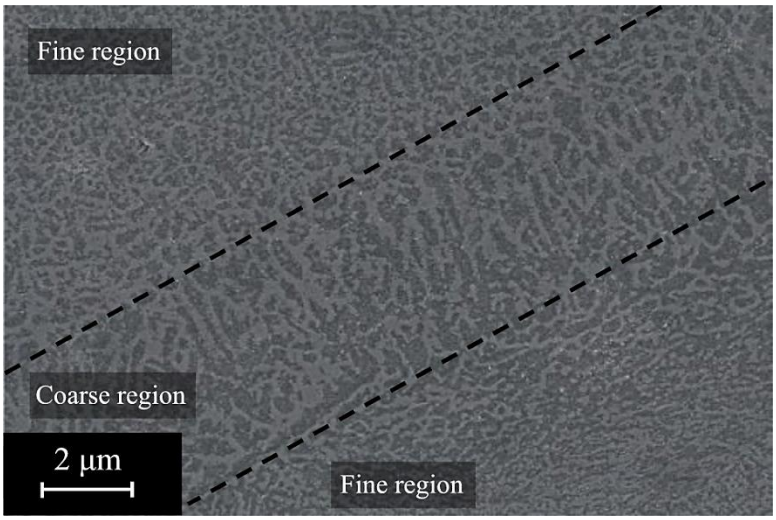

Figure 12 – Field emission scanning electron microscope (FESEM) micrograph of an AlSi10Mg part obtained through the direct metal laser sintering (DMLS) technology, at increased magnification (D. Manfredi 2013).

There are essentially two different forms of grain structure (Nesma T. Aboulkhair 2014). The inside of the melt pool, namely its core, is characterized by a fine microstructure whereas at the melt pool boundary coarser and elongated grains are found, as seen in Figure 12. At the melt pool borders, overlapping of the scan passages and consequent re-melting might occur. The coarser form of the grains located at this region is directly related to the longer time this region stays at higher temperatures, resulting in a slower solidification rate (Nesma T. Aboulkhair 2014, D. Manfredi 2013). In most cases, a heated affected zone is also distinguished close to the overlaps of the melting pools (Wei Pei 2017, Nesma T. Aboulkhair 2014).

The amount of overlapping of the scan and therefore the amount of coarse and fine regions will be affected by the AM process parameters. As seen in Figure 13, overlapping is directly related to the beam focus size, hatching distance and the scan power. By separately varying these parameters: the overlapping between the melt pools is increased by increasing the beam focus size or the scan power and by reducing the hatching distance.

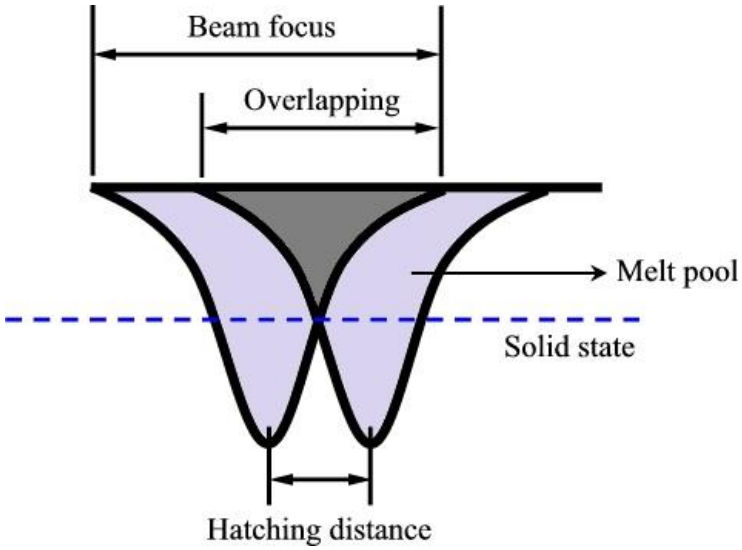

Figure 13 – Schematic representation of two adjacent melt pools and correspondent important dimensions and regions, in the fabrication of a part using an additive manufacturing technology.

The different complex and localized thermal cycles present on the fabrication of a part due to the inherent characteristics and process parameters of an additive manufacturing technology, results in a distinctive microstructure thus affecting the material mechanical properties.

One additional aspect of extreme importance that often occurs in the fabrication of parts through additive manufacturing is the existence of defects, internal or at the surface, which have an extremely important role on the mechanical properties of the final part. Defect generation is also influenced by the process parameters and by the correct calibration of the system's performance and metallic powder properties (Haijun Gong 2014).

In a part produced through AM processes, defects are usually present in the form of pores, voids or unmelted powder. The overall presence of defects can be estimated by measuring the porosity of a sample, through the comparison of its density to the nominal density value indicated for the material to be studied (Haijun Gong 2014). Examples of defects can be observed in Figure 14 to Figure 16.

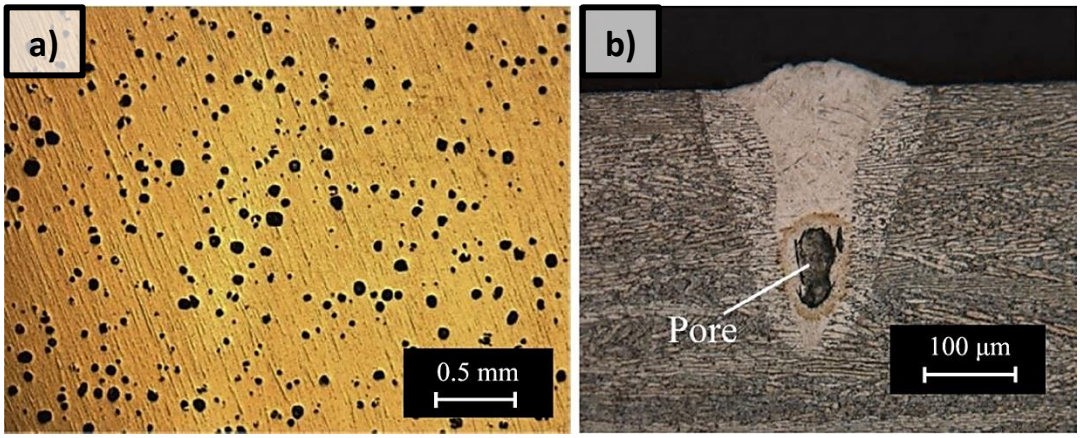

Figure 14 – Near-spherical defects directly correlated with excess energy input (Haijun Gong 2014). (a) Cross-section image of a SLM Ti–6Al–4V sample. (b) Melt pool profile of a SLM Ti–6Al–4V sample.

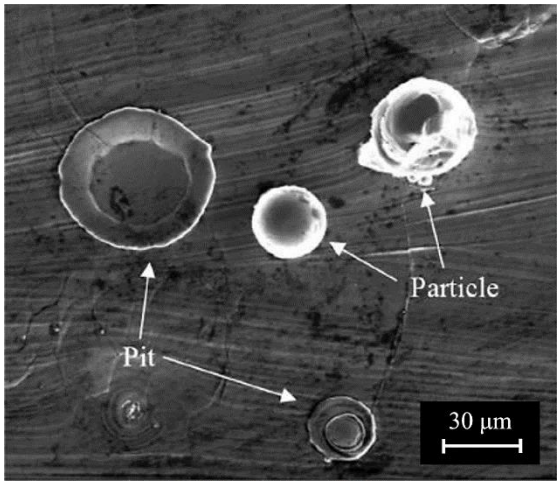

Figure 15 – Scanning electron microscopy (SEM) of the top surface of an SLM sample in which the presence of defects such as pits and small spherical particles are visible (Haijun Gong 2014).

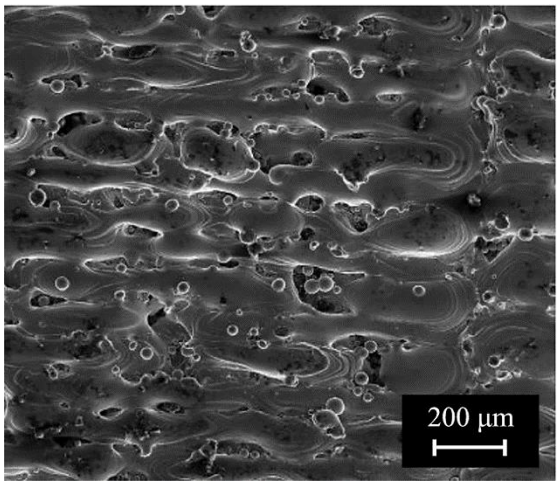

Figure 16 – Scanning electron microscopy (SEM) of the top surface of a SLM Ti–6Al–4V sample, showing defects related to insufficient energy input for full melting (Haijun Gong 2014).

In a study by H. Gong *et al.* (Haijun Gong 2014), defect generation mechanisms such as material vaporization, mass transfer phenomenon, melt pool discontinuity and process related instability are described and are summarized in this text.

Energy density is usually used to describe the average applied energy per volume of material during a powder bed fusion AM process (Haijun Gong 2014). It basically corresponds to the energy available to melt a certain volume of metallic powder and it can be expressed by the following equation (Haijun Gong 2014).

$$E = \frac{P}{V \cdot h \cdot t} \; [J \cdot mm^{-3}]$$

In this equation, P [W] corresponds to the scan power, V [mm·s^{-1}] is the scan speed, h [mm] is the hatch spacing and t [mm] is the layer thickness.

In this study, it was shown that the process parameters influence the level of porosity and therefore the level of defects on a sample. Upon the generation of porosity or not in relation to process parameters such as scan power and speed, four types of melting zones can be defined, as in Figure 17 (Haijun Gong 2014).

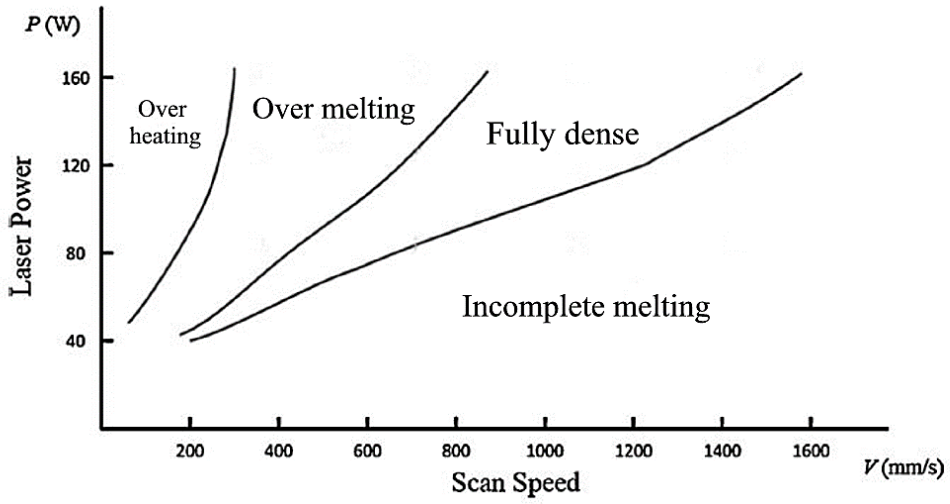

Figure 17 – Representation of the four types of melting zones in relation to the laser power and scan speed for SLM Raymor Ti–6Al–4V powder (Haijun Gong 2014).

Usually, only parts built using the combination of parameters in the over melting and incomplete melting zones contain measurable porosity, which implies the presence of defects. The defects generated by the over melting zone parameters are associated to excess energy, while the defects generated by the incomplete melting zone parameters are associated to insufficient energy (Haijun Gong 2014). Samples cannot be built using parameters on the overheating zone due to serious deformation caused by the excess heating of the samples (Haijun Gong 2014).

The excess energy input from the over melting zone parameters results in near-spherical defects as seen in Figure 14 and is described as the material vaporization defect generation mechanism. These defects can be attributed to gas bubbles formation when a higher laser energy is applied to the melt pool (Haijun Gong 2014). In a keyhole geometry melt pool, it was shown that gas bubbles may be formed far beneath the surface, as observed in Figure 14 b), due to vaporization of low melting point constituents of the alloy (Haijun Gong 2014). These defects are therefore trapped in the lower regions of the melt pool, since its rapid solidification does not give time for these bubbles to rise and escape (Haijun Gong 2014).

In addition to vaporization inside the melt pool as referred, molten material on the top surface can also be evaporated due to the intense thermal energy generated by excessive laser irradiation (Haijun Gong 2014). The evaporation process generates a recoil pressure on the melt pool and molten metal is ejected, rapidly solidifies and finally lands and gets welded as a spherical particle on the molten top surface (Haijun Gong 2014). This is described as the mass transfer phenomenon defect generation mechanism and it can be observed for the fully dense and over melting zones parameters (Haijun Gong 2014). Particles whose size is smaller than the layer thickness remain welded to the surface upon spreading of the subsequent layer, whereas particles larger than the layer thickness are removed by the recoating blade, as demonstrated in Figure 18 (Haijun Gong 2014).

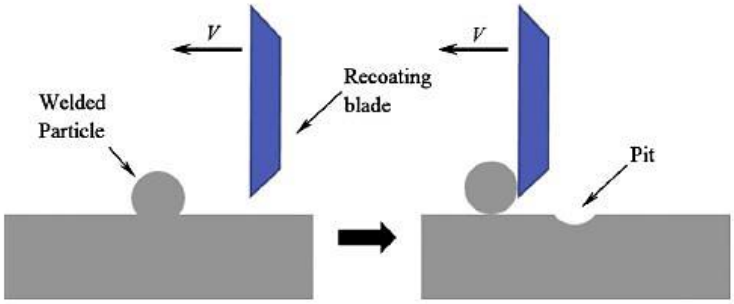

Figure 18 – Schematic representation of the formation of pits process (Haijun Gong 2014).

In these cases, pits are created on the surface of the layer and large enough pits could become as defects underneath the new layer to be formed (Haijun Gong 2014). Defects generated through this mechanism can be observed in Figure 15.

Moreover, defects such as pores and voids with entrapped powder particles can be formed due to melt pool discontinuities and lack of melt pool overlap, described as the melt pool discontinuity defect generation mechanism (Haijun Gong 2014). The insufficient or lack of overlap between hatch lines and/or by failing to wet the previous layer is a direct consequence where a lower energy density (incomplete melting zone parameters), large hatch spacing or even increased scan focus is used (Haijun Gong 2014). Examples of these defects can be seen in Figure 16.

Besides the defect generation mechanisms referred, defects can also occur if the system's performance and metallic powder properties are not correctly calibrated, thus referring to the process instability (Haijun Gong 2014). As an example, un-melted powder particles may become entrapped underneath the melt pool, caused by the reduced penetration depth of the scan as a result of power fluctuations (Haijun Gong 2014).

By understanding the mechanisms involved in the generation of defects and their relationship to the AM process parameters, it is therefore extremely important to correctly control these parameters values in order to avoid the generation of unwanted defects which will influence the final part mechanical and physical properties.

2.2 Direct metal laser sintering (DMLS)

Direct metal laser sintering (DMLS) is an additive manufacturing technology developed by EOS GmbH (Herderick 2011, E. Atzeni 2016) of Munich, Germany, and has been commercially available since 1995 (M. W. Khaing 2001). It offers a good balance between investment costs, range of materials and part quality (E. Atzeni 2016) by allowing high performance parts to be produced in just one fully automated production step (E. Atzeni 2016) without the need for tooling and posterior machining and/or thermal treatments to be applied. This process uses a laser beam as the heating source to selectively melt fine metal powder to create the final part, layer-by-layer. In Figure 19, an EOSINT M 280 machine that produces parts using the DMLS technology is shown.

Figure 19 – EOSINT M 280 machine, by EOS GmbH (GmbH 2010).

Because of its laser power and the use of an inert atmosphere in the building chamber to prevent the materials oxidation, it allows to process reactive materials such as cobalt-chromium, titanium and aluminum alloys (D. Manfredi 2013, E. Atzeni 2016). Other materials such as tool

steel and stainless steel can also be used (Herderick 2011). To guarantee the process repeatability with low porosity and suitable dimensional accuracy, tailoring of the powder and processing conditions is fundamental (Herderick 2011).

The production process starts by converting a 3D CAD model file to a STL file. The STL file contains the information of the part geometry and is then transferred to dedicated software which generates the required support structures and slices the part into layers of a designated thickness (D. Manfredi 2013). Each layer thickness depends on the material used and the thinner the powder layer, the greater the degree of interlayer bonding (Diego Manfredi 2013). The support structures main functions consist in holding unsupported geometries in place and to prevent the distortion of the part during fabrication, to fix the part to the building platform and to conduct excess heat away from the part (D. Manfredi 2013).

Figure 20 shows a schematic representation of the EOS machine and its components. The EOS device is equipped with a 200 W Yb (Ytterbium) fiber continuum laser, with a beam focus of 0.1 mm to 0.5 mm (E. Atzeni 2016, GmbH 2010). Its build volume depends on the specific EOS machine used. For the EOS M 280 machine, it is of 250 x 250 x 325 mm (Herderick 2011).

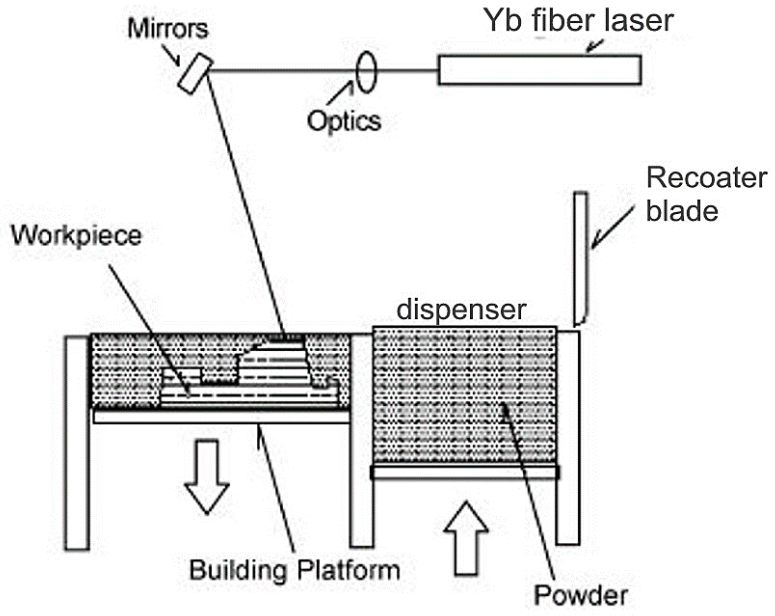

Figure 20 – Schematic representation of the EOS machine and its components (M. W. Khaing 2001).

Prior to the building process, the metal powder is sieved to ensure a maximum particle size in agreement with the layer thickness (Diego Manfredi 2013) and then placed in the dispenser inside of the building chamber. The chamber is then filled with an inert gas, namely argon, preventing the material to suffer from oxidation (D. Manfredi 2013, E. Atzeni 2016).

Once the process starts, a layer of powder is deposited onto the building platform using a recoater blade, preheated at 35 °C (D. Manfredi 2013). The laser beam then melts the powder according to the layer geometry in three consecutive steps: the laser starts by melting the contour of the section; it then melts the inner area by scanning it with parallel scan lines; to conclude, the contour is traced again to make sure that the part edges correspond exactly to the STL file data (Diego Manfredi 2013). Its intensity is defined so that the melted powder lightly penetrates the previous layer, to ensure at the same time a good connection between layers (D. Manfredi 2013).

Posteriorly to each layer formation, the building platform is lowered vertically by a distance equal to the layer thickness. The layer formation process is then repeated until the final part is formed. For each new layer to be formed, the direction of the scan lines over the inner area is rotated by 67 degrees, like observed in Figure 21, since a certain degree of rotation between layers leads to a better overlapping of these (Diego Manfredi 2013). The distance between two consecutive scan lines corresponds to the hatching distance. The same way as for the layer thickness, the process parameters such as scan power, velocity and hatching distance are also selected according to the material to be processed (E. Atzeni 2016).

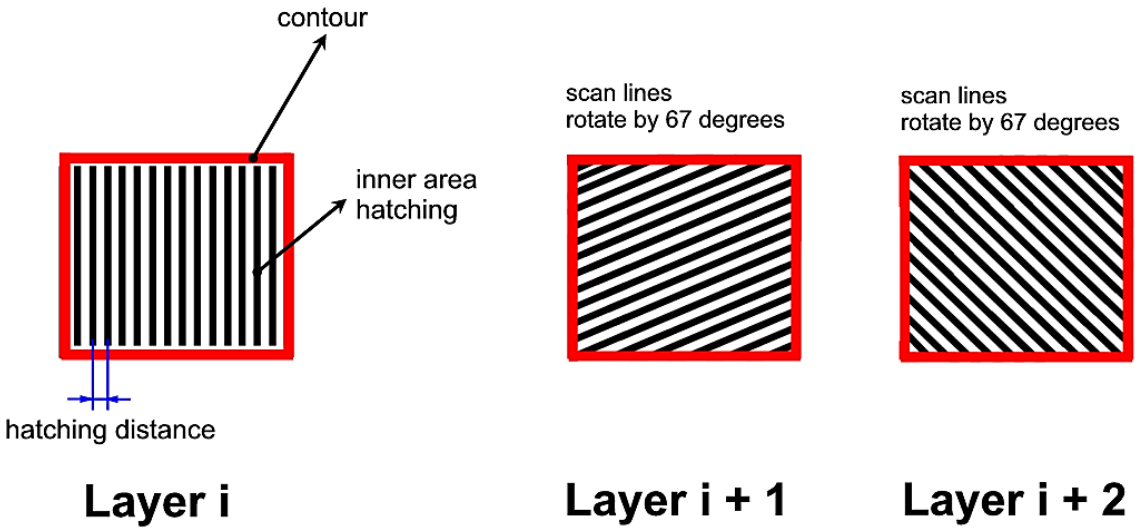

Figure 21 – Schematic representation of 3 consecutive layers and their contour, scan lines over the inner area and correspondent 67-degree rotation for each new layer, and hatching distance.

After to the building process, any excess powder is removed and a thermal treatment is applied to the part still in the platform to relieve stress (E. Atzeni 2016, M. W. Khaing 2001). Finally, the part can be removed from the platform after removing all the support structures (if existing) (D. Manfredi 2013).

2.3 Aluminum alloys - AlSi10Mg

Aluminum and its alloys are materials with broad applications due to their excellent balance of physical and mechanical properties. Examples of common applications of these materials include the airspace and automotive industries, beverage cans and cooking utensils (William D. Callister 2001).

They feature a high strength-to-weight and stiffness-to-weight ratios (σ/ρ and E/ρ respectively), with densities of around 3 times less than for steel (2.7 g/cm^3), high electrical and thermal conductivities and resistance to corrosion in some environments such as the ambient atmosphere (William D. Callister 2001). They are also characterized by its high ductility and its low melting temperature of around 660 °C (1220 °F), as being aluminum and aluminum

alloys main limitation (William D. Callister 2001). The mechanical strength of aluminum can be improved by cold work and by alloying with elements such as magnesium, silicon, copper, manganese and zinc (William D. Callister 2001).

As referred previously, to ensure the additive manufacturing process repeatability with low porosity and suitable dimensional accuracy, tailoring of the powder and processing conditions is fundamental (Herderick 2011).

EOS aluminum AlSi10Mg (Al, 10 wt-% Si, 0.3 wt-% Mg) is a specially tailored aluminum alloy powder to be used by EOS machines to create parts by direct metal laser sintering. Its chemical composition is comparable to the one of the correspondent typical casting alloy AlSi10Mg, which has good casting properties and is typically used for cast parts with complex shape (Systems 2014). Its composition is presented in Table 1.

Table 1 – Composition of the AlSi10Mg aluminum alloy powder (Systems 2014).

Al	Si	Fe	Cu	Mn	Mg	Ni	Zn	Pb	Sn	Ti
(balance)	9.0 – 11.0 wt-%	≤ 0.55 wt-%	≤ 0.05 wt-%	≤ 0.45 wt-%	0.2 – 0.45 wt-%	≤ 0.05 wt-%	≤ 0.10 wt-%	≤ 0.05 wt-%	≤ 0.05 wt-%	≤ 0.15 wt-%

The combination of silicon and magnesium improve the alloy mechanical properties and hardness (GmbH 2010). It has good strength, hardness and dynamic properties which allow the alloy to be used for parts subject to high loads. Parts made of this material are ideal for applications in which low weight, good thermal properties and a combination of high mechanical properties and low specific weight is required (Systems 2014). Typical applications include the direct manufacture of functional prototypes, small series products and spare parts (GmbH 2010).

The development and fabrication in a single step of a lightweight finger exoskeleton concept including joints, as reported by D. Manfredi (D. Manfredi 2013) and shown in Figure 22, is an example of an application of this aluminum alloy. The purpose of this concept consisted in the development of a system to overcome the EVA (Extra Vehicular Activities) glove stiffness of an astronaut, while strength, endurance and dexterity are maintained (D. Manfredi 2013).

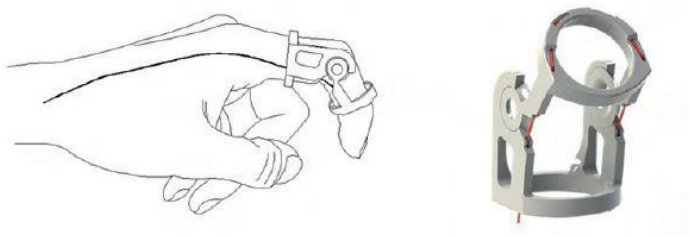

Figure 22 – Lightweight finger exoskeleton concept, made of AlSi10Mg using DMLS technology (D. Manfredi 2013).

Another example for the use of the AlSi10Mg aluminum alloy is on the production of lightweight aluminum lattice structures, as reported by the same study and shown in Figure 23 (D. Manfredi 2013). These cellular structures have been used for heat exchangers and in the aerospace and automotive industries, among others, due to their low density, high strength, good energy absorption and good thermal properties (D. Manfredi 2013).

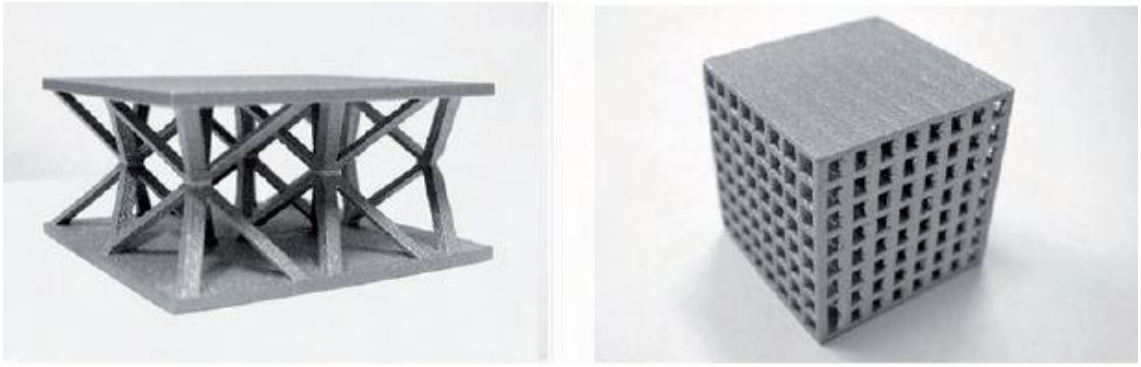

Figure 23 – Lightweight AlSi10Mg lattice structures, produced using DMLS technology (D. Manfredi 2013).

Because aluminum alloy powders have poor flowability, high reflectivity and high thermal conductivity promoting rapid heat dissipation, a higher laser power is needed to melt the powder and overcome these characteristics (Nesma T. Aboulkhair 2014). At the conditions present during the additive manufacturing process, aluminum alloys are highly susceptible to oxidation

(Nesma T. Aboulkhair 2014). As referred previously, an inert atmosphere is then used inside the building chamber to prevent it.

Heat treatment is frequently applied to a cast part produced using this alloy, to improve the mechanical properties. However, the laser-sintering process in AM is characterized by extremely fast melting and solidification which produces a metallurgy and consequent mechanical properties in the as-built part which are similar to the heat-treated cast parts. For this reason, such hardening heat treatments are not recommended or currently finding wide spread applications for parts produced through additive manufacturing. Instead, only a stress-relieving thermal treatment is done (Systems 2014).

Currently, there is limited published data on the mechanical properties of materials used in additive manufacturing. Most of the published mechanical properties have been reported for Ti-6Al-4V alloy (Seifi 2016). The mechanical properties of the EOS aluminum AlSi10Mg, as stated by EOS except for hardness values, are presented in Table 2. Hardness values were determined in a study by D. Manfredi (Diego Manfredi 2013) through Vickers microhardness measurements using a Leitz instrument with a load of 50 g for 30 s.

Table 2 – Mechanical properties of the EOS aluminum AlSi10Mg, as stated by EOS (Systems 2014).

		As built	**Heat treated: stress relieve**
Ultimate tensile strength (MPa)	Horizontal direction (xy)	460 ± 20	345 ± 10
	Vertical direction (z)	460 ± 20	350 ± 10
Yield strength (Rp 0.2 %) (MPa)	Horizontal direction (xy)	270 ± 10	230 ± 15
	Vertical direction (z)	240 ± 10	230 ± 15
Young's modulus (GPa)	Horizontal direction (xy)	75 ± 10	70 ± 10
	Vertical direction (z)	70 ± 10	60 ± 10
Strain to failure (%)	Horizontal direction (xy)	9 ± 2	12 ± 2
	Vertical direction (z)	6 ± 2	11 ± 2
Hardness (HV)		Approx. 107 ± 4	

As already stated, the production of a part using an additive manufacturing process involves local and complex thermal cycles which will influence the microstructure of the material and therefore its mechanical properties. Different microstructures are formed for the powder deposition plane (xy plane) and build direction (z direction), as observed in Figure 11. From the literature values presented in Table 2 and except for the material hardness, it is evident that the mechanical properties values are slightly different on the powder deposition plane and on the build direction, as expected.

Furthermore, as previously referred, the chemical composition of the EOS aluminum AlSi10Mg aluminum alloy powder is comparable to the one of the correspondent typical casting alloy AlSi10Mg, namely the A360.0 alloy (Systems 2014, Diego Manfredi 2013). However, due essentially to the very fine microstructure formed on the additive manufacturing process by the rapid and localized melting and cooling rates (Diego Manfredi 2013), the EOS AlSi10Mg alloy shows different values of mechanical properties. When compared to the as-fabricated A360.0 cast alloy, it shows higher values of yield strength corresponding to an increase of about 43 % for the xy plane and 36 % along the z direction (Diego Manfredi 2013, D. Manfredi 2013). Moreover, ultimate tensile strength shows little higher values, whereas the elongation at break is higher for the xy plane but slightly lower along the z direction (Diego Manfredi 2013, D. Manfredi 2013).

2.4 Scanning electron microscopy (SEM)

Scanning electron microscopy (SEM) is a technique used for the visualization and characterization of material surfaces, capable of conduct examinations at a very high magnification (Silva 2012 , Joseph Goldstein 2012). It is believed that the first contribution to the idea of a scanning electron microscope was made by H. Stintzing in 1927 (Reichelt 2007, Silva 2012). However, just in 1942 SEM was truly described and developed by Zworykin and only in 1965 the prototype for the first commercial SEM was developed by Pease and Nixon (A. Bogner 2006).

SEM is now a well-established method for the visualization and characterization of surfaces in many fields such as materials and surface sciences, semiconductor research and industry, life

sciences, mineralogy, geology, the oil industry, archaeology and food research, among others (Reichelt 2007).

It consists in the emission of a fine probe of electrons, with energies typically up to 40 KeV, focused on the specimen surface to be analyzed and scanned along a pattern of parallel lines (A. Bogner 2006). This process occurs inside of a vacuum chamber (de Assumpção Pereira-da-Silva and Ferri 2017, Silva 2012) with pressure typically to about 10^{-4} Pa, allowing the beam of electrons to travel to the specimen with little interaction with residual gas molecules (Reichelt 2007). It then collects the several signals generated as a result of the impact of the incident electrons on the specimen, to form an image or to analyze its surface (A. Bogner 2006).

These generated signals correspond mainly to high-energy electrons backscattered from the primary beam, secondary electrons with energy levels of just a few tens of eV and characteristic X-rays (A. Bogner 2006). Due to the low energy of the secondary electrons, these can be bent round corners and thus allow for the topographic contrast (R. E. Smallman 1999). On the other hand, the emission of X-rays characteristic of the material being bombarded with high-energy electrons allows to gather information on the chemical composition of the material.

The use of this technique has shown to be extremely useful for fractographic analysis to evaluate, study and determine the correspondent failure mechanisms of materials produced using additive manufacturing processes. Correlating fractography with measured mechanical properties such as yield strength (YS), ultimate tensile strength (UTS) and strain to failure (ε_f), conclusions on the controlling deformation mechanisms, their significance on properties and linkages to microstructures and processing can be made.

A good example of a typical ductile failure is shown in Figure 24. In this fracture surface and at higher magnifications (Figure 24 b) and c)), it is possible to observe that very fine dimples completely cover the surface which reveals a great ability to dissipate the energy of the fracture (Diego Manfredi 2013). In fact, for samples that failed by ductile fracture, microvoid size as seen on the fracture surface is inversely proportional to strain to failure, meaning that smaller void diameters are an indicative of higher strain to failure values (Nimer 2011). In addition to microvoid dimples on the fracture surface, ductile fracture can be preceded by necking, corresponding to a decrease of the sample cross-sectional area at the point of failure (Nimer 2016).

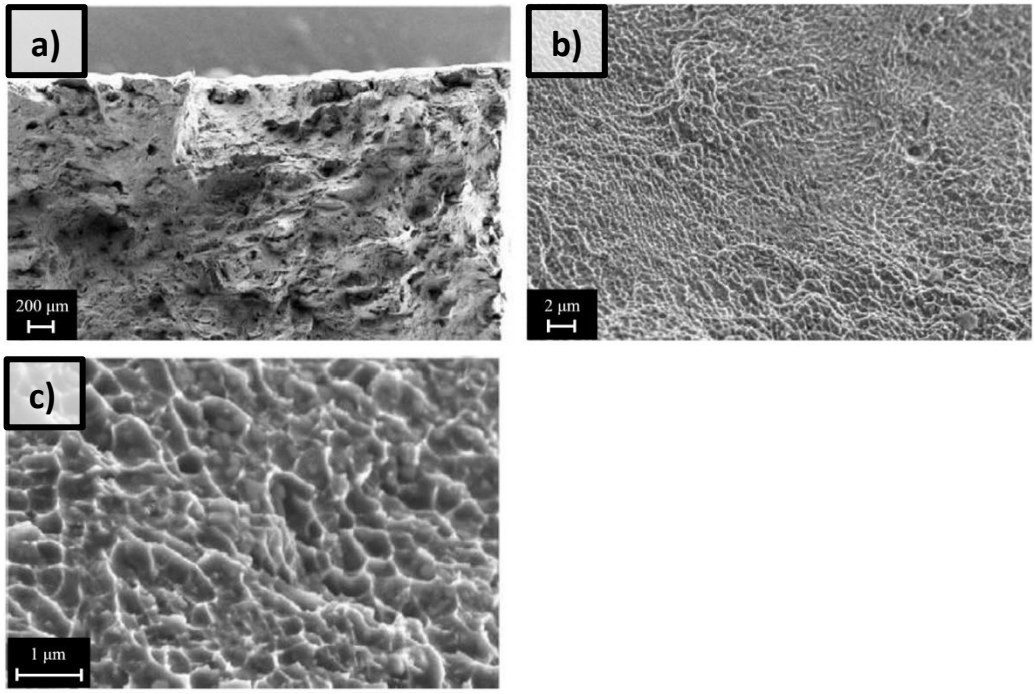

Figure 24 – Field emission scanning electron microscopy (FESEM) at different magnifications of the fracture surface of an aluminum alloy produced using DMLS technology (Diego Manfredi 2013).

A brittle fracture can also occur, as seen in Figure 25, due to the lack of dimples present and instead the presence of a smooth fracture surface and slip bands (Nimer 2011). This image shows cleavage failure (Nimer 2011).

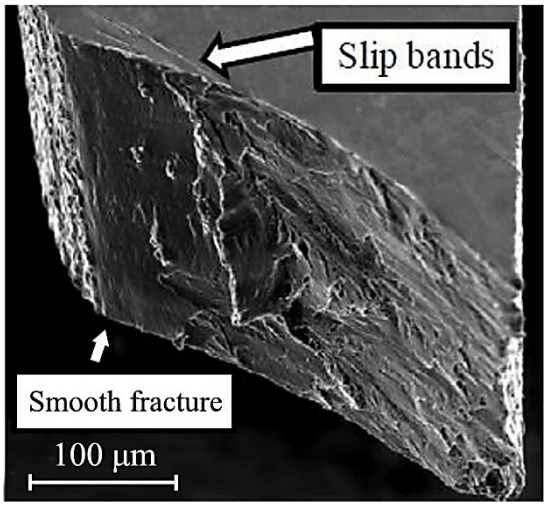

Figure 25 – SEM image of the fracture surface of a Ti-5111 specimen taken from the retreating interface in the middle of the weld produced using friction stir welding (FSW) (Nimer 2011).

In addition to ductile and brittle failure mechanisms, defects can also be seen in fracture surfaces using the SEM technique (Amanda J. Sterling 2015, Ming Tang 2016), which allows to evaluate their possible influence on the failure of a specimen. Although most pores are spherical, irregularly shaped pores can also be formed (Amanda J. Sterling 2015). Specially pores with sharp angles and pointed cavities, such as in Figure 26 pointed with an arrow, can be detrimental for the mechanical behavior of a part by producing large stress concentrations (Amanda J. Sterling 2015).

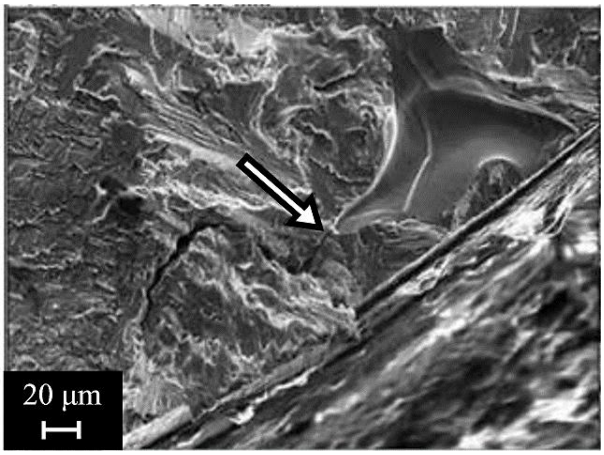

Figure 26 – SEM image of an irregularly shaped pore of a Laser Engineered Net Shaping (LENS) Ti–6Al–4V specimen fracture surface (Amanda J. Sterling 2015).

The size, shape and topology of the fracture surface explains how the microstructure is controlling microscale properties.

2.5 Summary

This review of the state of the art showed the importance of process parameters of an additive manufacturing technology on the microstructure of the final part and thus on its macroscale properties, due to the complex and localized thermal cycles deriving from this process. However, the influence on the microstructure and properties of the material of different AM technologies is currently not well characterized, understood or controlled.

The purpose of this work consists in studying the orientation-dependency of the mechanical properties of parts made of an aluminum alloy, specifically AlSi10Mg, produced using additive manufacturing. For this study, a novel technique consisting in microsample testing (using samples whose gage section is 1.78 mm long with a square shaped cross-section of 250 μm x 250 μm) was used to directly measure the mechanical properties of this alloy at a length scale that will explore the inhomogeneous material performance.

To produce the part to be analyzed, direct metal laser sintering (DMLS) was used by means of an EOS machine in collaboration with Johns Hopkins University Applied Physics laboratory. Microsample testing was carried out using a custom-built elevated temperature microsample testing system designed and developed by Nimer (Nimer 2016) in the Micromaterials Laboratory at the University of Maryland, Baltimore County (UMBC). Posteriorly, fracture surfaces of the tested microsamples were analyzed using a scanning electron microscope FEI Nova NanoSEM 450 in the department of physics at UMBC.

3 Material Production

3.1 Introduction

Additive manufacturing is a technology used to create parts from a 3D CAD model, consecutively adding layers of material until the final part is formed. It is starting to be widely used due to its proposed advantages such as reduced component lead time, reduced material waste, energy usage and carbon footprint (Herderick 2011), among others.

However, it is a manufacturing process still in development and while AM has great promise it is far from its potential. Notable characterization and understanding of the mechanical behavior of the produced materials is limited (Nimer 2016). The process parameters of AM such as laser scan power and focus, scan velocity, hatching distance and layer thickness are highly influential on the resultant material microstructure and on the creation of defects in the final part. The microstructures defect formation involves local complex thermal evolutions on the layer being scanned and on the adjacent previous layers. Consequently, the process parameters local build geometry as well as the macro build location all directly affect the mechanical properties of the as-built part.

For this reason, characterization and understanding of the mechanical and physical behaviors of materials produced using this manufacturing process is necessary. Currently, there is limited published data on the mechanical properties of materials used in AM. Most of the published mechanical properties have been reported for Ti-6Al-4V alloy (Seifi 2016). Moreover, studies to characterize the mechanical behavior of materials produced with AM technologies have been made using standard sized samples in short databases for design (Diego Manfredi 2013).

In this work, a novel technique designated as microsample testing was employed to characterize the local mechanical behavior of an AlSi10Mg aluminum alloy part produced using direct metal laser sintering (DMLS). The test results are linked to material process parameters as well as to build geometry. This technique was carried out to determine the final part mechanical properties in the three different building directions (Figure 27): x and y (parallel to the powder deposition plane) and z (parallel to the build direction). Afterwards, a scanning electron microscope was used to analyze the microsamples fracture surface.

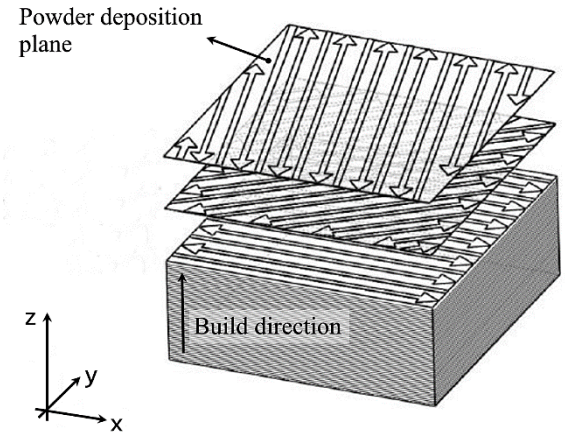

Figure 27 – Schematic representation of the powder deposition plane and build direction orientations, on the fabrication of a part through direct metal laser sintering (DMLS) (Diego Manfredi 2013).

Although microsample testing has been carried out for several material studies as referred in the literature, the use of this novel technique on parts produced through additive manufacturing is still very limited. The relevant information that can be obtained through microscale tensile testing and the correspondent fracture analyses of microsamples makes this a unique technique that can be used for this purpose.

In this chapter, a description of the manufacturing steps necessary to produce the DMLS AlSi10Mg aluminum alloy part to be posteriorly analyzed is made.

3.2 AlSi10Mg part production

In order to be able to study the local mechanical behavior through microscale tensile testing of an AlSi10Mg aluminum alloy part manufactured using DMLS, a simple rectangular prism part as represented in Figure 28 was produced using an EOSINT M 280 (Figure 19) in collaboration with the Johns Hopkins University Applied Physics laboratory. In this work, standard EOS process parameters defined for AlSi10Mg parts production were used.

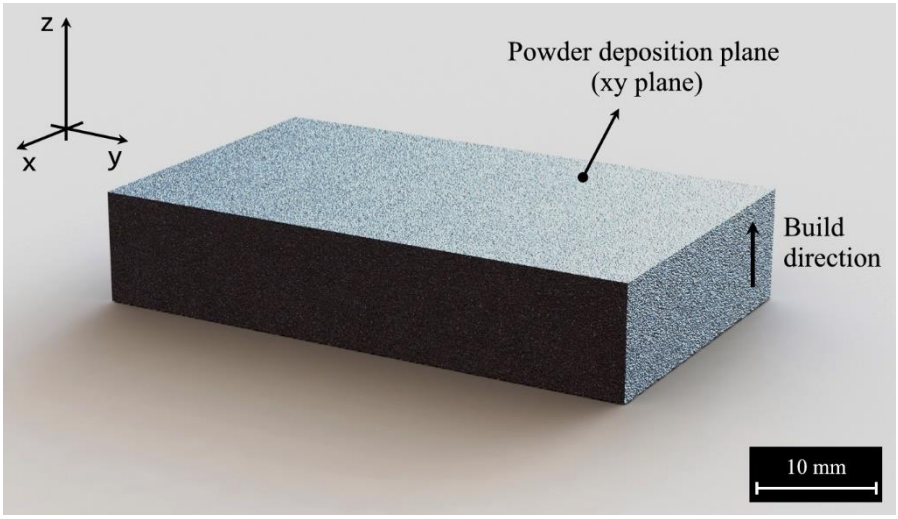

Figure 28 – Representation of the AlSi10Mg rectangular prism part produced using DMLS.

The production of this part started by converting the 3D CAD model to an STL file, which contains the information of the part geometry and the correspondent information of each layer to be printed.

The EOS aluminum AlSi10Mg powder was supplied by EOS GmbH, being sieved to ensure a maximum particle size in agreement with the layer thickness and placed in the dispenser inside of the building chamber (Figure 20). The chamber was afterwards filled with argon, which is in accordance to the material being processed, to prevent the material to suffer from oxidation during its fabrication (D. Manfredi 2013, E. Atzeni 2016).

Once the process started, a layer of powder was spread over the building platform, preheated at 35 °C, using a recoater blade. The layer thickness depends on the material used and for AlSi10Mg powder it corresponds to 30 μm. The thinner the powder layer, the greater the degree of interlayer bonding.

Then, a 200 W Yb fiber laser, with a beam focus of 0.1 mm to 0.5 mm, melted the powder according to the layer geometry in three consecutive steps (Figure 29): the laser starts by melting the contour of the section (step 1); it then melts the inner area by scanning it with parallel scan lines (step 2); to conclude, the contour is traced again (step 3).

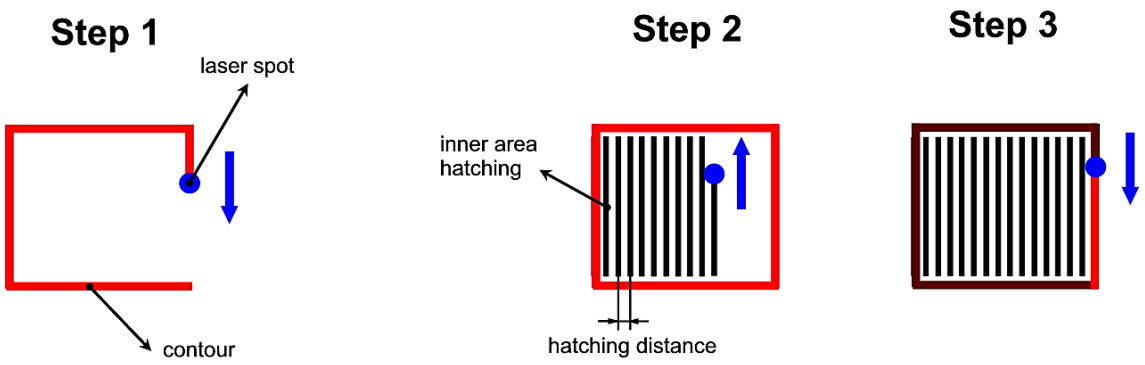

Figure 29 – Schematic representation of the three steps involved in the scanning of one layer.

At the end of the formation of each layer, the building platform was lowered vertically by a distance equal to the layer thickness of the part and the process was repeated until the final part was obtained. For each new layer formed, the direction of the scan lines on the inner area was rotated by 67 degrees (Figure 21) leading to a better overlap between layers (Diego Manfredi 2013).

The same way as for the layer thickness, the process parameters such as scan power, velocity and hatching distance are also material dependent and corresponded to the standard EOS parameters for the AlSi10Mg powder (E. Atzeni 2016). The EOS machine uses different parameters for the core of a part, for its lower and upper surfaces parallel to the powder deposition plane (down-skin and up-skin) and for the contour, as it can be observed in Figure 30 (Diego Manfredi 2013).

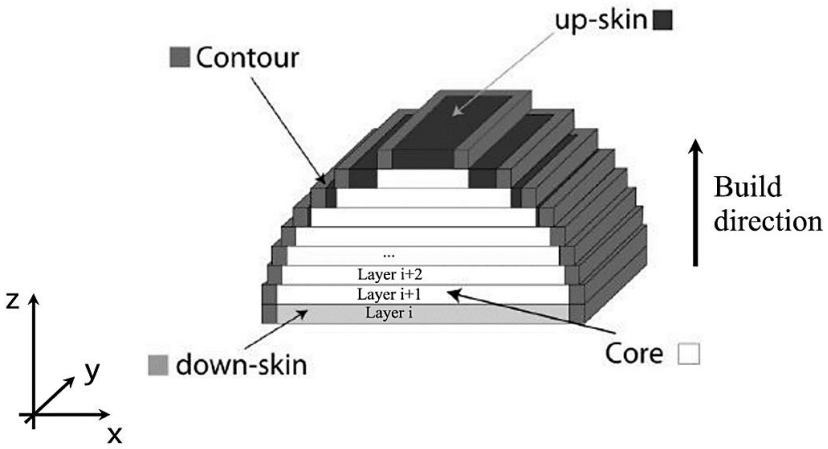

Figure 30 – Schematic representation of the different AM process parameters employed for different zones in the production of a part (each color represents a specific set of parameters) (Diego Manfredi 2013).

Once the part was made, excess powder was removed and a thermal treatment of 2 hours at 300 °C was applied to the part still mounted on the building platform to relieve stress (D. Manfredi 2013), preventing the bending of the part due to the high residual thermal stresses resultant from the high thermal gradients at which it was subjected (Diego Manfredi 2013). The referred thermal treatment parameters employed were also specifically indicated for the aluminum alloy powder used in this study. Finally, the part was removed from the platform and was ready for posterior microsample extraction and mechanical behavior study.

4 Microsample Testing

4.1 Introduction

A common and straightforward method used to characterize the mechanical behavior of materials consists in performing either uniaxial tensile or compression tests to standard macro sized samples, with dimensions of cm, as shown in Figure 31.

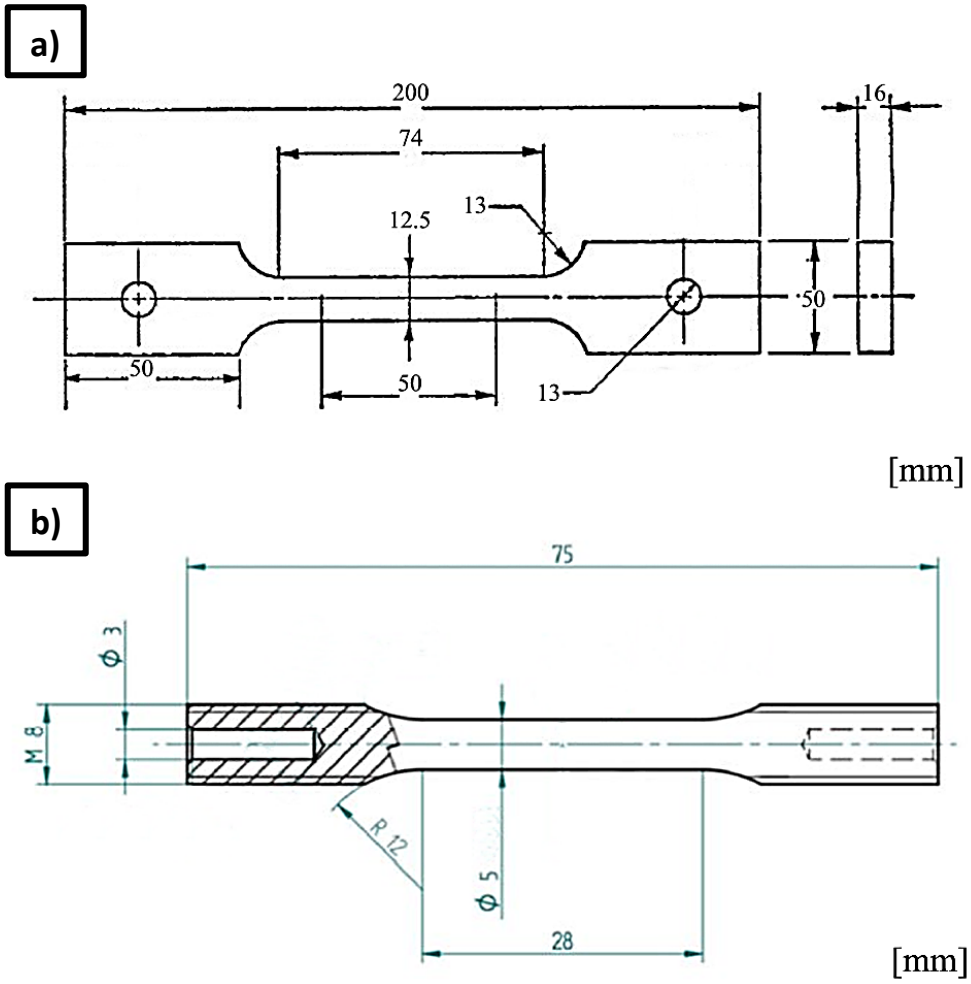

Figure 31 – Examples of standard uniaxial tensile samples: (a) ASTM standard pin-loaded tension test specimen (ASTM International. 100 Barr Harbour Dr.); (b) EN ISO standard cylindrical tension test specimen (E. Balducci 2017).

The information obtained through these tests is sufficient to characterize materials that present a homogeneous microstructure. However, not all materials have homogeneous microstructures. When the used manufacturing process results in anisotropic microstructures and

inhomogeneities of the material due to the local material evolutions involved, tensile tests using larger scale samples are unable to deeply characterize the mechanical behavior of the material as they will average the effect of its microstructural inhomogeneities and its performance.

Additive manufacturing (AM) and friction stir welding (FSW) are straightforward examples of material processing methods that involve local complex material evolutions resulting in inhomogeneities and anisotropy of the material (Nimer 2016). As for additive manufacturing, the AM process parameters influence the final part microstructure as a result of the local complex thermal evolutions involved on the layer being scanned and on the adjacent previous layers.

To address to this challenge, a microscale tensile testing approach has been developed which changes the sample length scale and allows anisotropic material responses to be evaluated. Several studies have been made on this field leading to the design and development of reliable microsample testing systems (Cheng 2008, M. Zupan 2001, Nimer 2016). Microscale tensile and compression testing consists in performing tensile or compression tests to specimens as shown in Figure 32, whose volume of the test region is roughly 500,000 times smaller than a standard sample (D. A. LaVan and W. N. Sharpe 1999). Currently, progress is being achieved on microscale tensile testing of materials across different conditions, for example at elevated temperatures (Nimer 2016).

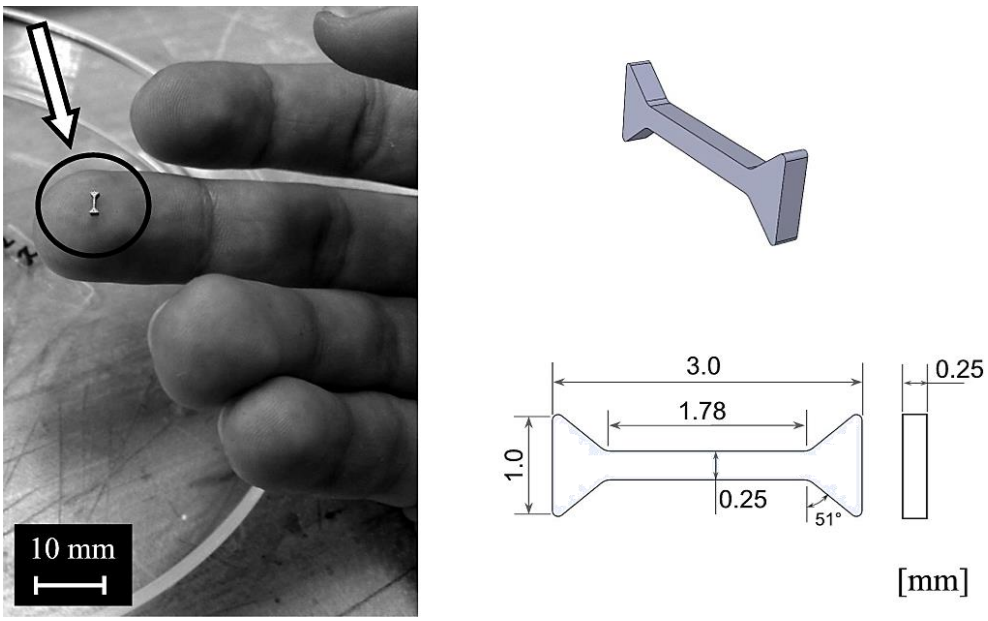

Figure 32 – (left) Picture of a microsample in a finger-tip and (right) schematic representation of a microsample used for tensile testing and correspondent dimensions and geometry.

Figure 33 gives to the reader a better perspective on the dimensions difference between a microsample and a standard sample, used for uniaxial tensile testing.

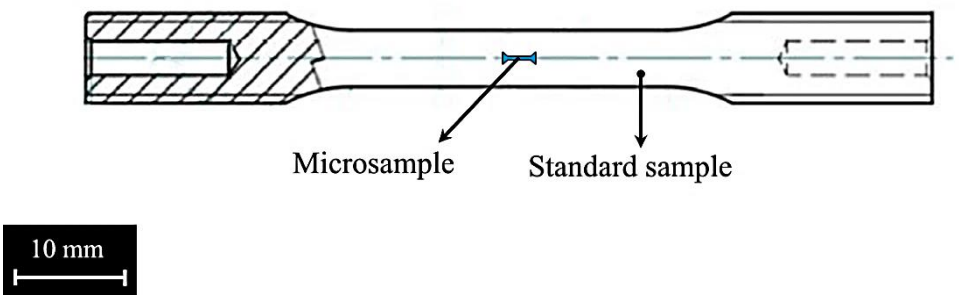

Figure 33 – Dimensions comparison between a microsample and a EN ISO standard cylindrical tension test specimen (E. Balducci 2017).

In addition to this technique, efforts to characterize the mechanical behavior of small volumes of materials have led to the development and use of other test methodologies like Vickers and nanoindentation hardness tests, thermal cycling experiments, in situ X-ray diffraction experiments, thin film bulge testing, resonance tests of thin film cantilevers and M-test electronic measure (K.J. Hemker and W.N. Sharpe 2007).

Nevertheless, the use of microsample tensile testing presents several advantages to these test methodologies, making it a more simple and powerful method used to characterize the local mechanical behavior of a material. This method allows for collection of samples from bulk materials, not being limited to thin films, and it is a direct method since stress and strain values (σ and ε respectively) are measured without having to imply stress state. The measured values correspond to absolute measurements and not to relative values, i.e. vickers hardness values are often relative within a single alloy. It enables to obtain the stress-strain responses of the material, from which mechanical properties such as Young's modulus (E), yield strength (σ_y), ultimate tensile strength (UTS) and strain to failure (ε_f) can be determined. Furthermore, the data obtained from microsample tensile tests is directly comparable to hand books and familiar to designers. Moreover, the resultant stress and strain measurements scale with the power of one, being less affected by possible small experimental errors.

In a more general point of view, microsample tensile testing holds several other advantages. As already referred, the use of this technique makes it possible to study and characterize the local mechanical behavior of materials with anisotropic microstructures and inhomogeneities. It also enables one to build a strong database on the mechanical properties of a material with small amounts of material. Moreover, the mechanical behavior of expensive materials or materials obtained through extremely rigorous, expensive and difficult to replicate processes can be studied.

Microsample testing has proven to be more than effective for a wide range of material analysis, including but not limited to base metal, heat affected zones and different weld regions of weldments (Figure 34) (Nimer 2011, Rafal M. Molak 2008, Nimer 2016), copper bullet jacket (Figure 35) (Cheng 2008), nanocrystalline copper (Figure 36) (Y.M. Wang 2003), silicon dioxide thin films (Figure 37) (D.S. Gianola and W.N. Sharpe 2004) and elevated temperatures materials behavior (Figure 38) (Nimer 2016, M. Zupan 2001, K.J. Hemker and W.N. Sharpe 2007). However, there are significant challenges related to the preparation, handling, testing and strain measurement of microsamples due to its small size and fragility.

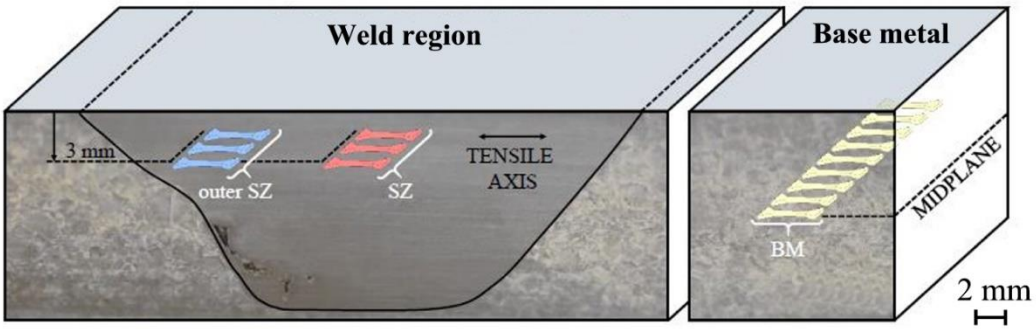

Figure 34 – Schematic representation of the weld region and base metal of friction stir welding (FSW) and the location of the extracted microsamples (Nimer 2016).

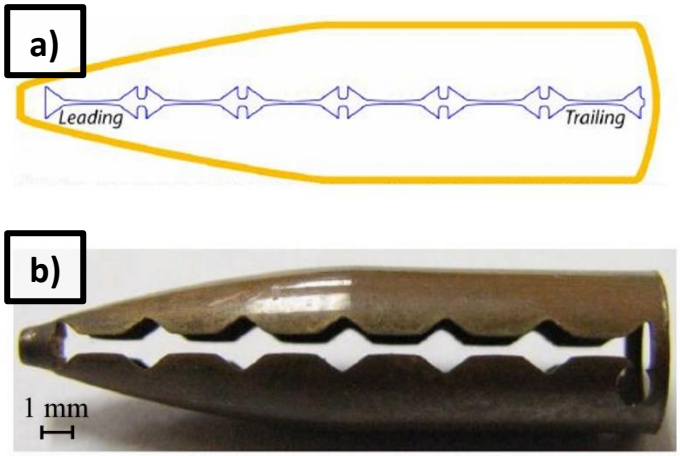

Figure 35 – (a) Schematic representation of a copper bullet jacket and location of the microsamples to be extracted. (b) Image of the copper jacket with removed microsamples (Cheng 2008).

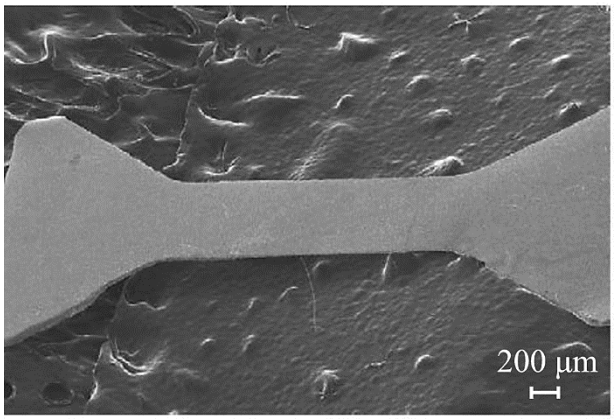

Figure 36 – SEM image of a nanocrystalline copper microsample with a cross-section of 0.5 x 0.015 mm^2 (Y.M. Wang 2003).

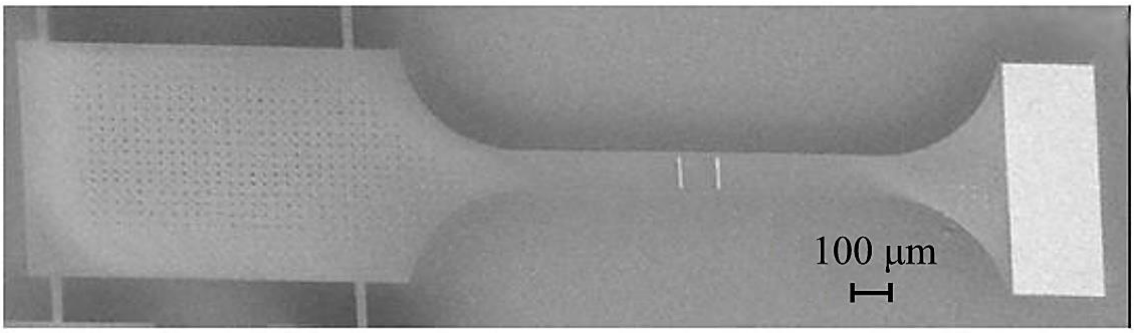

Figure 37 – Gold tensile specimen used to represent the silicon dioxide tensile specimen, which by being transparent makes it difficult to be photographed (D.S. Gianola and W.N. Sharpe 2004).

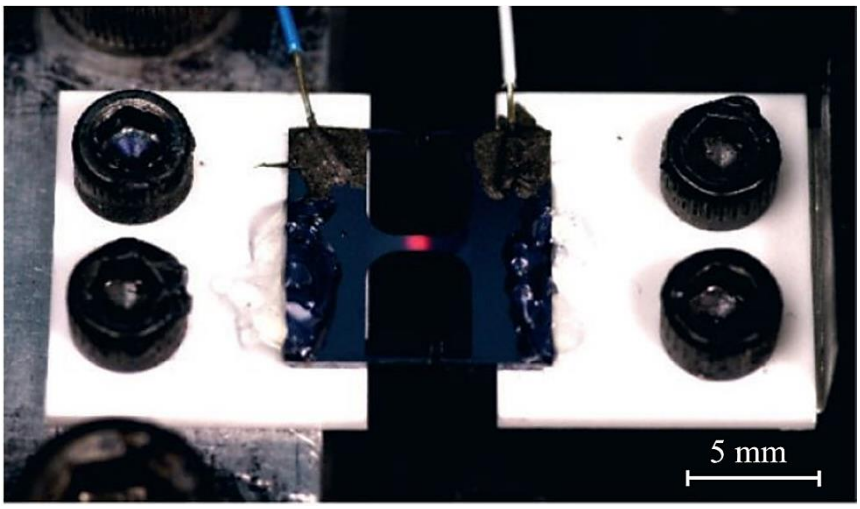

Figure 38 – Glowing polysilicon microsample ready to be tested at 670 °C, resistively heated (K.J. Hemker and W.N. Sharpe 2007).

Although microsample testing has been carried out for several material studies as referred, studies using this novel technique on parts produced through additive manufacturing are still very limited.

According to ASTM, additive manufacturing is "The process of joining materials to make objects from 3D model data, usually layer upon layer, as opposed to subtractive manufacturing methodologies" (Flaviana Calignano 2017). For that purpose, several AM technologies are available such as direct metal laser sintering (DMLS), selective laser melting (SLM) and selective laser sintering (SLS), among others.

The AM process parameters such as scan power, velocity and hatching distance are highly influential on the microstructure, porosity and quality of the part, as it involves local complex thermal evolutions on the layer being scanned and on the adjacent previous layers, which influence the mechanical properties of the as-built part.

Therefore, characterization and understanding of the mechanical behavior of materials produced using this manufacturing process is of extreme importance. The relevant information that can be obtained through microscale tensile testing and the correspondent fracture analyses of microsamples makes this a unique technique that can be used for this purpose.

In this work, microsample testing was carried out to determine the mechanical properties in the three different building directions x and y (parallel to the powder deposition plane) and z (parallel to the build direction) of an AlSi10Mg aluminum alloy part produced using additive manufacturing.

4.2 Microsample extraction and preparation

There are significant challenges related to the preparation, handling, testing and strain measurement of microsamples due to the small size and fragility. To produce accurate and repeatable microsample specimens, specialized machining methods such as Electrical discharge machining (EDM) are used as an alternative to normal mechanical machining. Traditional machining methods are not well suited for microsample since they can produce a damaged layer that is comparable to the volume of material to be tested (K.J. Hemker and W.N. Sharpe 2007).

EDM is a machining method that involves a thermal process and that overcomes the challenges associated with microsamples extraction. It consists in removing metal by applying a series of carefully controlled and rapidly recurring electric discharges between an electrode and the workpiece in the presence of a direct fluid, vaporizing a small volume of metal in front of the electrode (Cheng 2008, D. A. LaVan and W. N. Sharpe 1999). The workpiece is machined to a high degree of precision achieved through the control of its position by a computer numerical control (CNC) system, also allowing for repeatability in production (Cheng 2008). Figure 39 to Figure 41 show examples of the use of EDM.

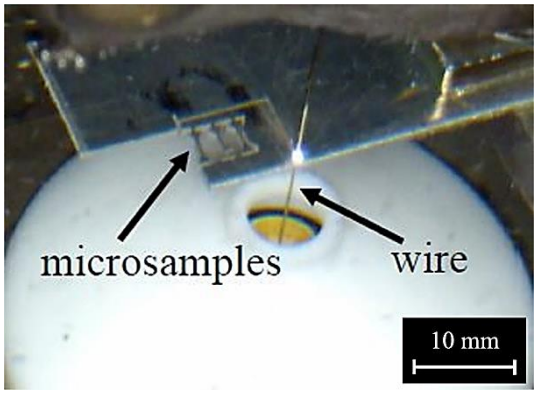

Figure 39 – Example of microsamples being cut using EDM (Nimer 2016).

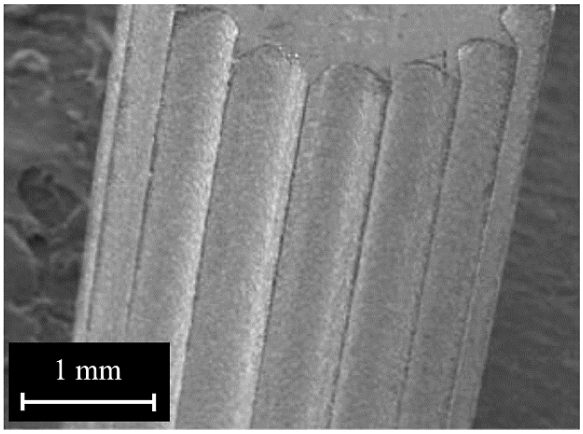

Figure 40 – Spur microgear (3.58 mm diameter, 17 teeth, 6 mm height, 660 µm pitch, 70 µm fillet radius) of copper, produced using conventional wire EDM (Mohammad 2008).

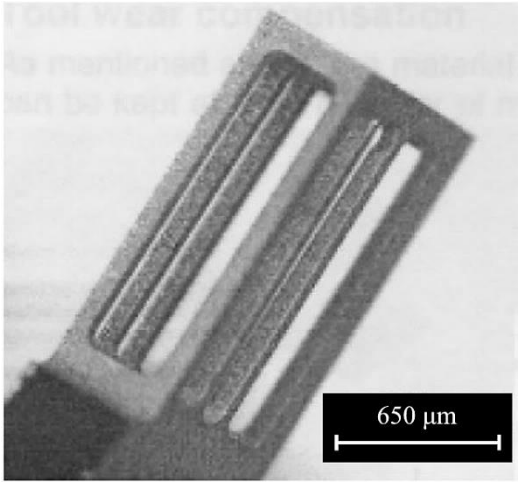

Figure 41 – Silicon microstructure produced using EDM (Masuzawa 2000).

The microsample geometry and dimensions used in this work are shown in Figure 42. It has a nominal over all foot print of 3 mm long and 1 mm wide, with a gage length of 1.78 mm long and 0.25 mm wide.

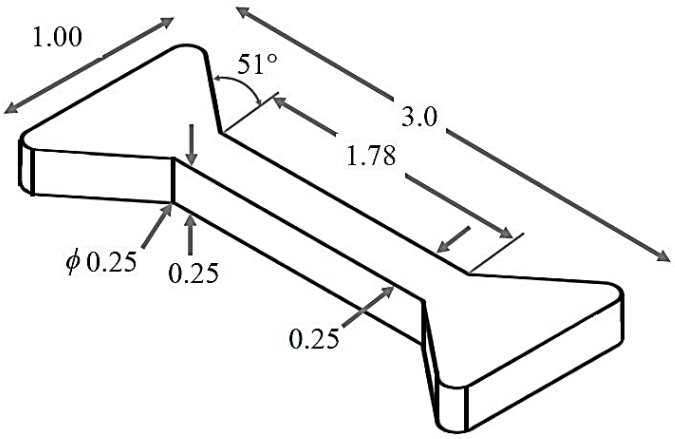

Figure 42 – Microsample geometry and dimensions (all units in mm) (Nimer 2016).

The bow-tie-shaped microsample geometry used is directly related to its functionality. It fits into tapered grips on the tensile testing system, is self-aligning and requires no clamping or gluing of the sample in order to be tested (D. A. LaVan and W. N. Sharpe 1999).

As seen in Figure 43, the microsamples are extracted by first slicing the bulk material obtained through additive manufacturing into ≈1 mm thick sections along the build direction (z direction) and along the powder deposition plane (xy plane). One slice of material was cut along the build direction and two slices were cut parallel to the powder deposition plane. The full extraction process in this work was accomplished using a Fanuc Alpha OiE wire electric discharge machine at Johns Hopkins University.

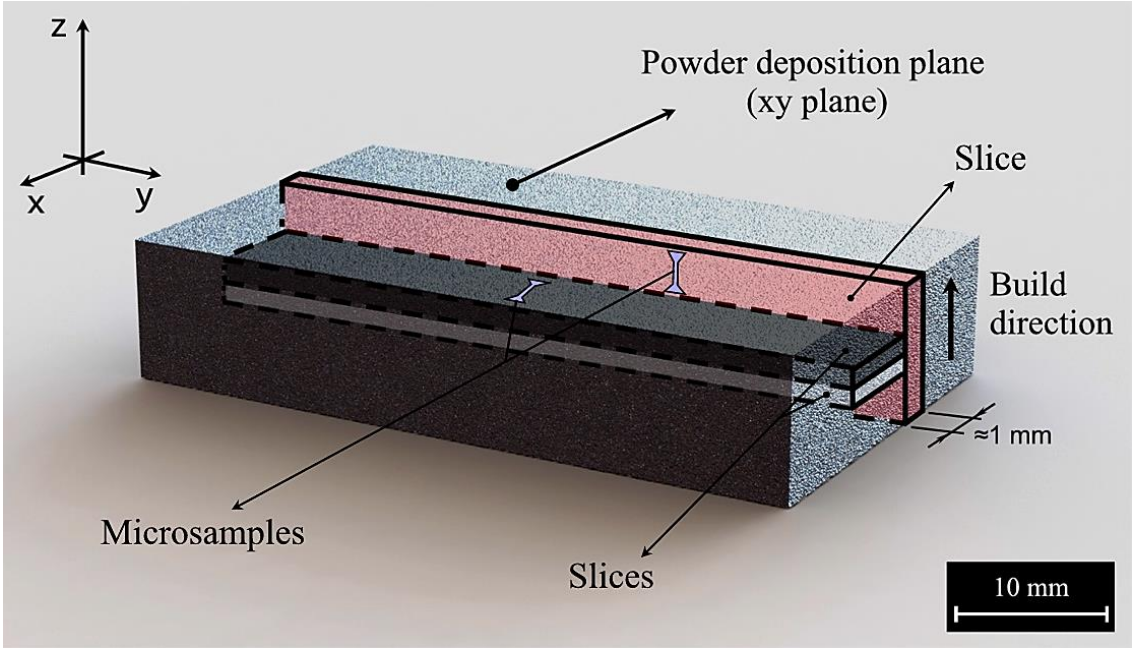

Figure 43 – Representation of the location of the ≈1 mm thick slices removed from the part obtained through additive manufacturing, on each of the building directions.

By introducing the CAD file of the microsample design into the EDM machine, they were afterwards sequentially machined on the slices using a finishing pass setting resulting in a slow and controlled cutting process with minimal damage to the material (Nimer 2016). The microsamples initial thickness corresponded to the thickness of the slices they were machined from. A simplified representation of the location and direction of the specimens removed from the slices referred previously is presented in Figure 44.

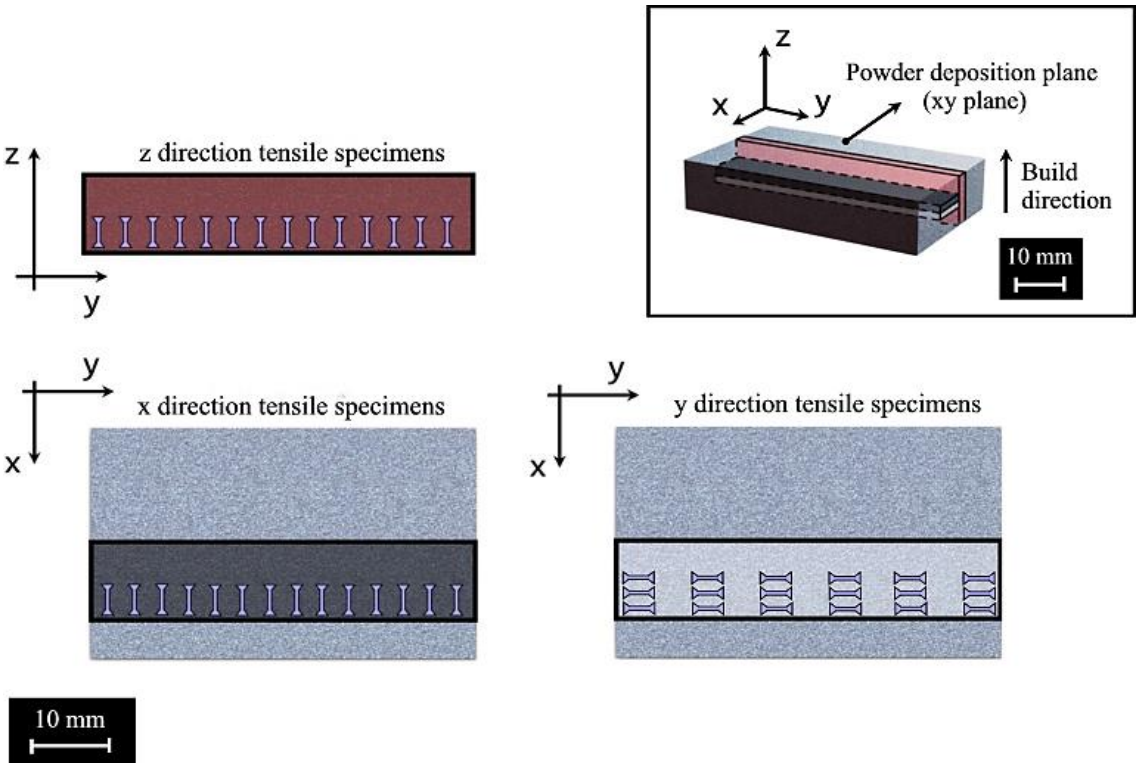

Figure 44 – Simplified representation of the location and direction of the specimens removed from the slices.

Although the sample is not subjected to mechanical stress during this process, some molten metal redeposits on the cut surface forming a recast layer (D. A. LaVan and W. N. Sharpe 1999). However, as indicated by LaVan and Sharpe (D. A. LaVan and W. N. Sharpe 1999) and showed by Nimer (Nimer 2016), the EDM settings used allows for the recast layer to be reduced to less than a micrometer or not visible through the cross-section examination of the sample, respectively. It has been proven through testing that any EDM machining artifacts does not affect the measured microsample mechanical results. Figure 45 shows the result from machining the microsamples using EDM.

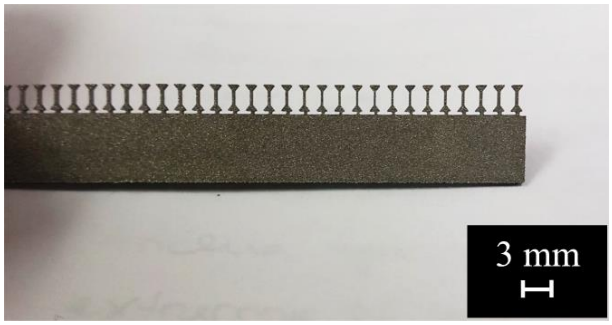

Figure 45 – Image of the result of microsamples machined using EDM, oriented along the x direction.

To keep track of the microsamples, they were duly identified with a number as shown in Figure 46 simplified. The numeration of each microsample correspondent to the x and z directions increases from the left of the slice to its right. The same happens to the y direction microsamples, however the numeration will also increase from upper to lower samples.

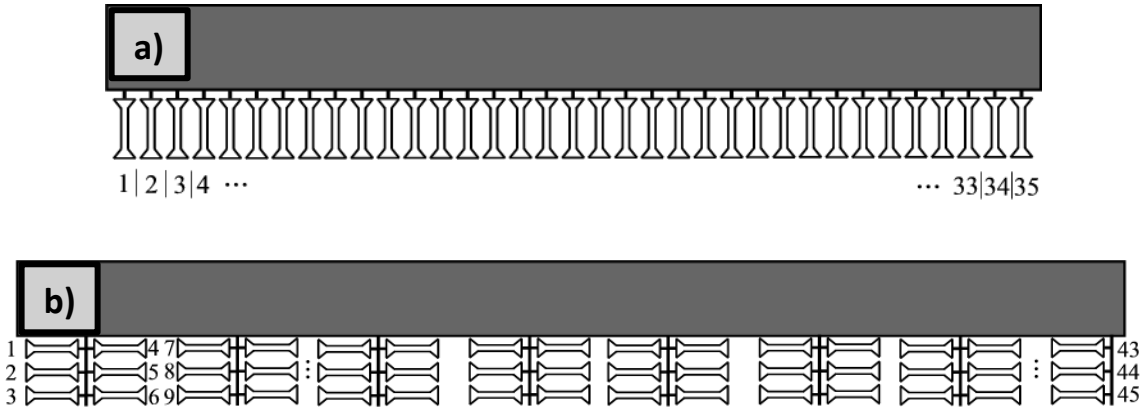

Figure 46 – (a) Simplified representation of the microsamples correspondent to the x and z directions and their identification (b) Simplified representation of the microsamples correspondent to the y direction and their identification.

Each microsample was removed from the respective slice using a diamond saw. Following the identification above, the 10 middle samples from each direction were utilized in this study.

After extraction, the microsamples require preparation prior to testing. Microsamples were mechanically polished using typical metallographic methods to a mirror finish using 320, 600, 800 and 1200 grit SiC paper (Nimer 2016), followed by a final polish using 1 μm deagglomerated alumina suspension. Due to the small size and challenges associated with handling the samples, a special procedure is used to assist on the polishing process for each of their sides. The microsamples and 4 polishing guides pins are mounted on a circular glass disc using Crystalbond™ and the heat from a hot plate, as it can be observed in Figure 47.

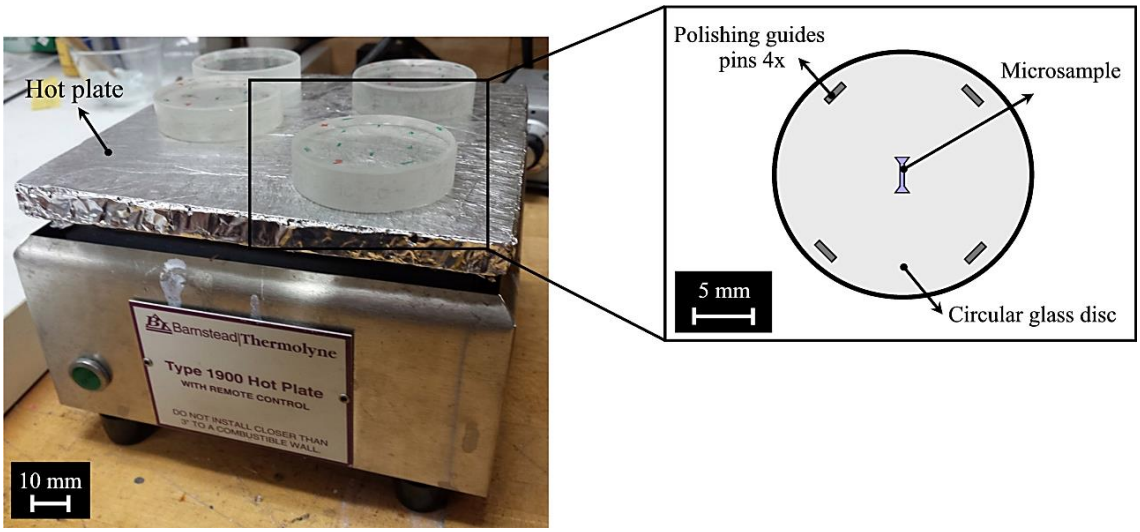

Figure 47 – Picture of glass discs being heated on a hot plate, to posteriorly mount the microsamples and polishing guides pins using Crystalbond™, as schematically represented on the image on the right.

The glass disc makes it easier to hold the samples throughout the polishing process and the polishing guides enables to control their thickness during this same process, with the use of a caliper. Since the polishing guides are mounted on the outermost part of the glass disc and the samples on the inside part of it, the polishing guides thickness dictates the samples thickness. To make sure the samples have a planar polished surface the polishing guides thickness should all be the same. Moreover, several samples can be polished at the same time. Figure 48 shows a microsample after it has been polished to completion.

Figure 48 – Microsample surface polished to a mirror finish, observed through the Olympus BX51 microscope.

After the polishing process is completed for one side, the samples are removed from the glass disc and then cleaned, repeating afterwards the mounting and polishing processes for the opposite side. Posteriorly to complete the polishing process, a final thickness of ≈250 μm was targeted to achieve a gage section of an approximated square shaped cross-section. After polishing, the samples were cleaned in an ultrasonic cleaner.

In addition to the actual preparation of the microsamples, the samples gage section thickness and width were measured using the AmScope 3.7 software, through the observation on the Olympus BX51 microscope. This method allows the as fabricated microsample dimensions to be determined.

Due to the small size of microsamples, directly contacting the sample for strain measuring would result in parasitic measurements. Traditional strain measurement gages are often bigger or of the same scale as the sample and would act to reinforce the material giving rise to errors both in strain and stress. Because of the small size of the samples, any rigid body motion or machine compliance would be a comparatively large amount of the total displacement that would be measured if cross head displacement was used to measure strain.

Therefore, non-contact methods such as digital image correlation (DIC) are used. This method requires the application of a speckle pattern to the surface of the microsample that must meet certain requirements to ensure its good quality (Nimer 2016). The quality of the speckle pattern is ensured by painting a random pattern that provides a high contrast with the background and each speckle should be nominally the same size and small enough to measure the desired deformations on a microscale (Nimer 2016).

As observed in Figure 49, high heat white spray paint was applied to the sample, fully covering it, to create a high contrast background. Posteriorly, the speckle was painted using an airgun with a 45 psi air pressure and a black paint mixture of acetone and high heat black paint in a 6:5 ratio.

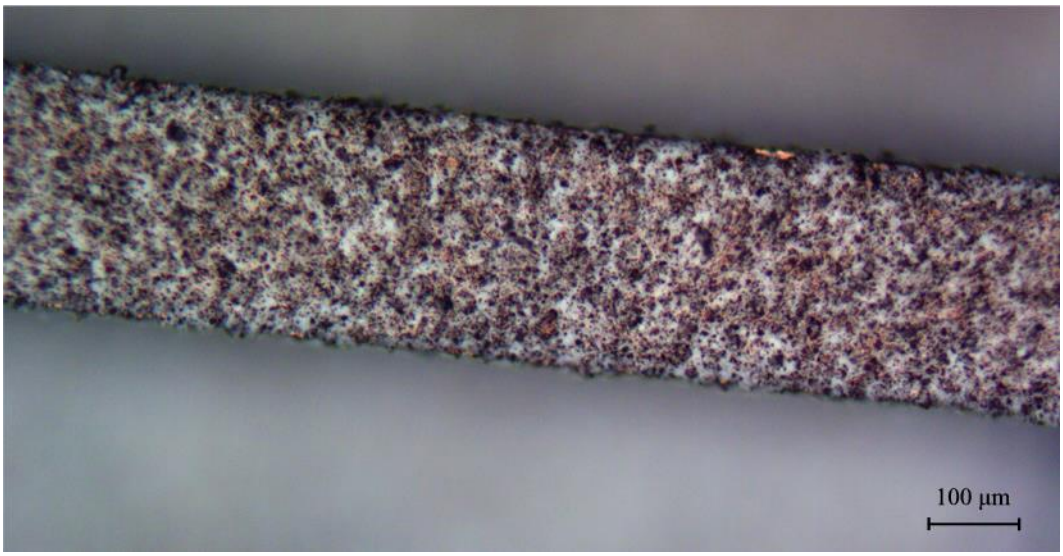

Figure 49 – Microsample gage section surface after the application of the speckle pattern, observed through the Olympus BX51 microscope.

When applying the paint speckles using an airgun, both air pressure and dilution are two of four major factors that influence the pattern and the values used were optimized to get the best speckle results. The two other factors such as airflow setting and spraying distance were adjusted to the best results over trial and error (Nimer 2016).

4.3 Microsample testing

Unlike the ASTM standard tensile tests, one cannot simply place a microsample in a commercial test machine and test it in a predefined way (K.J. Hemker and W.N. Sharpe 2007). Because of their microscale size, there are challenges associated to the application of small forces, stress and strain measurement and elevated temperature testing (K.J. Hemker and W.N. Sharpe 2007). In a microscale, frictional forces may be on the same order of magnitude as the loading forces and so must be considered to understand the true material response (Nimer 2016).

In terms of sample loading, an appropriated high-resolution method for applying displacements must be used such as picomotors, piezoelectric actuators and atomic force microscopes. Also, suitable sensors to measure force at small levels must be used (Nimer 2016). As referred

previously, a non-contact method to measure strain such as digital image correlation must be used.

A custom-built tensile testing machine has been developed to face and meet these requirements. In this work, an elevated temperature microsample testing system designed and developed by Nimer (Nimer 2016) in the Micromaterials Laboratory at UMBC, University of Maryland, Baltimore County was used. Figure 50 shows pictures of an overview and a more detailed view of this testing machine and its components.

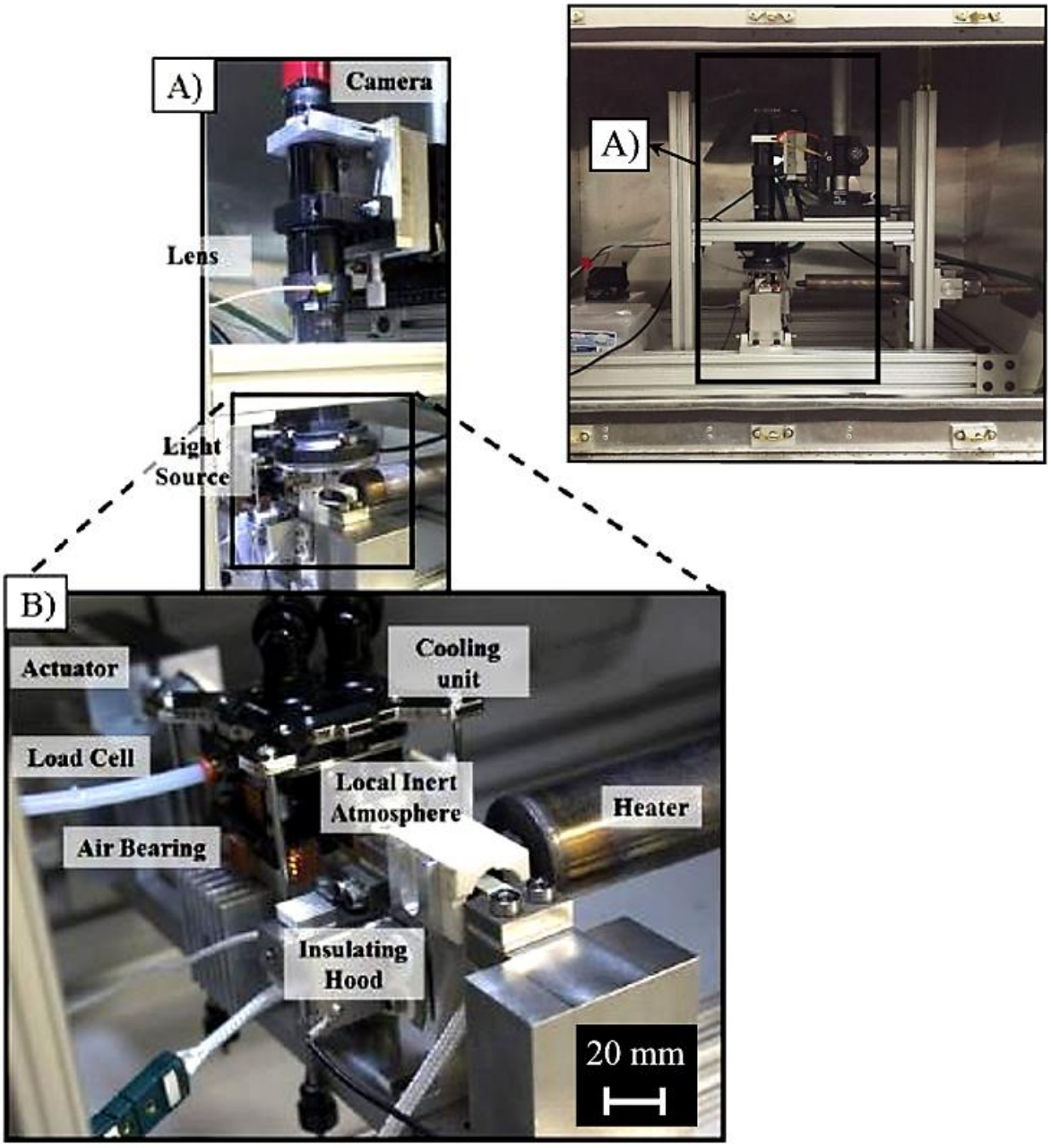

Figure 50 – Overview and detailed view of the microsample testing system designed and developed by Nimer (Nimer 2016) at UMBC. (a) camera, lens and light source used for DIC measurement and (b) heating system and load frame (Nimer 2016).

This machine comprises a load frame with a piezoelectric actuator controlled by software producing a quasi-static strain rate of 10^{-4} s^{-1} and a maximum strain rate of 1 s^{-1}. It also provides an axial load capacity of up to 120 N and a stroke of 25 mm total (Nimer 2016). A load cell is placed in line between the actuator and a linear air bearing, as seen in Figure 50, used to overcome any friction during the test and ensures uniaxial loading (Nimer 2016, D. A. LaVan and W. N. Sharpe 1999).

It has tapered grips capable to fit bow-tie-shaped microsamples (Figure 51). As it was referred previously, the geometry of the sample is directly related to its functionality. It results from a series of considerations on how to hold the sample to perform the tensile test. Although gripping or gluing is possible, it presents several challenges. Gripping small samples can easily destroy them and small misalignments create large bending strains. On the other hand, gluing prevents rapid successive tests due to the long cure and debonding times of appropriate adhesives. To overcome these concerns, a bow-tie-shaped specimen was adopted that fits into tapered grips, is self-aligning, i.e. upon initial loading the sample will move into place and eliminate any misalignment, and requires no clamping or gluing of the sample (D. A. LaVan and W. N. Sharpe 1999).

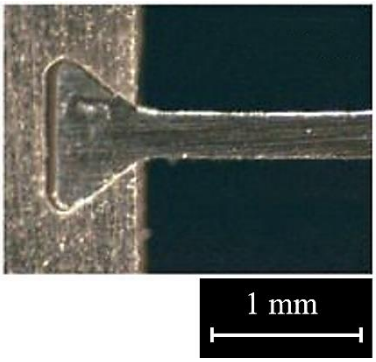

Figure 51 – Image of the detail of a bow-tie-shaped microsample held in self-aligning tapered grips (K.J. Hemker and W.N. Sharpe 2007).

The samples are illuminated using a white LED source and their images are taken with a lens and a camera mounted on top of where the testing is taking place (Figure 50), as the method employed to further perform DIC analysis. It is essential to check the accuracy of the alignment of the camera and its focus on the sample's surface since these are factors that can affect the

DIC results (Nimer 2016). Load, displacement and temperature values are recorded at the same rate as pictures are being taken, whereat each value is synced with each image. To measure strain, a DIC analysis is carried out to the samples previously coated with a speckle using the commercial software VIC-2D 6 by Correlated Solutions (Nimer 2016).

Even though the tensile tests were carried out at room temperature, this testing system is also equipped with a tubular gas heater (Figure 50) allowing for microsamples to be tested at high temperatures. It uses argon gas as the heating media to prevent oxidation of the microsamples, a pure titanium mesh on the heater nozzle that serves as a getter as the hot argon passes across it and a cooling unit used to ensure the electronics of the load frame remain at a safe temperature (Nimer 2016).

Tensile tests were carried out at a quasi-static strain rate of 10^{-3} s^{-1} until the fracture of the sample, while images of its surface were captured. Values of stress, load and displacement were obtained. Stress values were directly calculated by inserting the microsample cross-sectional area values into the data acquisition software.

4.4 Strain measurement – Digital image correlation

The knowledge of the strain values of a microsample associated to a tensile test is essential for material property determination such as Young's modulus, yield strength and strain to failure. Due to the small size of microsamples, directly contacting the sample for strain measuring is impossible (Nimer 2016). Therefore, non-contact methods must be used. Non-contact methods such as the interferometric strain/displacement gage (ISDG) and digital image correlation (DIC) are being used to measure strain (Nimer 2016, D. A. LaVan and W. N. Sharpe 1999).

ISDG is a method that uses two reflective markers on the sample surface to reflect the light from a laser, creating an interference pattern that is captured by two charge-coupled device (CCD) cameras. As the microsample suffers deformation, the indents move apart and the corresponding fringe movement can be analyzed to measure strain (Nimer 2011, Cheng 2008). Although this technique works well, it has a limited maximum strain range as the optical signal gets degraded by the deformation of the sample surface (Nimer 2016).

Digital image correlation (DIC) has gained popularity as a result of the improvement of imaging technology (Nimer 2016) and has been commonly used for the surface deformation measurement (Bing Pan 2009). It is the non-contact optical method used in this study to measure strain of the microsamples.

When compared to the interferometric optical techniques this method is of simple application. It involves a simple experimental setup and specimen preparation as it only requires one fixed CCD camera to record the digital images of the test sample surface during the test, as in Figure 52, and the microsample preparation can be made by simply spraying paint against its surface (Figure 49). Also, a white light source can be used to illuminate the sample during the test, instead of using a laser source, and a wide range of measurement sensitivity and resolution is possible (Bing Pan 2009).

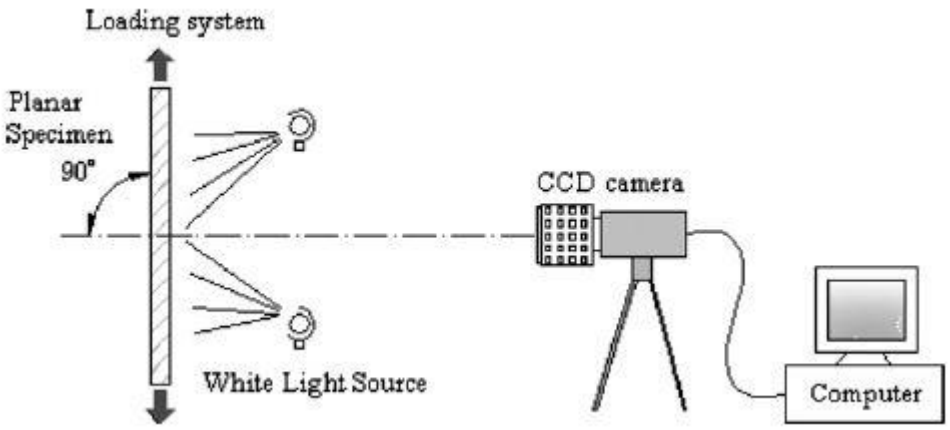

Figure 52 – Schematic of a typical system used for the digital image correlation method (Bing Pan 2009).

To perform DIC analysis, the application of a speckle pattern to the surface of the microsample by paint or gold deposition is needed and must meet certain requirements to ensure its good quality (Nimer 2016). The quality of the speckle pattern is the parameter that affects the accuracy of DIC strain measurement the most (Nimer 2016). It should be a random pattern that provides a high contrast with the background and each speckle should be nominally the same size and small enough to measure the desired deformations on a microscale (Nimer 2016).

Posteriorly to the speckle application to the microsample, digital images of the sample are recorded during its testing. It is necessary to check the accuracy of the alignment of the camera and its focus as well as the illumination variation on the sample's surface since these are other

factors that can affect the DIC analysis results (Nimer 2016). Full-field bi-axial displacements and strains are then obtained by comparing the images captured during the test to the un-deformed initial state image (reference image) (Bing Pan 2009), with the use of a dedicated software. In this study, the commercial software VIC-2D 6 by Correlated Solutions was used.

For image processing purposes on the DIC analysis using the VIC-2D 6 software, a region of interest in the images is selected, specifically at the microsamples gage section. This region comprises numerous smaller regions called subsets, each one of them containing a distribution of speckles that is exclusive to it. By this mean, the motion and deformation of each subset is tracked and the displacements of each subset measured. By differentiating the displacements, strain can be obtained (Nimer 2016). Each subset must be sufficiently large so that it contains enough speckles for it to be unique. However, a balance must be done when deciding the subset size, since a smaller subset can result in less error due to the increased spatial resolution (Nimer 2016).

To analyze all the samples strains with VIC-2D 6 software, the settings listed in Table 3 were used.

Table 3 – DIC analysis settings used, using VIC-2D 6 software.

Subset size	41
Step	4
Subset weights	Gaussian
Interpolation	Optimized 4-Tap
Low-Pass filters	Enabled
Incremental correlation	Enabled
Exhaustive search	Enabled
Prediction margin (pixel)	0.02
Confidence interval (pixel)	0.1
Matchability (pixel)	0.1
Strain filter size	15

Finally, the average strain values are measured for each image by placing a line “extensometer” across the microsamples gage section length, at the center of its width (Nimer 2016).

4.5 Summary

In this chapter, the application of a novel technique consisting in microsample tensile testing was described, including the samples extraction and preparation required to be able to use it.

Values of load and displacement were directly obtained through the microsample tensile tests and the engineering stress values were determined by inserting the measured microsample initial cross-sectional area values into the data acquisition software. Afterwards, a DIC analysis was applied to the captured images during the tensile tests of the microsample gage section surface to determine the strain values involved in these tests.

Microsample testing allowed to obtain the engineering stress and strain values (σ and ε respectively) for different build directions, parallel to the powder deposition plane and parallel to the build direction, of an additively manufactured part of AlSi10Mg. The obtained results from the microtensile tests and from the posterior fracture surface analyses using SEM are going to be presented and discussed in the following chapter.

5 Results and analysis

Additive manufacturing is a process that allows to directly produce parts from a 3D CAD model by consecutively adding layers of material until the final part is formed. The process parameters used in the part fabrication are highly influential on the final microstructure and therefore on both the local material and global part mechanical properties. These microstructures arise from the complex local thermal evolutions involved. However, notable characterization and understanding of their influence on the microstructure and mechanical behavior of the material, both local and global, produced through AM processes is still very limited.

In order to better understand the material mechanical and physical behavior of an AlSi10Mg aluminum alloy part produced using direct metal laser sintering (DMLS), the microsample testing technique was used and microsamples were tested along the three different building directions: x, y and z as shown in Figure 53.

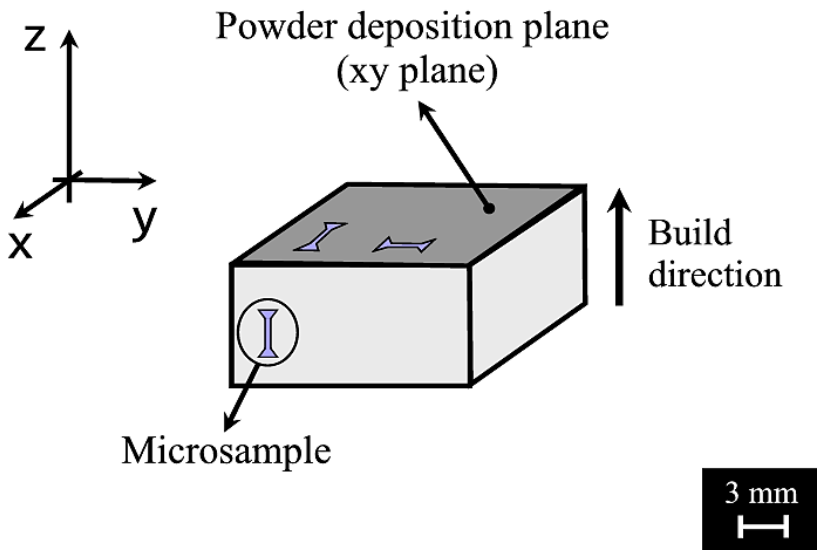

Figure 53 – Schematic representation of the orientation of the microsamples tested, from a part produced through AM.

In this chapter, results from the microsample tensile tests are presented and a discussion about their linkage to the additive manufacturing process and its process parameters is made. Postmortem, fractographic analyses using SEM to study and determine the correspondent failure mechanisms are described.

5.1 AlSi10Mg mechanical properties analysis

Microsample tensile tests were made for a total of 28 microsamples oriented along three different directions: x and y (parallel to the powder deposition plane) and z (parallel to the build direction) as shown in Figure 53. The identification of the microsamples tested in this work and correspondent location on the additive manufactured part, for each orientation, is presented in Figure 54.

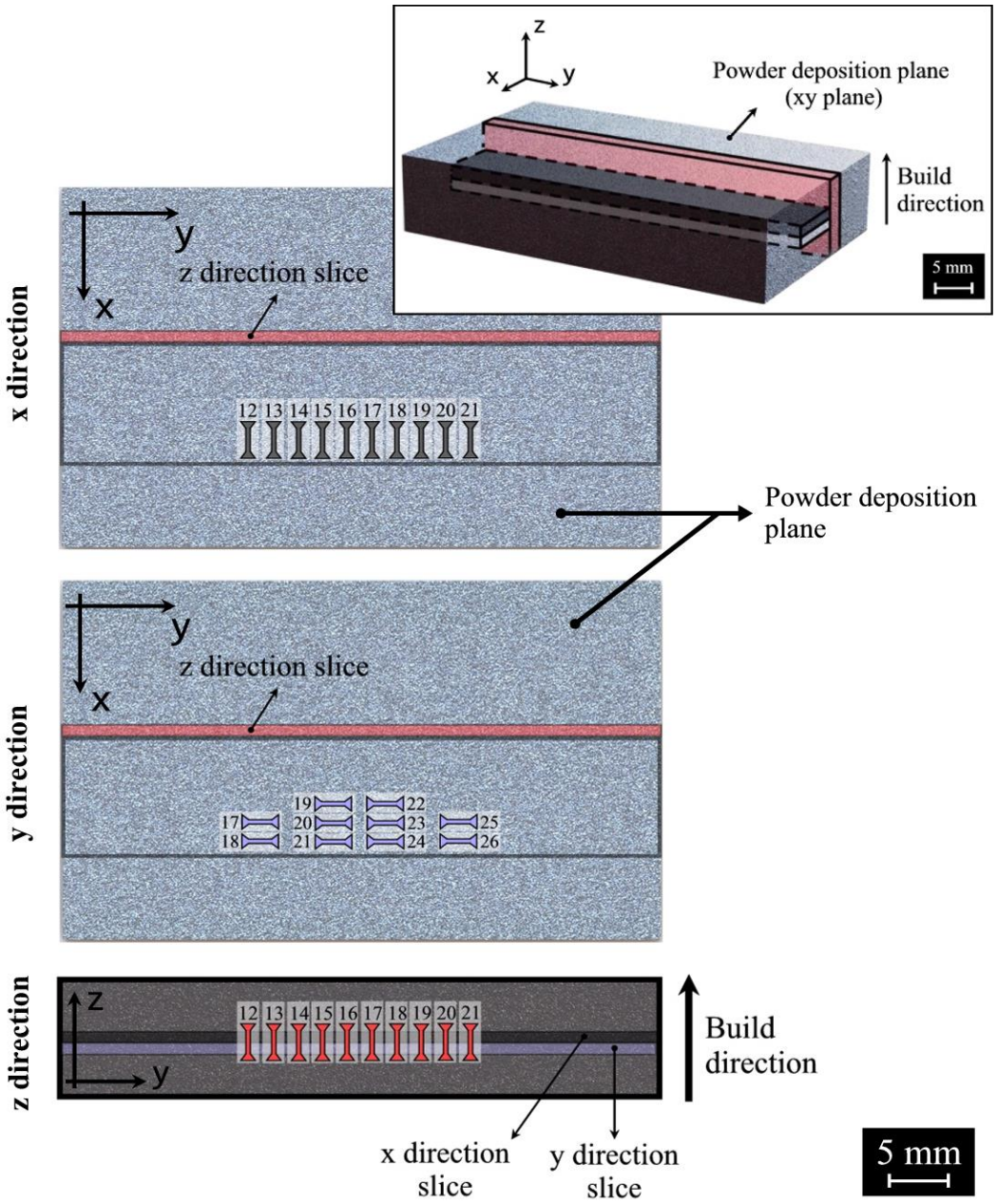

Figure 54 – Schematic indicating the identification used for the microsamples tested in this work and correspondent location on the additive manufactured part, for each orientation.

Moreover, Figure 55 shows how the location of the microsamples oriented along the x direction is related to the location of the microsamples oriented along the y direction, with a superposition of these two sets.

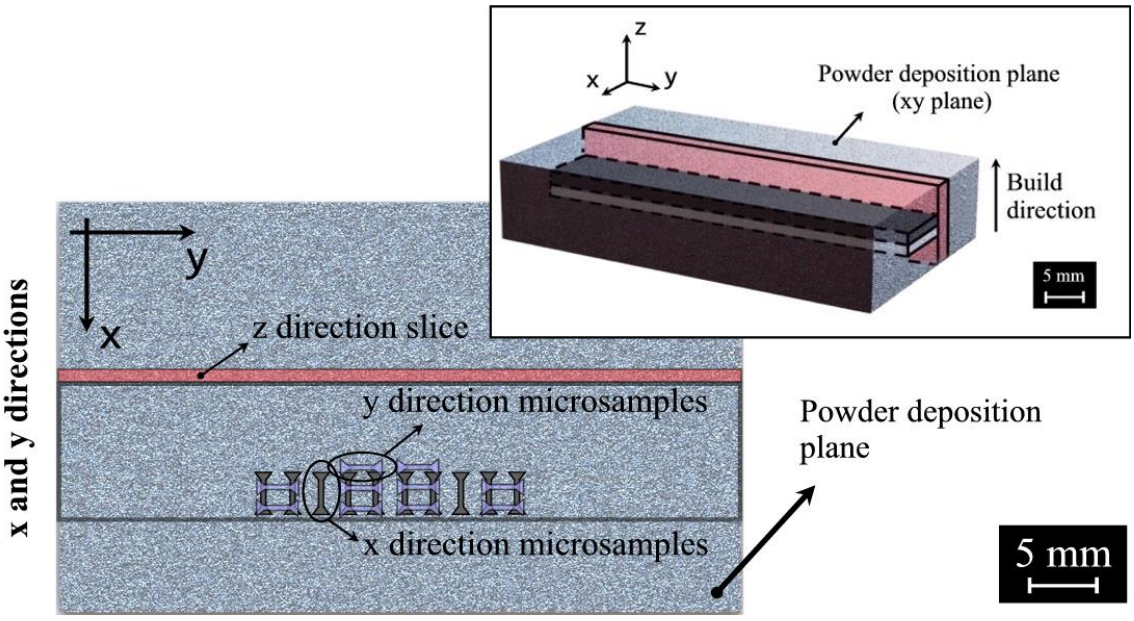

Figure 55 – Schematic showing the relation between locations of the microsamples oriented along the x direction to the ones oriented along the y direction.

Values of load and displacement were directly obtained through the microsample tensile tests and engineering stress values were determined. Post test, DIC analysis was applied to images captured during the testing of the microsamples gage to determine the corresponding engineering strain for a given stress. The collected data was then organized and used to generate the engineering stress-strain responses for each microsample.

It was observed that the microsamples were subjected to plastic strain, for which it is more meaningful to represent the true stress-strain curves (William D. Callister 2001, Fonseca 2014) to further characterize the strain behavior of the material (R. E. Smallman 1999). Therefore, true stress and strain values were determined using the following relationships, valid to the onset of necking (William D. Callister 2001).

$$\sigma_T = \sigma(1+\varepsilon)$$

$$\varepsilon_T = \ln(1+\varepsilon)$$

These equations relate the true stress and true strain, σ_T and ε_T respectively, to the engineering stress and strain values, σ and ε.

The true stress and strain responses of all the microsamples tested oriented along each direction are presented in Figure 56 to Figure 58.

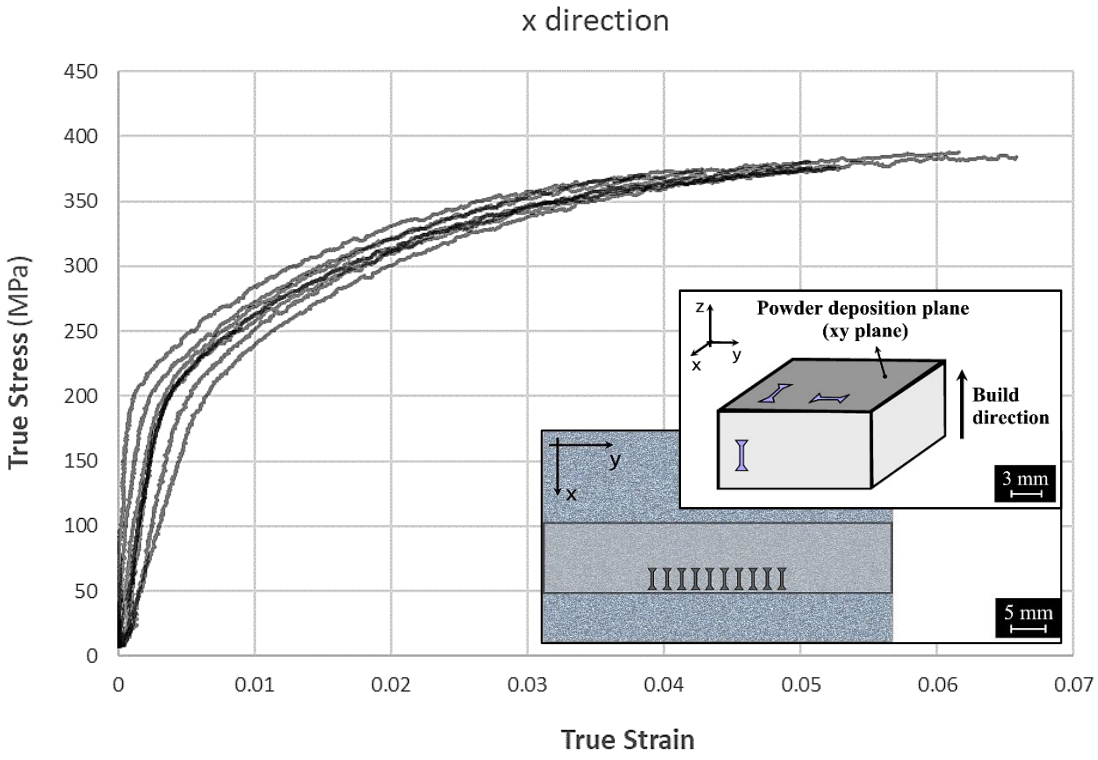

Figure 56 – Stress-strain responses of the microsamples oriented along the x direction, on the powder deposition plane.

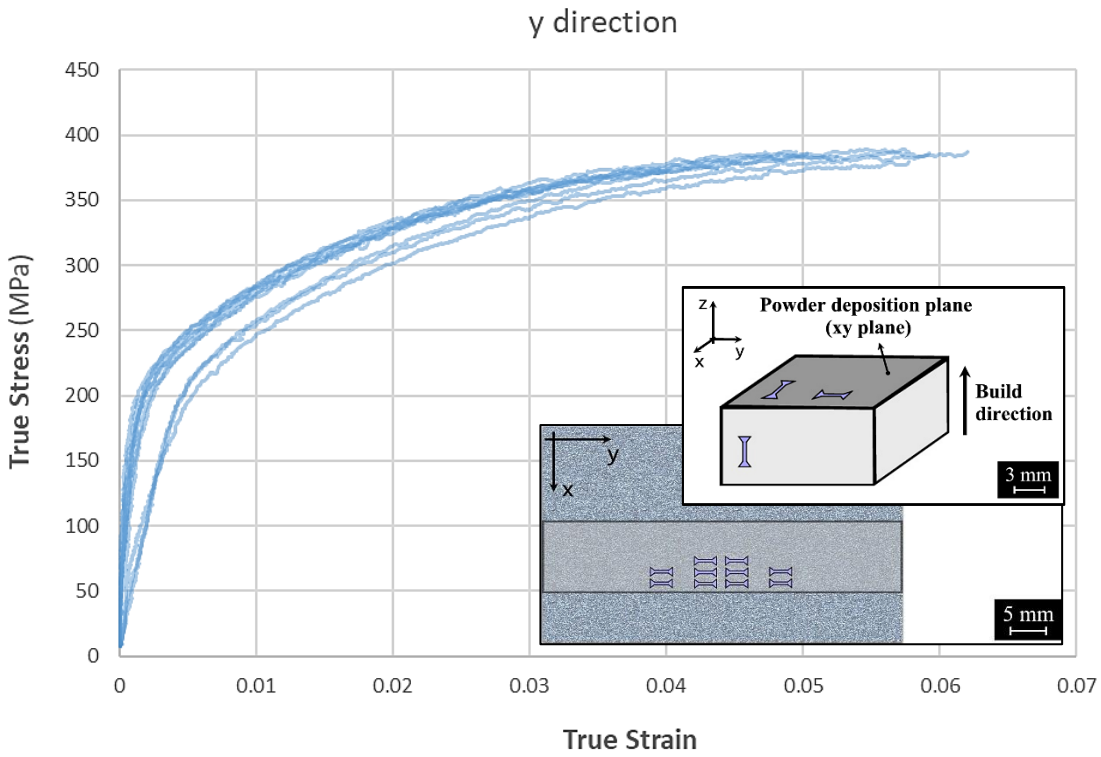

Figure 57 – Stress-strain responses of the microsamples oriented along the y direction, on the powder deposition plane.

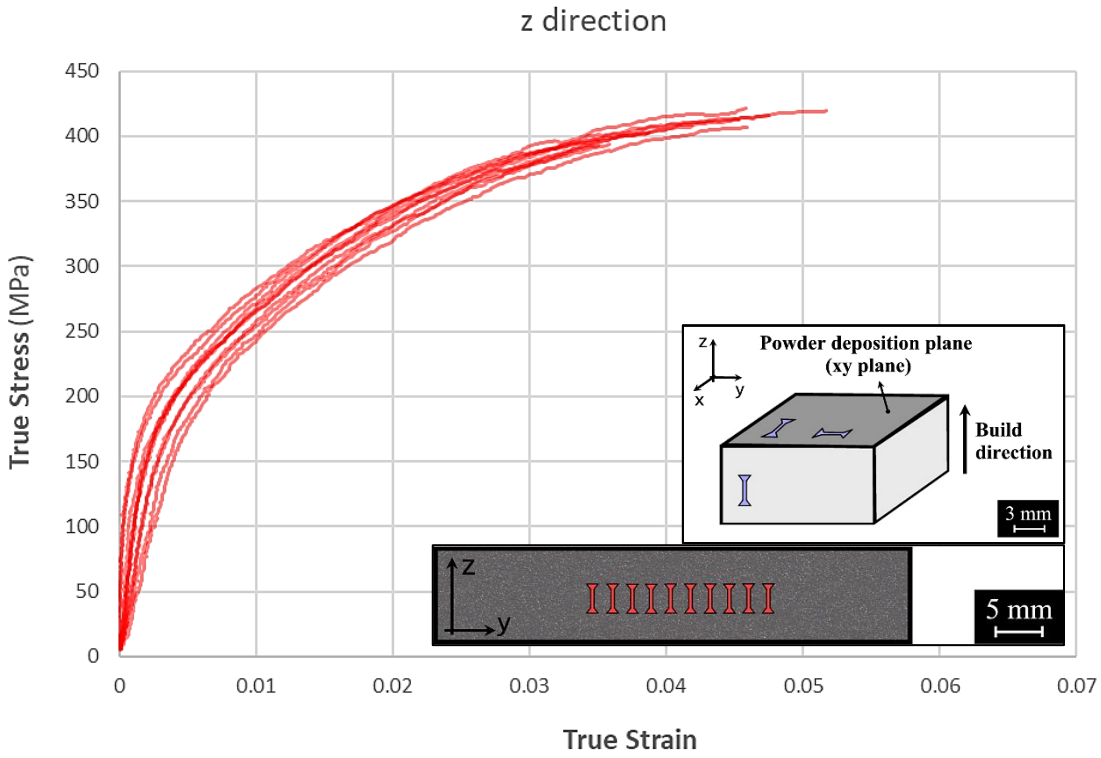

Figure 58 – Stress-strain responses of the microsamples oriented along the z direction, on the build direction.

For each microsample tested, the Young's modulus values, E, were determined through the analysis of the linear elastic region slope on each of the stress-strain responses. Yield strength values at a 0.2% offset yield method were also determined through the direct analysis of the stress-strain responses. A parallel line to the elastic region distanced by 0.002 of strain was drawn and the stress value of the intersection of that line to the response curve was recorded, corresponding to the yield strength value at a 0.2% offset. On the other hand, ultimate tensile strength (UTS) values were determined by analyzing the maximum stress values for each microsample over the entire data obtained from the tensile tests.

Figure 59 to Figure 61 shows the determined Young's modulus, yield strength and UTS values for the tested microsamples oriented along the x, y and z directions as a function of the sample identification number, i.e. its location on the part. On the yield strength and UTS plots, the difference between the maximum and minimum values of the respective mechanical property is also presented, as a percentage of the maximum mechanical property value.

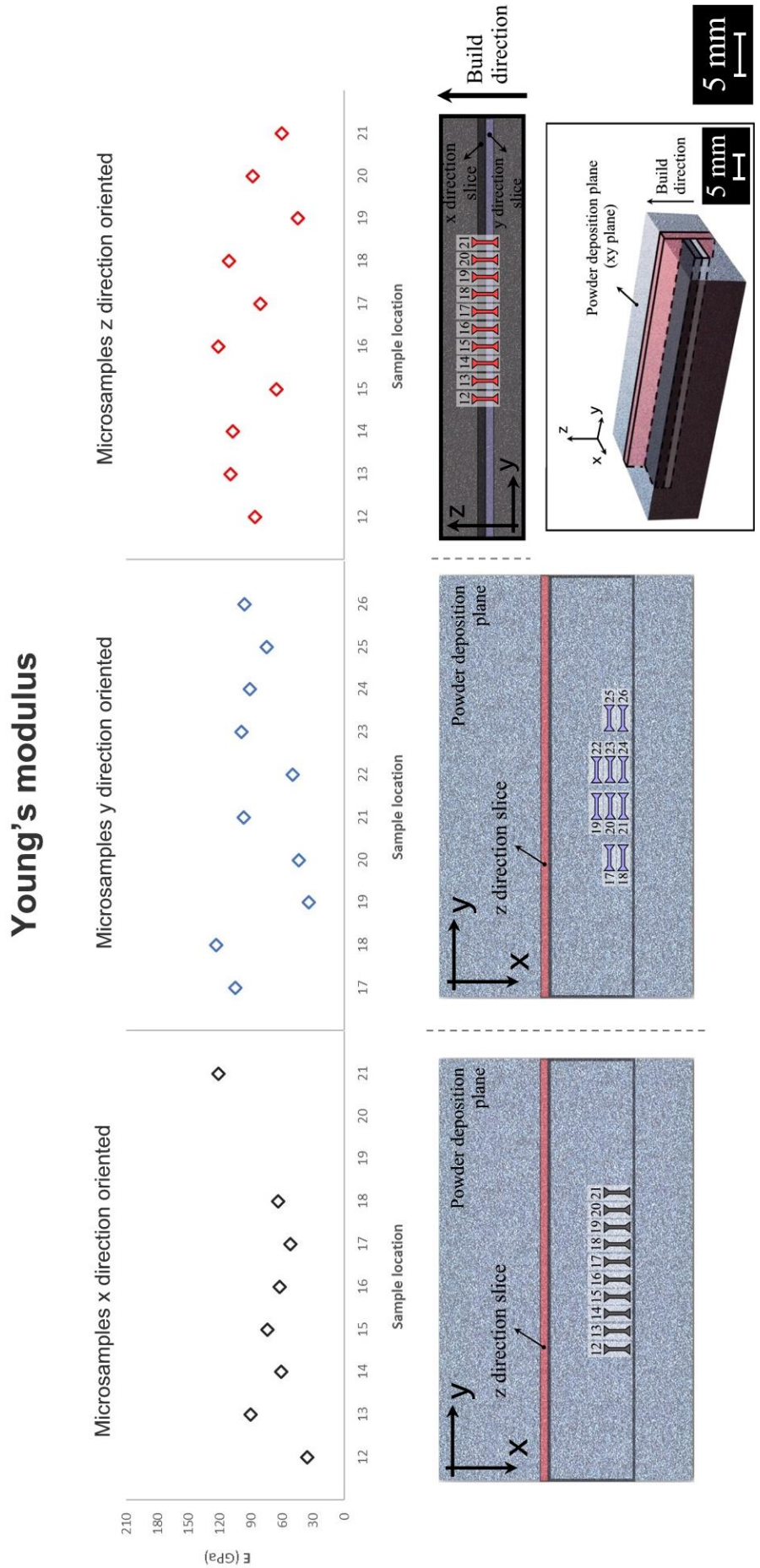

Figure 59 – Young's modulus values of the microsamples tested oriented along the x, y and z directions, as a function of the sample location on the additive manufactured part.

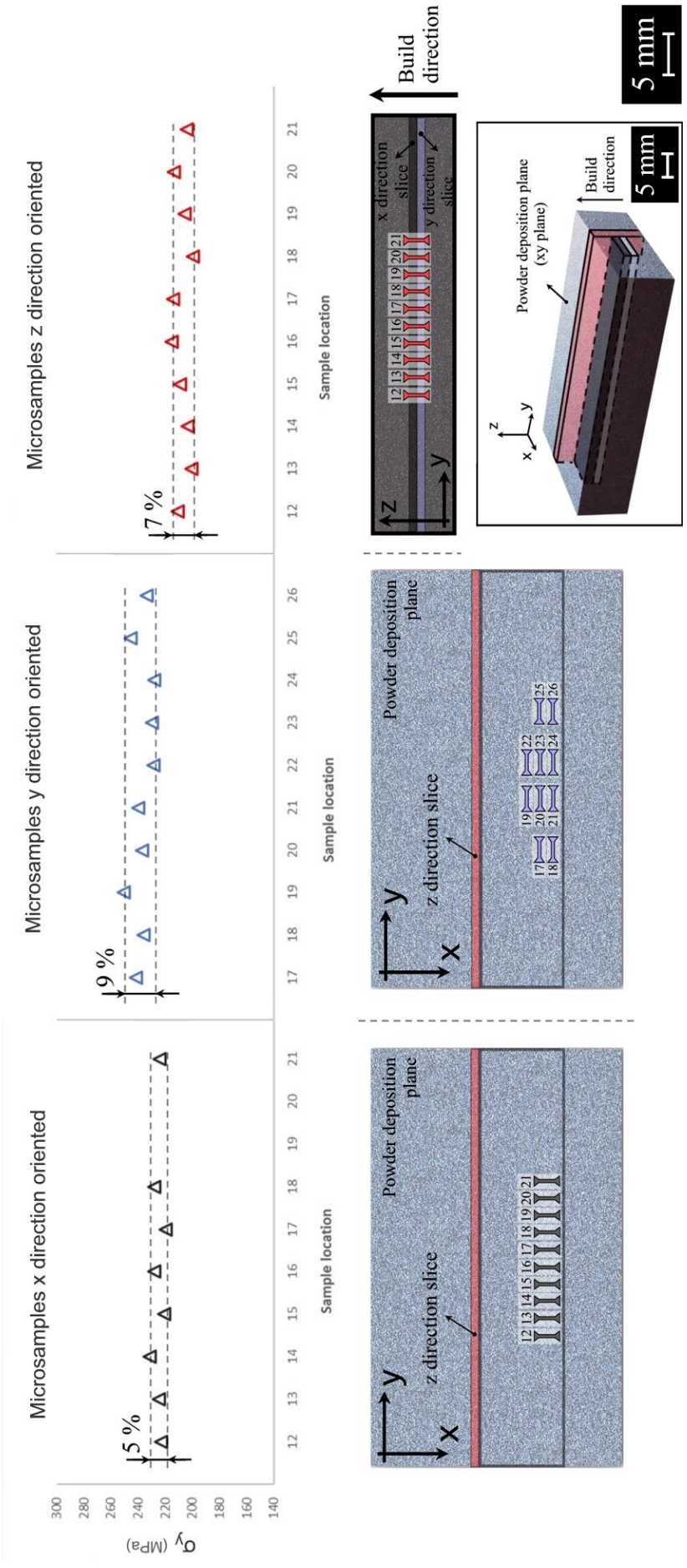

Figure 60 – Yield strength values of the microsamples tested oriented along the x, y and z directions, as a function of the sample location on the additive manufactured part.

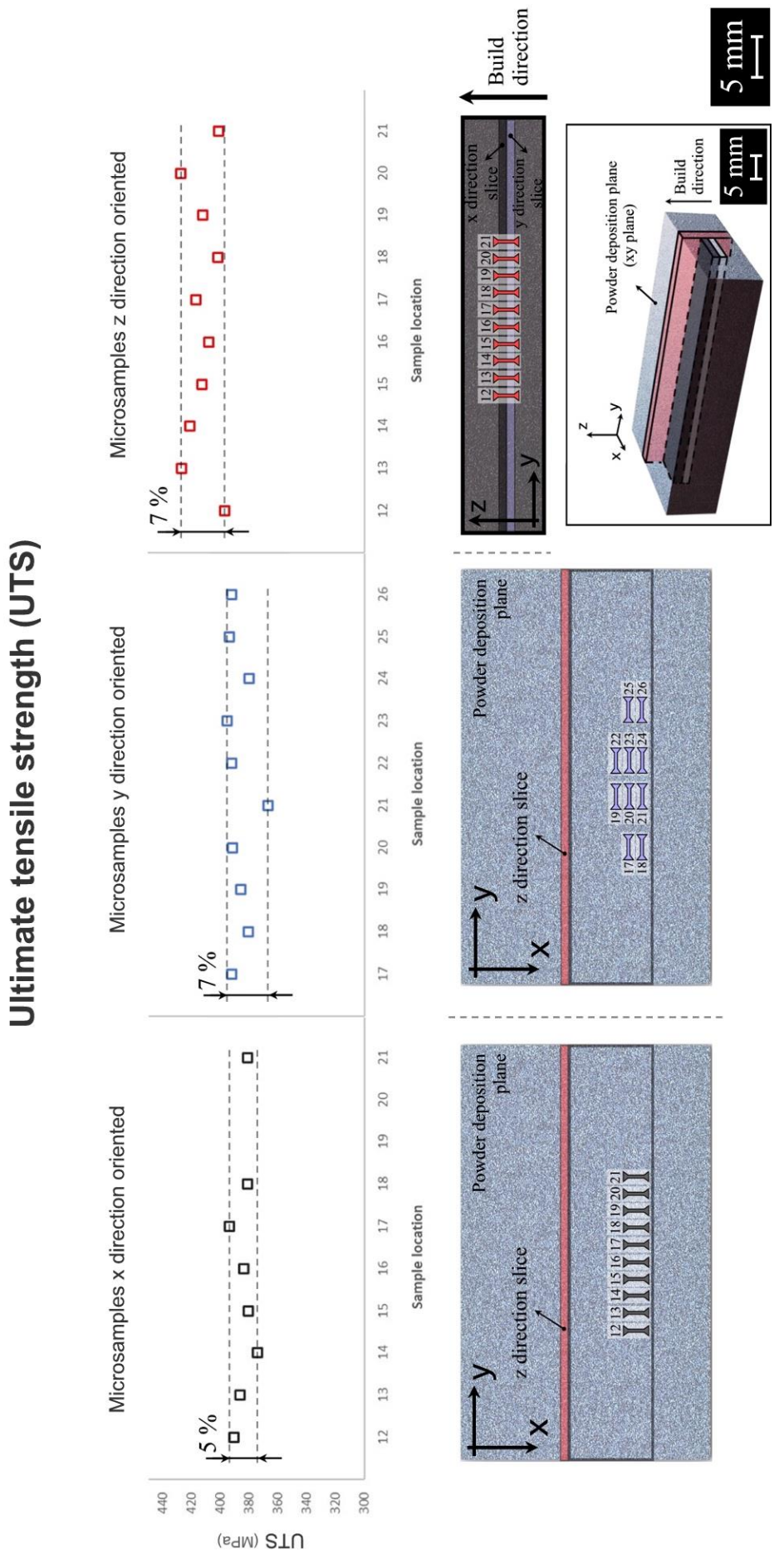

Figure 61 – Ultimate tensile strength (UTS) values of the microsamples tested oriented along the x, y and z directions, as a function of the sample location on the additive manufactured part.

Moreover, mean and standard deviation of the Young's modulus, yield strength and UTS values for each orientation were determined and are presented in Table 4.

Table 4 – Values of mean and standard deviation of Young's modulus, yield strength and UTS, for each orientation.

		Orientation		
		x	y	z
Young's modulus	**Mean** (MPa)	70.42	81.24	87.52
	Standard deviation (MPa)	26.00	29.45	25.25
Yield Strength	**Mean** (MPa)	225.07	237.46	207.67
	Standard deviation (MPa)	3.97	7.47	5.78
UTS	**Mean** (MPa)	384.03	387.34	412.34
	Standard deviation (MPa)	6.24	8.85	10.69

Table 5 shows a comparison between the mechanical properties mean values obtained from the microsample tensile tests to the ones presented in literature obtained using larger sized samples (Diego Manfredi 2013). Also, a comparison to the mechanical properties means of the correspondent typical casting alloy A360.0 is shown (Diego Manfredi 2013).

Table 5 – Mechanical properties means of a DMLS AlSi10Mg obtained through: microsample tensile tests; large standard samples tensile tests, presented in literature (Diego Manfredi 2013). Also, mechanical properties mean values of the correspondent as-fabricated A360.0 F casting alloy.

Material	**Orientation**	**Young's modulus** (GPa) Means	**Yield strength** (MPa) Means	**UTS** (MPa) Means
DMLS AlSi10Mg (microsamples)	x	70.42	225.07	384.03
	y	81.24	237.46	387.34
	z	87.52	207.67	412.34
DMLS AlSi10Mg (large size samples)	xy plane	73	244.22	343.20
	z	72	231.69	340.52
A360.0 F (as-fabricated)	-	71	170	317

As seen in Table 5, the mechanical properties values obtained do not match the ones presented in literature, obtained using large size samples. Inclusively, measurable differences were obtained for the x and y directions, while in literature the material is considered to have isotropic properties along the xy plane (powder deposition plane, Figure 53). The inherent small size of microsamples allowed therefore to obtain information that could not otherwise be obtained through the use of standard size samples, as expected.

The Young's modulus values show a relatively high variation throughout the part (Figure 59), for each orientation, featuring high standard deviation values. Young's modulus values vary from 36 GPa to 122 GPa for the x direction oriented microsamples, from 34 GPa to 123 GPa on the y direction and from 45 GPa to 122 GPa on the z direction. However, values of this mechanical property and correspondent variations along the part shows similarities when comparing the three different orientations analyzed, as seen in Figure 62.

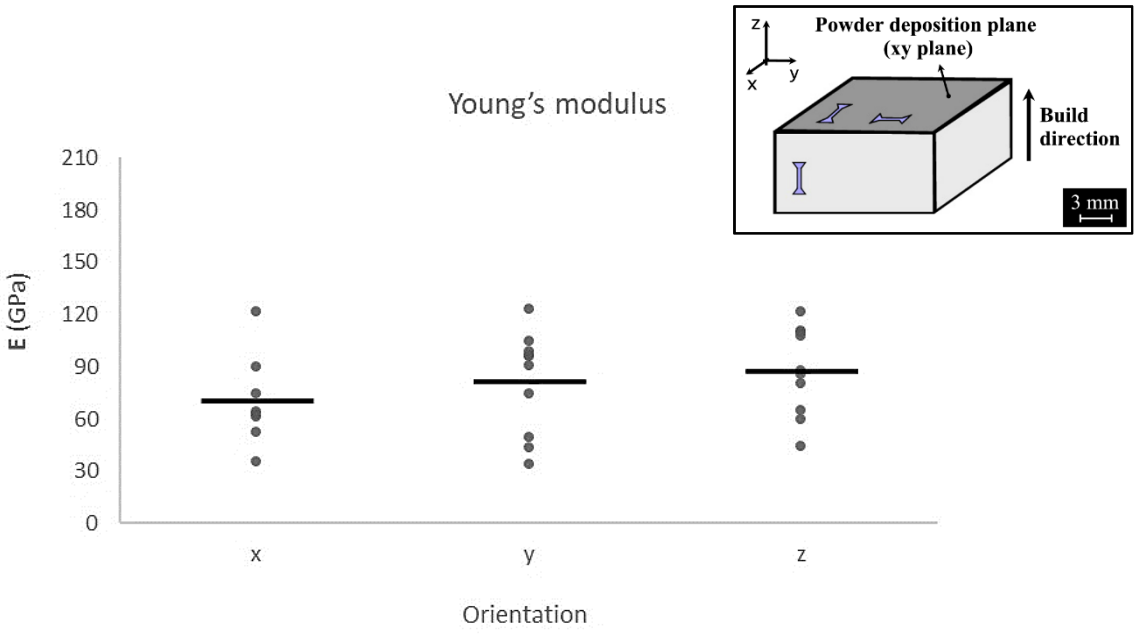

Figure 62 – Young's modulus values and respective means for each orientation on the part produced through additive manufacturing.

Resulting from the material fabrication, a polycrystalline material microstructure is constituted by several grains, each one with a specific associated crystallographic orientation (Silva 2012), as demonstrated in Figure 63. The variation of Young's modulus values along the part, for a given orientation, suggests that the microsample elastic deformation is locally controlled by grains with a given FCC crystal structure orientation which prevail over grains with crystal structures oriented differently.

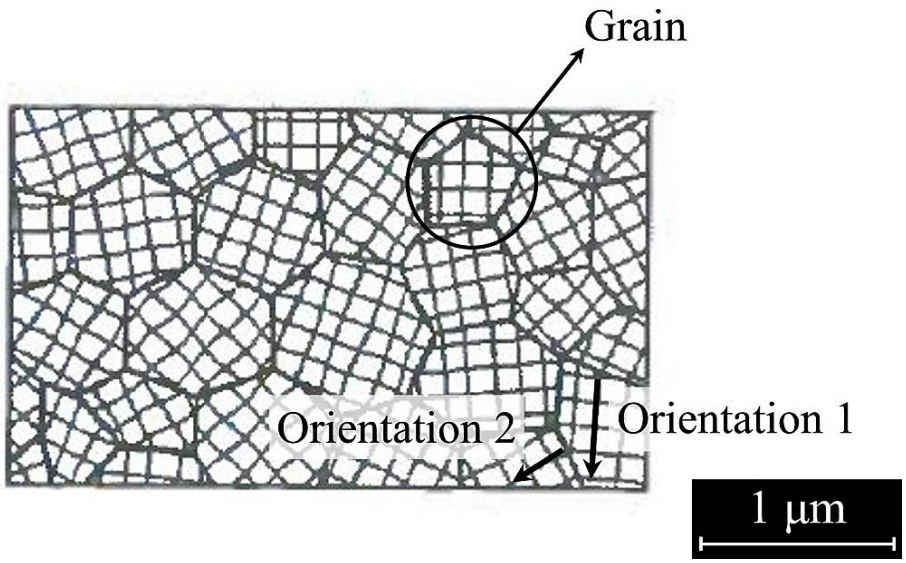

Figure 63 – Schematic of a polycrystalline material microstructure, showing different crystallographic orientations for different grains (Silva 2012).

As for the Young's modulus, yield strength values also show measurable variations along the part, for a given orientation (Figure 60), as observable from the percentage values represented in the plots and standard deviations. When comparing the yield strength values of each of the studied orientations, as shown in Figure 64, differences of this mechanical property values are also evident.

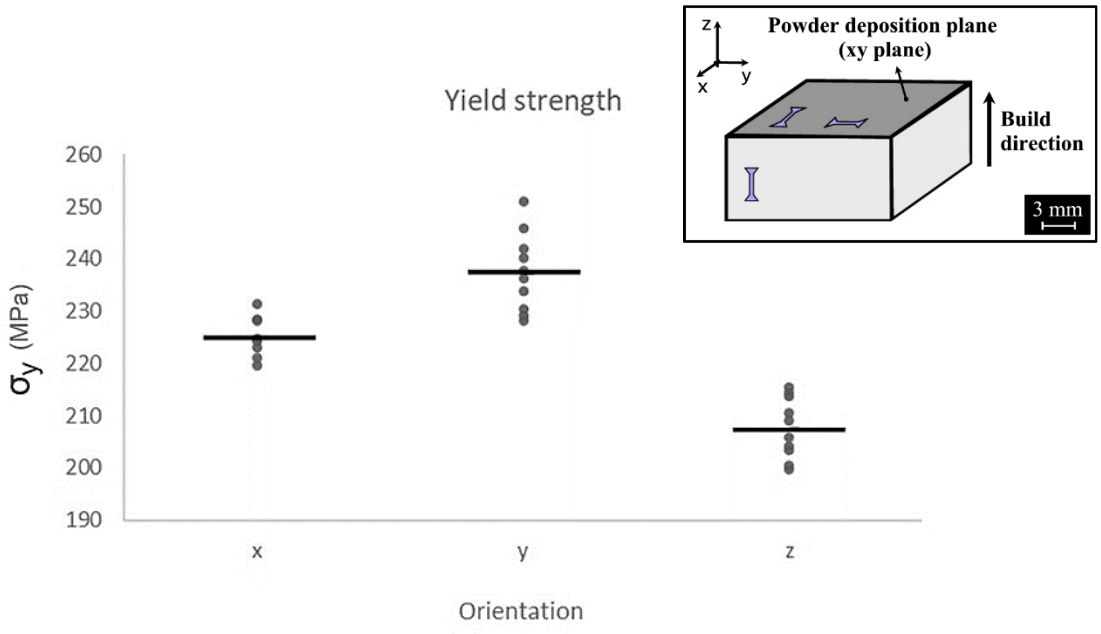

Figure 64 – Yield strength values and respective means for each orientation on the part produced through additive manufacturing.

Yield strength values show to be different for the x and y directions (parallel to the powder deposition plane), in contradiction to what is referred in literature. Higher values were obtained on the y direction, followed by the x and z directions, respectively.

In line with what is observable from the yield strength values, ultimate tensile strength (UTS) values within the same orientation also show measurable variations, as seen in Figure 61. These variations are highlighted with the indication of the correspondent percentage of variation, Figure 61, and standard deviations. Furthermore, differences of UTS values are noticeable when compared between different orientations, as shown in Figure 65.

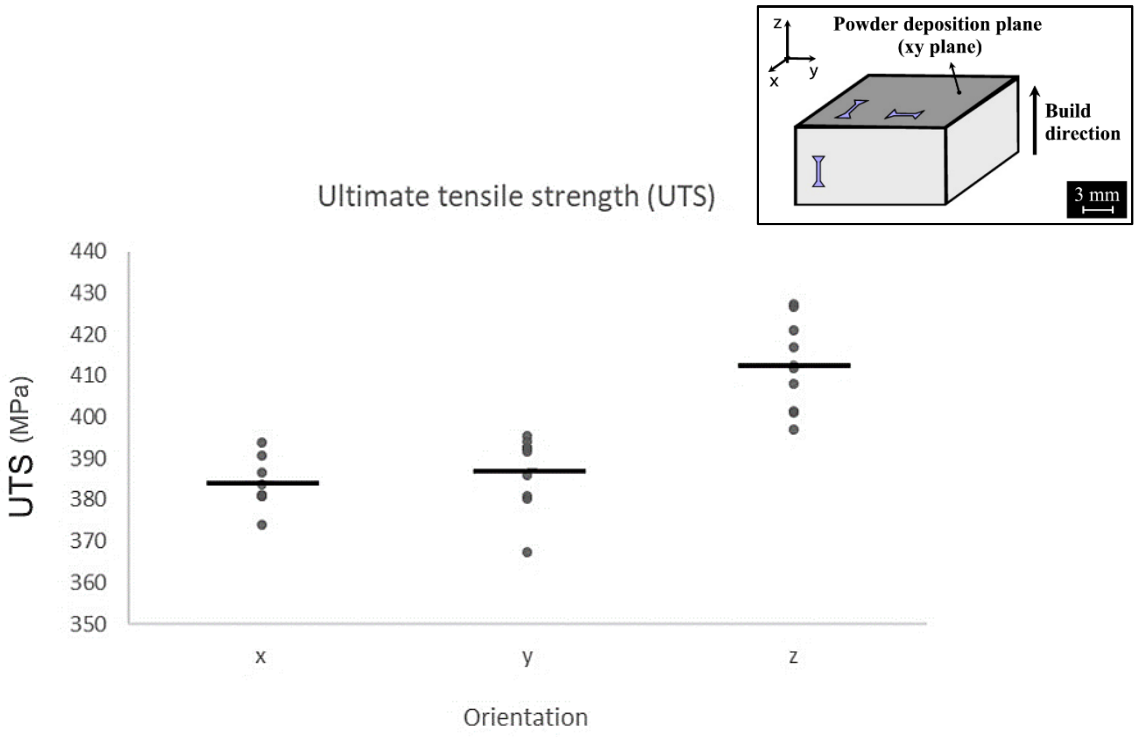

Figure 65 – Ultimate tensile strength (UTS) values and respective means for each orientation on the part produced through additive manufacturing.

Ultimate tensile strength (UTS) values show to be higher for the z direction, followed by the y and x direction respectively. However, UTS values for the y direction are only slightly higher than the ones observed for the x direction.

As shown in literature for parts produced through additive manufacturing, different microstructures are formed for the powder deposition plane and for the build direction (Figure 11), due to the building strategy used and the complex local thermal evolutions involved in the process of the part fabrication. As seen in Figure 66, melt pool lines resultant from the metallic powder melting during the part fabrication are parallel to the powder deposition plane and oriented along several directions, corresponding to the 67 degrees scanning path rotation for each consecutive layer formed. Furthermore, melt pools present similar dimensions due to the use of the same process parameters on the fabrication of the core of a part, from where microsamples were removed.

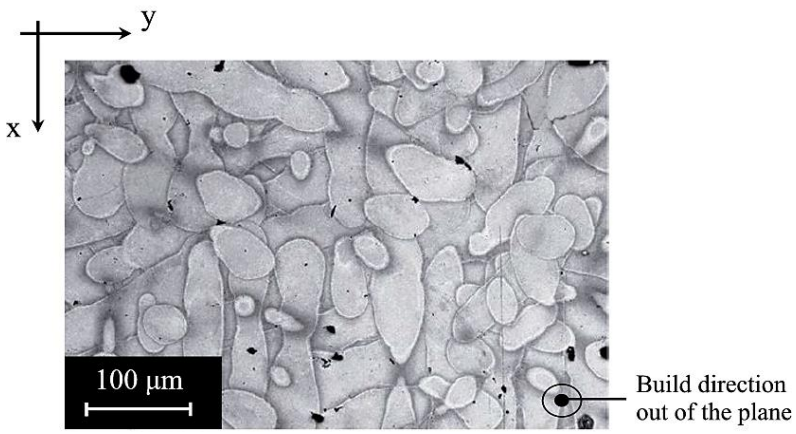

Figure 66 – Optical micrograph of a cross-section parallel to the powder deposition plane (xy plane) of an AlSi10Mg part obtained through direct metal laser sintering (DMLS) (D. Manfredi 2013).

For microsamples oriented along the x and y directions, i.e. directions parallel to the powder deposition plane, just a few layers of the additive manufactured material are comprised within the microsamples thickness due to their small size, as seen in Figure 67.

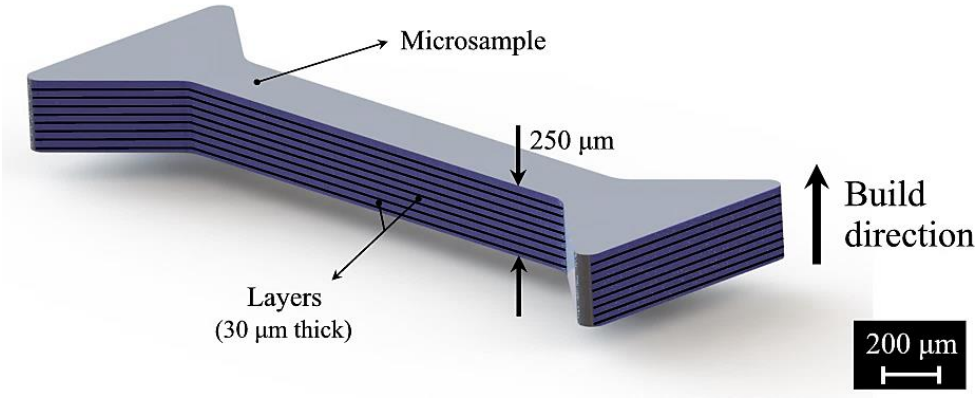

Figure 67 – Schematic representation of the layers of the additive manufactured part on a microsample oriented along the x or y directions.

During the fabrication of the part through additive manufacturing, the scanning path is rotated by 67 degrees for each consecutive layer, which allows for overall similar microstructures to be formed for the x and y directions. The use of standard large size samples to obtain the material mechanical properties would average across an infinite number of layers and therefore

similar mechanical properties values would be obtained for these two directions. However, the finite number of layers within the microsample thickness can stand for locally slightly different microstructures for the x and y directions, which has a direct and measurable influence on the mechanical behavior of the material. It therefore justifies the difference observed between the yield strength and UTS values for the x and y directions (Figure 64 and Figure 65, respectively).

The observed variations of yield strength and UTS values along the part (Figure 60 and Figure 61, respectively), for a given orientation, can also be justified by the small size of microsamples. Even though the microsamples tested were removed from locations subject to the same scanning strategy and process parameters, the order of magnitude of their cross-sectional area ($\approx 250\ \mu m \times 250\ \mu m$) is sufficiently small so that locally different microstructures can be present. Therefore, slightly different mechanical properties were obtained.

On the other hand, the mechanical behaviors differences observed between the microsamples oriented along x and y directions (parallel to the powder deposition plane) to the microsamples oriented along the z direction (parallel to the build direction) can be justified by the different microstructures formed for these directions during the production of the part, as seen in Figure 11.

Whereas the tensile characteristics of the x and y directions oriented microsamples are dictated in its majority by the very fine microstructure of the melt pool core (Figure 68 a) and b)), the tensile characteristics of the z direction oriented microsamples are dictated by the coarser and elongated grains of the melt pool boundaries and overlaps (Figure 68 c)). When comparing the microsamples along the z direction to the ones along the x and y directions, this results in higher yield strength values for the microsamples oriented along the x and y directions, but lower ultimate tensile strength (UTS). Furthermore, strain to failure values have shown to be higher for the x and y direction microsamples.

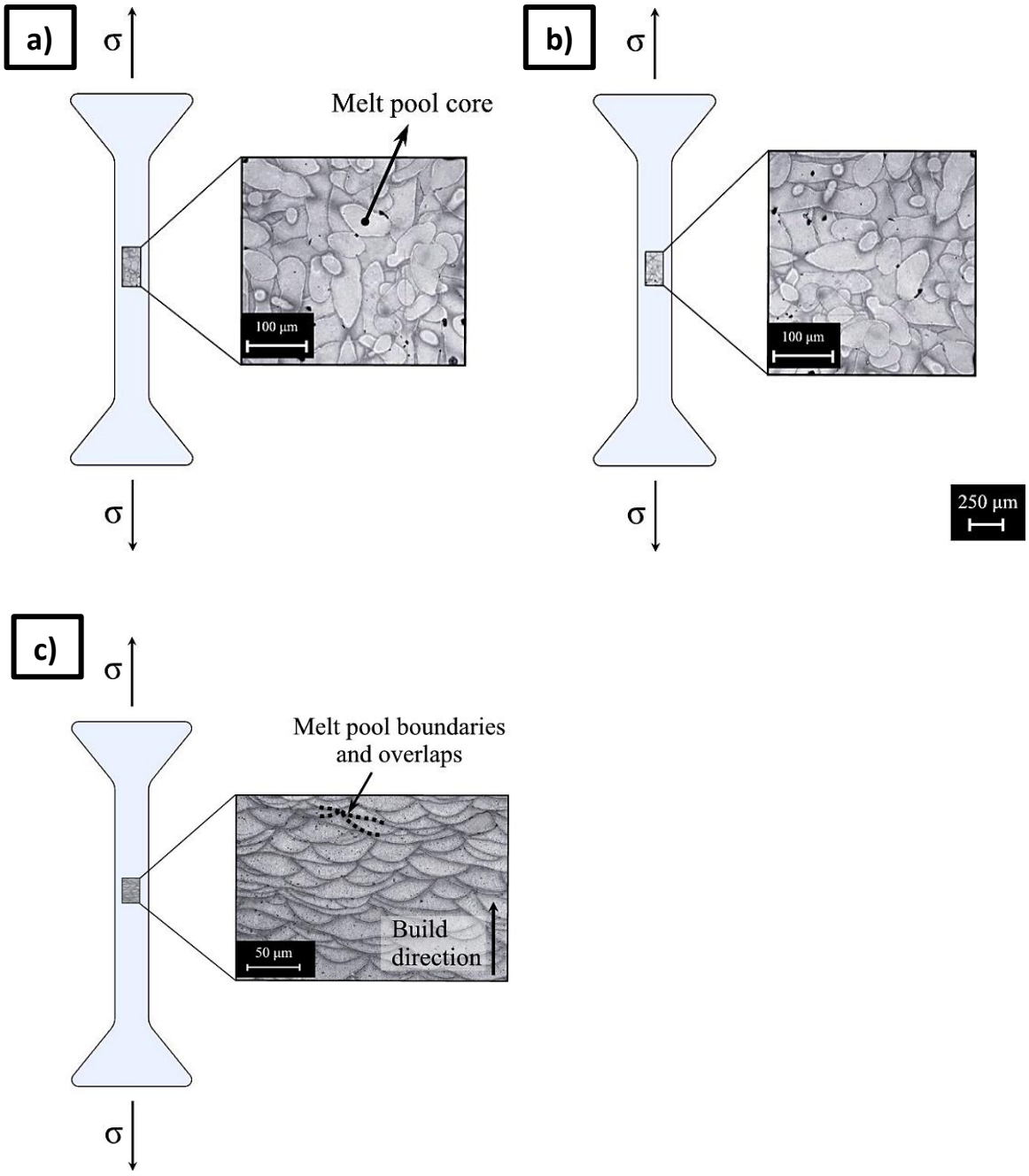

Figure 68 – Representation of the microsamples microstructures: (a) oriented along the x direction, (b) oriented along the y direction and (c) oriented along the z direction (D. Manfredi 2013).

5.2 Statistical significance

In order to conclude about the statistical significance of the difference between yield strength and UTS values for the different studied orientations, a statistical hypothesis test was made.

The selection of the hypothesis test to be used depends on factors such as the type of values to be analyzed, i.e. means or variances, if two different and independent sets of samples are compared and the sizes of the sets (Rui Campos Guimarães , Wilfrid J. Dixon 1950). In this study, a localization test was needed to compare both yield strength and UTS means ($\overline{YS}$ and $\overline{UTS}$ respectively) of two independent sets of microsamples, each one corresponding to microsamples oriented along a specific direction. Since each set was formed by 10 microsamples at most, it was considered to be of small dimensions. Therefore, a t-test was used.

Because the test is addressed to the comparison of two sets of microsamples, three tests were made, i.e. directions x – y, x – z and y – z, for each one of the two mechanical properties being analyzed. Since the sets of microsamples are of small dimensions, the test statistic follows a Student's t-distribution under the null hypothesis (initial hypothesis to conduct the test), with an established number of degrees of freedom (Rui Campos Guimarães). The degrees of freedom and the test statistic are determined using the mean, variance and sets size values from both sets being analyzed. Also, the p value represents a measure of how much the data contradicts the initial hypothesis. The smaller it is, the more the data contradicts the initial hypothesis and therefore the more convincing might be to reject that same hypothesis (Rui Campos Guimarães).

The results of the t-test analysis conducted with a level of significance, α, of 0.05 (5 %) and under the initial hypothesis of equality between the mean values of the mechanical properties for the directions studied are summarized in Table 6.

Table 6 – Summary of the t-test analysis results, applied to the mean values of yield strength (YS) and UTS for each one of the orientations on the AM part.

	Yield Strength			**UTS**		
Initial hypothesis	$\overline{YS_x} = \overline{YS_y}$	$\overline{YS_x} = \overline{YS_z}$	$\overline{YS_y} = \overline{YS_z}$	$\overline{UTS_x} = \overline{UTS_y}$	$\overline{UTS_x} = \overline{UTS_z}$	$\overline{UTS_y} = \overline{UTS_z}$
α	0.05					
p value (2 tailed)	6.47E-04	1.99E-06	9.26E-09	3.85E-01	5.88E-06	2.10E-05
Acceptance	Rejected. **Statistically different**	Rejected. **Statistically different**	Rejected. **Statistically different**	Not rejected. **Statistically equal**	Rejected. **Statistically different**	Rejected. **Statistically different**

The t-test results showed that there was no statistical significant difference between UTS values for the x and y directions. In fact, UTS values for the y direction are only slightly higher than the ones observed for the x direction. However, the t-test showed that there was a statistical significant difference between the yield strength values for the x and y orientations, as already seen from the results.

Furthermore, the statistical test results showed that there was also statistical significant difference between yield strength and UTS values, respectively, of the build direction to the ones from the orientations parallel to the powder deposition plane (Figure 53). As referred previously, the different mechanical properties observed for the powder deposition plane orientations and for the build direction can be justified by the different microstructures formed during the part fabrication (Figure 11), due to the additive manufacturing process building strategy. Yield strength values showed to be lower for the build direction, however ultimate tensile strength values showed to be higher.

5.3 Fractographic analysis - scanning electron microscopy (SEM)

In order to study and better understand the failure mechanisms of materials produced using additive manufacturing, a fractographic analysis was made to the fracture surfaces of 3 microsamples for each orientation using scanning electron microscopy (SEM). For that, a scanning electron microscope FEI Nova NanoSEM 450 in the department of physics at UMBC was used.

5.3.1 Microsample preparation for SEM imaging and parameters used

After microsamples were tested, their preparation to perform a fractographic analysis using SEM was required. Microsamples were cleaned in an ultrasonic cleaner to remove the painted speckle from their surface, which was previously used to perform a DIC analysis for strain measurement. They were afterwards glued to a block, as seen in Figure 69, to make it easier for microsamples to be handled in the scanning electron microscope.

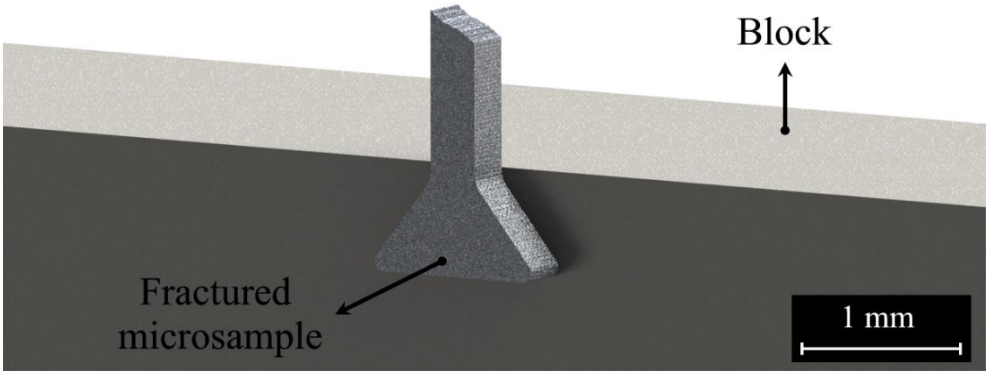

Figure 69 – Schematic representation of a microsample mounted in a block for fractographic analysis using SEM.

SEM images were obtained by the means of backscattered electrons. They were taken at a 4.3 to 5 mm distance from the microsamples surfaces, with magnifications ranging from 1,000x to 5,000x. Moreover, 20 – 30 kV of the emitted probe of electrons energies were used.

5.3.2 Fractographic analysis

Figure 70 shows SEM images of the fracture surfaces of the microsamples used for fractographic analysis, for different locations and orientations on the additive manufactured part in accordance with Figure 54.

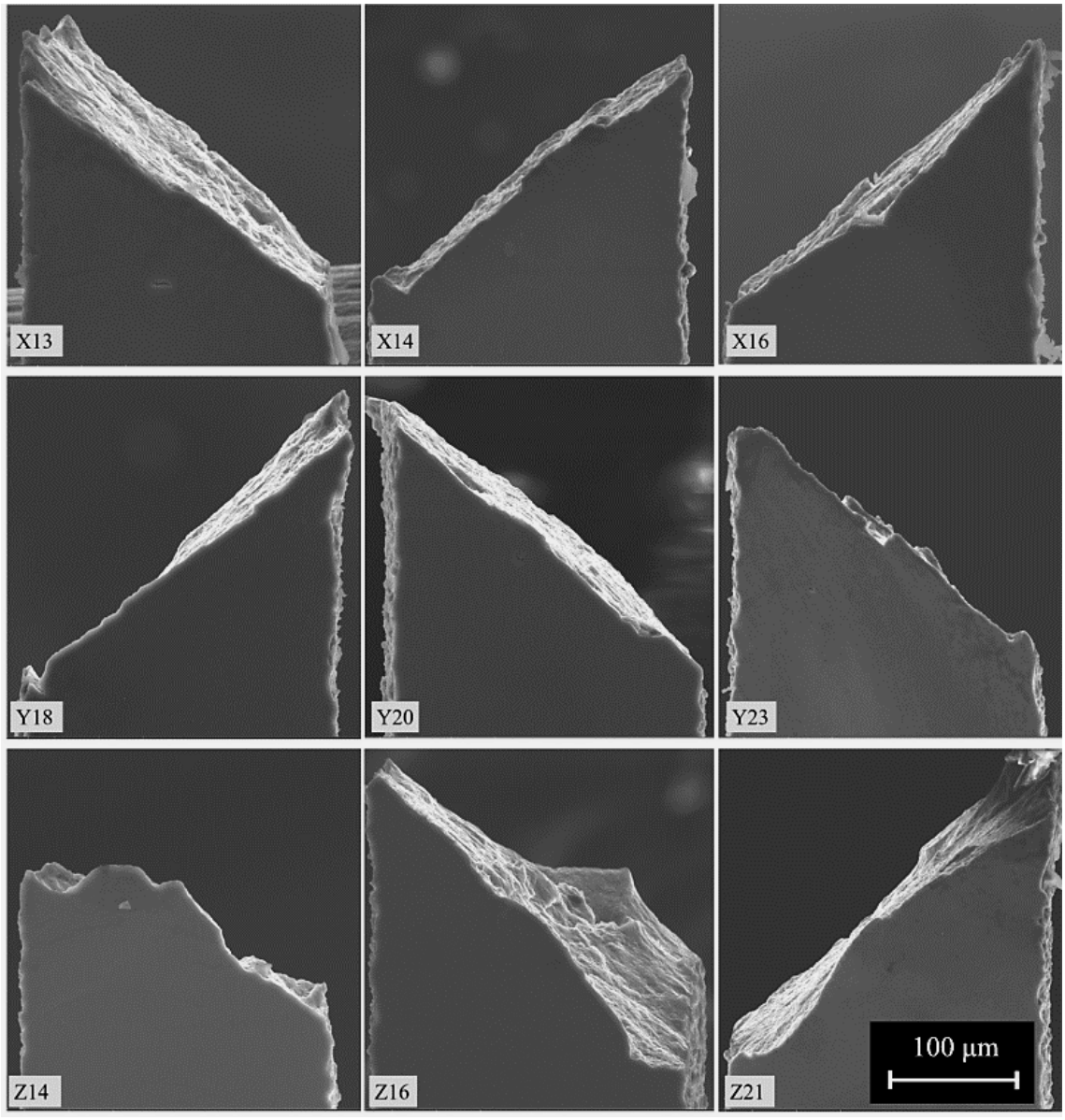

Figure 70 – SEM images of the fracture surfaces of the microsamples used for fractographic analysis, with respective identification number and orientation on the AM part.

The review of the microsamples fracture surfaces angles in Figure 70 shows that the samples harvested from the x and y orientations, in which the fracture surfaces make ≈ 37 - 38 degrees to the tensile axis. The two mimic each other and the deviation from 45 degrees is attributed to microstructural texturing that results from the AM processing. It is noted that the z oriented microsamples present a fracture surface that is closer to 45 degrees and has more out of plane features. These angle variations and out of plane features are attributed to the fact that the z oriented microsamples are composed of processed material layers that are loaded in tensions (Figure 68 c)). The shape of these layers expresses themselves on the materials fracture surface.

Powder deposition plane – x direction

Figure 72 to Figure 74 shows SEM images of the fracture surfaces of microsamples oriented along the x direction, parallel to the powder deposition plane. Also, Figure 71 shows a schematic representation of a microsample oriented along the x direction on a part produced using additive manufacturing.

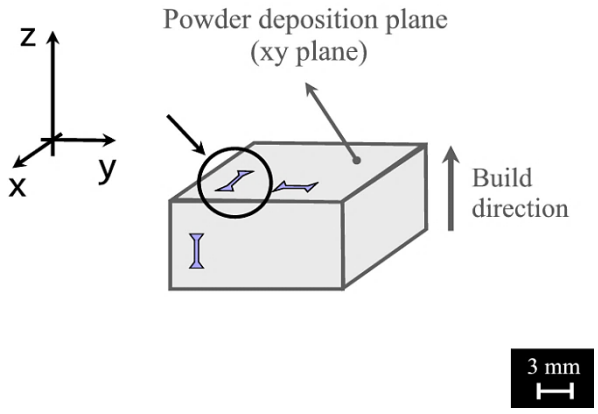

Figure 71 – Schematic representation of the microsamples oriented along the x direction on a part produced using AM.

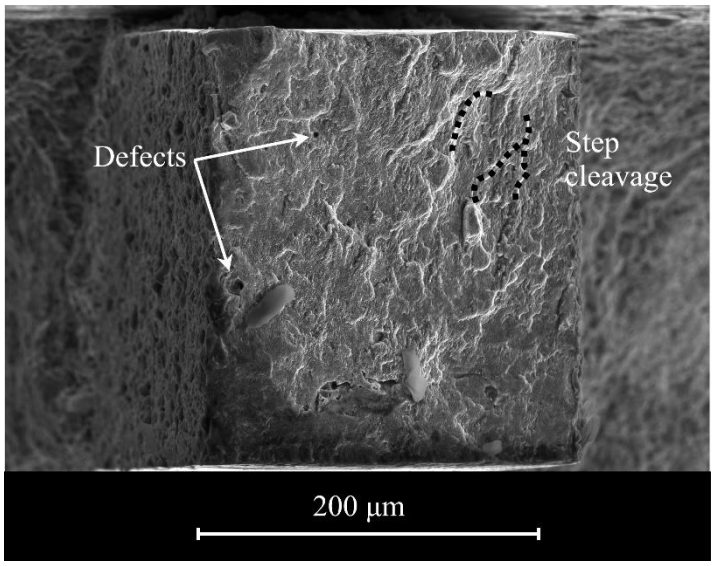

Figure 72 – SEM image of the fracture surface of the microsample number 13, oriented along the x direction.

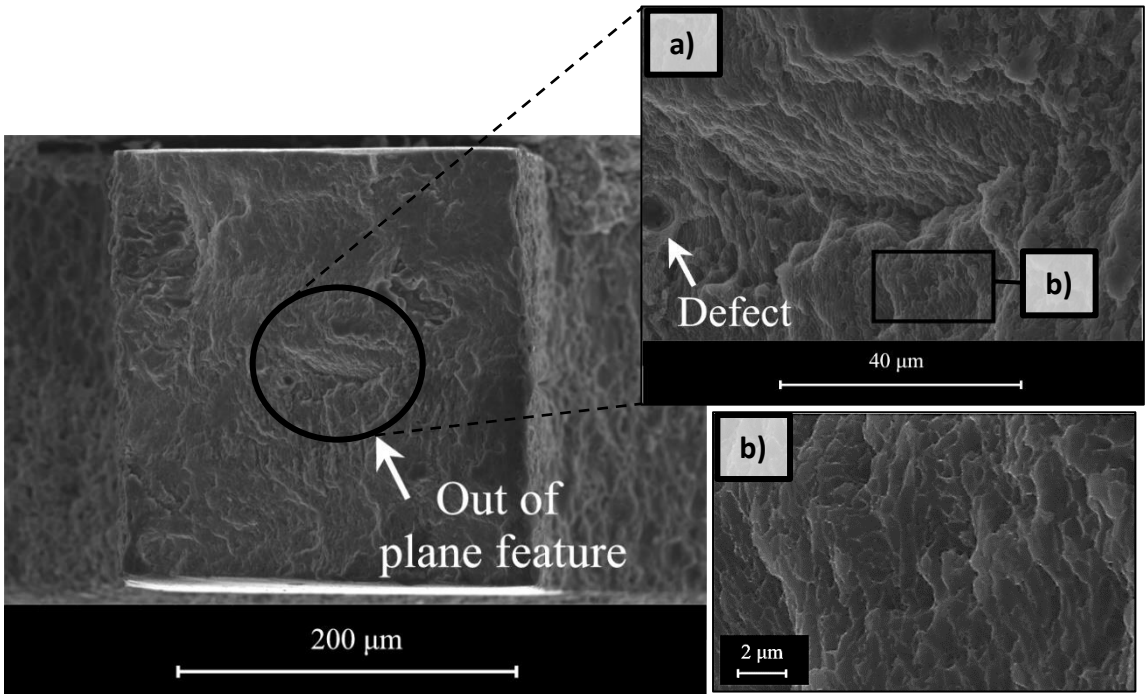

Figure 73 – SEM image of the fracture surface of the microsample number 14, oriented along the x direction. (a) and (b) Higher magnifications of the fracture surface.

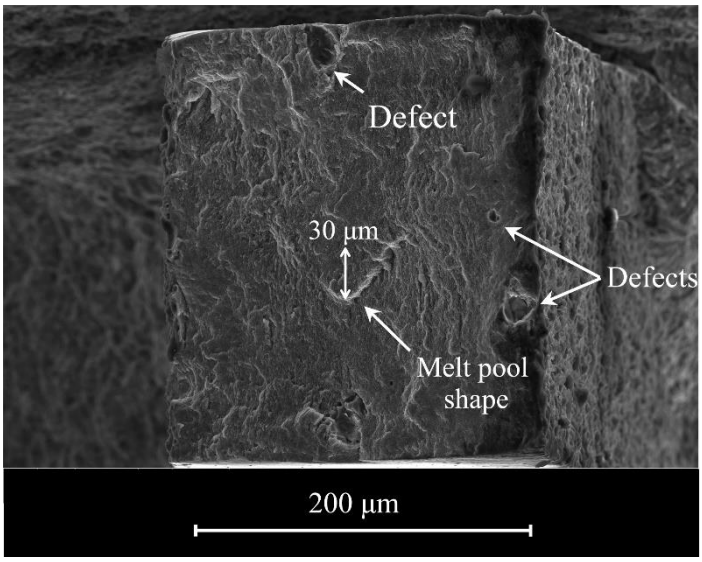

Figure 74 – SEM image of the fracture surface of the microsample number 16, oriented along the x direction.

For the x oriented microsamples, all fracture surfaces seen in the SEM images (Figure 72 to Figure 74) show ductile failure mainly due to the presence of very fine dimples, which can be observed at higher magnifications as in Figure 73 b). Necking of the microsamples was not evident. The fracture surfaces also show river like patterns that rise out of the plane, which can be attributed to deformation in the boundaries of the melt pools resulting in step cleavages, as indicated in Figure 72. These step cleavage features are a brittle response.

The distinctive features of the AM process create a unique microstructure in the AlSi10Mg parts and microtensile samples. The characteristics of the resultant microstructure are dependent on the thermal gradient G and the growth rate R (Yan et al. 2015, Thijs et al. 2013). G is determined by the difference of the temperature over a certain distance and varies with the time and place inside the melt track, R depends on the laser scanning speed and angle between the laser moving direction and the growth direction of the solidifying material. The G over R ratio (G/R) determines the morphology of the microstructure.

An equiaxed dendritic, columnar dendritic, cellular and planar are successively expected when the G/R ratio continuously changes from low to high value. The fineness of the microstructure is determined by the cooling rate (T = G x R). The higher cooling rate will lead to greater undercooling, and thus the finer microstructure. The AM processed used in this study is capable of generating a high cooling rate, due to the rapid scanning velocity of the laser beam and high thermal gradient (about 105 °C/m) of the processing (Thijs et al. 2013). Because of these

processing features, the fine microstructure of the as-built AM AlSi10Mg material is achieved. This fine microstructure controls the deformation and is expressed by the small ductile facture dimples on the fracture surface, as in Figure 73 b).

The SEM image in Figure 73 shows a peculiar detail on the fracture surface of the microsample. Its observation at higher magnifications, as in Figure 73 a), suggests that the failure within that region might have started next to the defect that is nearby the out of plane feature. It must have then extended across the coarser grains from a melt pool overlap, forming the local observable out of plane feature.

In Figure 74, a melt pool shape with a height of 30 μm, i.e. same as the layer thickness, can be noticed at the fracture surface. During deformation along the tensile axis, the melt pool core must have deformed slightly less than the melt pool overlaps, i.e. being pulled on deformation of the microsample, originating the melt pool shape on the fracture surface.

Because of the Gauss distribution of the laser energy, the under cooling changes over the melt track, which reaches the maximum at the centerline, then gradually decreases along the cross-section and finally goes to the minimum at the boundary of the melt track. From this point of view, the cellular size attains the minimum at the center of the melt track, and the maximum value on the boundary of the melt track. Because of this, incomplete and nonuniform features will present themselves in the microstructure. This is acutely apparent by the number of inherent defects found within each of the samples evaluated in the scanning electron microscope, seen in Figure 72 to Figure 74.

Powder deposition plane – y direction

Furthermore, Figure 76 to Figure 78 shows SEM images of the fracture surfaces of microsamples oriented along the y direction, also parallel to the powder deposition plane. Figure 75 shows a schematic representation of a microsample oriented along the y direction on a part produced using additive manufacturing.

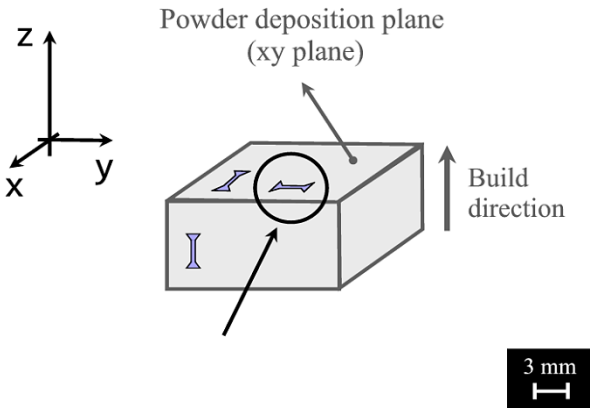

Figure 75 – Schematic representation of the microsamples oriented along the y direction on a part produced using AM.

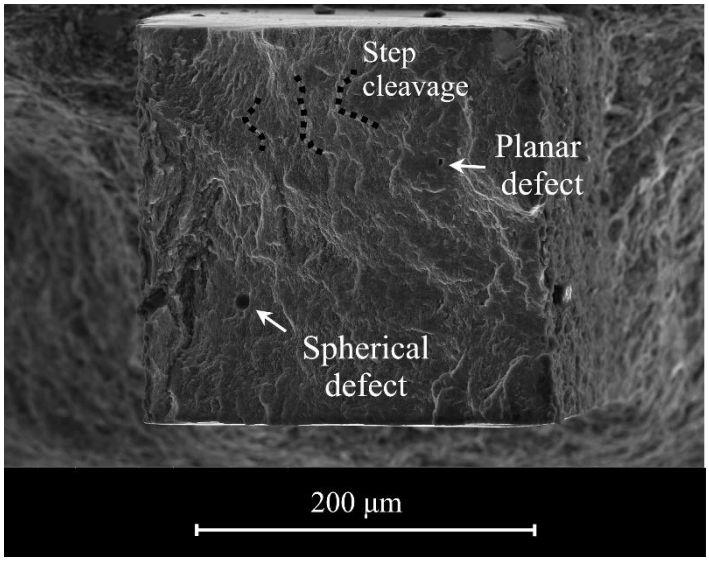

Figure 76 – SEM image of the fracture surface of the microsample number 18, oriented along the y direction.

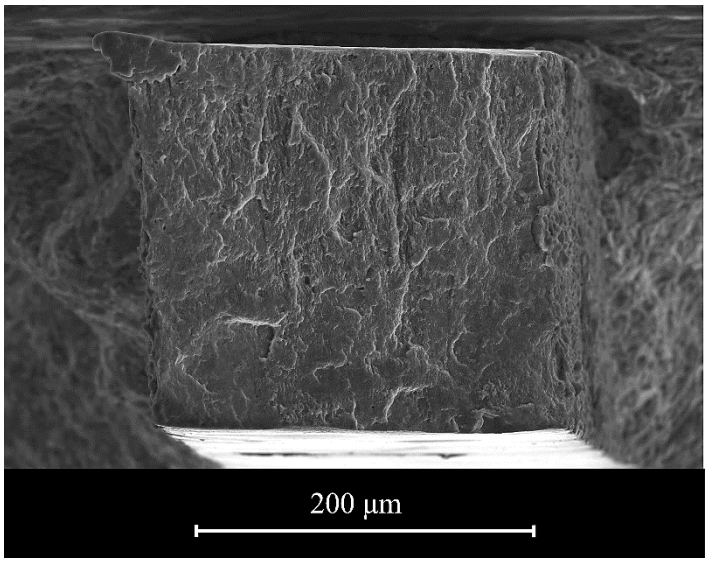

Figure 77 – SEM image of the fracture surface of the microsample number 20, oriented along the y direction.

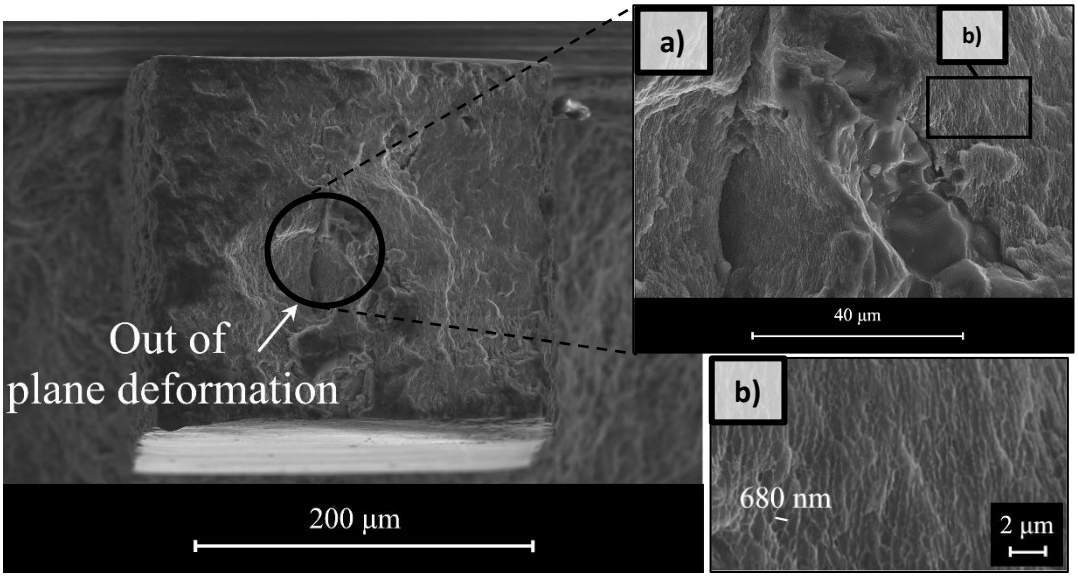

Figure 78 – SEM image of the fracture surface of the microsample number 23, oriented along the y direction and (a) higher magnification of the fracture surface.

The same way as for the x oriented microsamples, the fracture surfaces of the microsamples oriented along the y direction seen in the SEM images (Figure 76 to Figure 78) all show ductile failure in its majority due to the presence of very fine dimples. These fine dimples can be observed at higher magnifications in Figure 78 b) and their overall size is of 680 nm. As referred previously, the small ductile facture dimples visible on the fracture surface are an indication of the fine microstructure, formed due to the AM process characteristics, which controls the deformation of the material. Apart from that, necking of the microsamples was also not evident and step cleavages are visible in the fracture surfaces, as indicated in Figure 76. These step cleavage features are a brittle response.

The observable out of plane deformation in Figure 78 and a higher magnification of it in Figure 78 a) suggests that the deformation of a melt pool overlap prevailed over the deformation of the melt pool core. It might be justified by the presence of a defect deep in the slope, which might have given rise to a failure extended across the coarser and larger grains of a melt pool overlap on that region.

In addition to this, a small defect can be found in the SEM image of the fracture surface of the microsample in Figure 76, which can be associated to localized lack of overlap between melt pools.

Build direction - z direction

SEM images of the fracture surfaces of microsamples oriented along the z direction, parallel to the build direction, are show in Figure 80 to Figure 82. Also, Figure 79 shows a schematic representation of a microsample oriented along the z direction on a part produced using additive manufacturing.

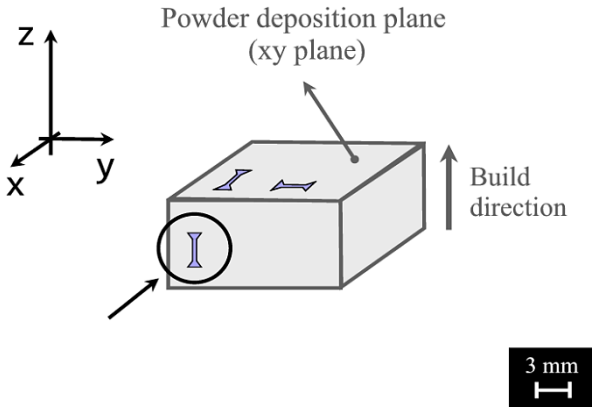

Figure 79 – Schematic representation of the microsamples oriented along the z direction on a part produced using AM.

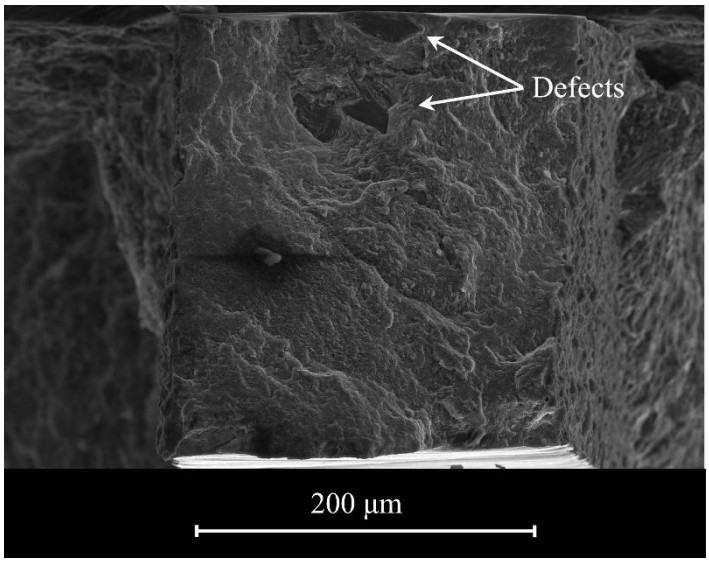

Figure 80 – SEM image of the fracture surface of the microsample number 14, oriented along the z direction.

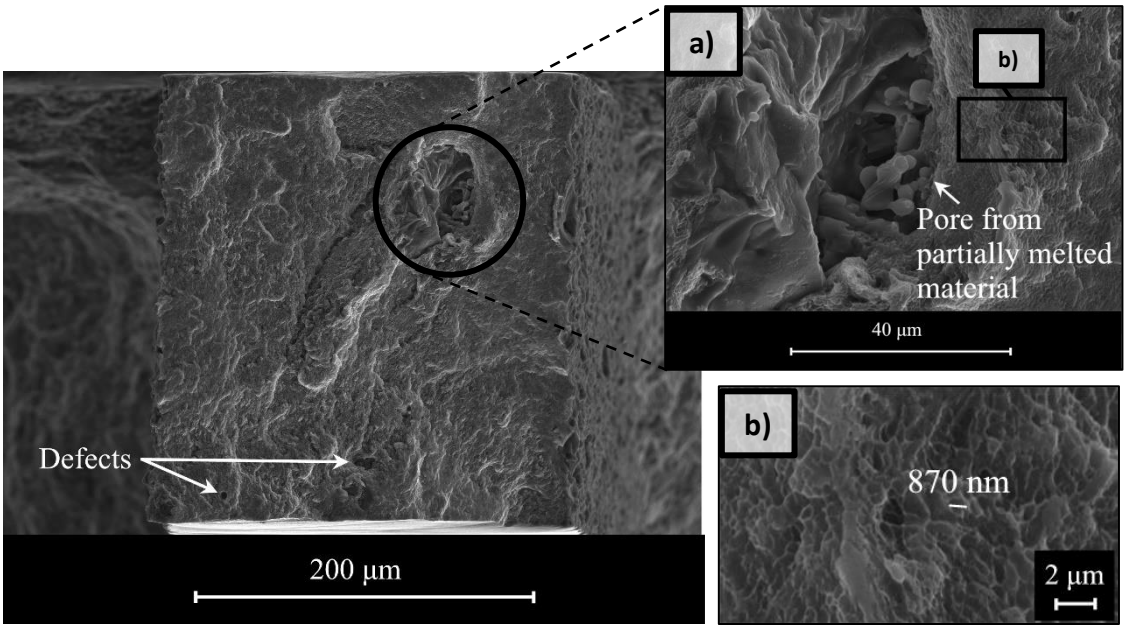

Figure 81 – SEM image of the fracture surface of the microsample number 16, oriented along the z direction and (a) higher magnification of the fracture surface.

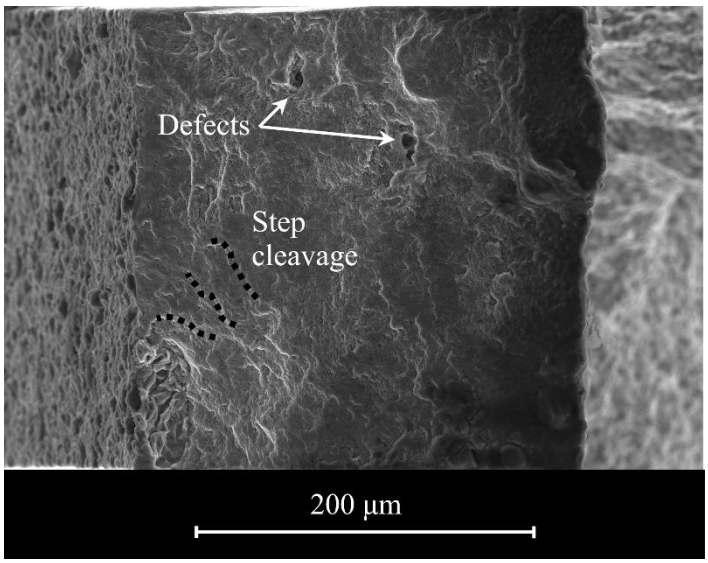

Figure 82 – SEM image of the fracture surface of the microsample number 21, oriented along the z direction.

The fracture surfaces of the microsamples oriented along the build direction, i.e. z direction, seen in the SEM images in Figure 80 to Figure 82, all show ductile failure mainly due to the presence of fine dimples, as seen in Figure 81 b). These fine dimples overall size is of 870 nm and, as mentioned previously, they are an indication of the fine microstructure formed due to the AM process features. This fine microstructure thus controls the deformation of the material. Necking of the microsamples was not evident and step cleavages are visible in the fracture surfaces, as indicated in Figure 82. These step cleavage features are a brittle response.

The size differences of the fine dimples observable on the fracture surfaces of microsamples oriented along the powder deposition plane directions (Figure 78 b)), to the ones observed for the build direction (Figure 81 b)) is correlated to the fact that strain to failure was lower for the build direction. As referred in literature for a ductile failure, dimples size is inversely proportional to strain to failure. In comparison to the results for the x and y directions, dimples size was higher for the z direction and therefore it explains the lower strain to failure values for this direction.

As it happened for some of the other fracture surfaces already studied, the one observed in Figure 81 also presents a peculiar detail. A magnified SEM image of this detail can be seen in Figure 81 a) and unlike the out of plane features observed in Figure 73 and Figure 78, this presents a smooth surface on the left side of the slope and on its core. This might be due to the fact that there was no deformation of the material in that region, suggesting it is a large defect. It is possibly justified by a lack of overlap between melt pools caused by a momentary process instability.

Furthermore, small defects can be found in the SEM images of the fracture surfaces seen in Figure 81 and Figure 82, while larger defects can be seen in Figure 80. The reason behind their formation, as already stated, might be related to localized lack of overlap between melt pools.

It is known that the microstructure of the AlSi10Mg alloy can be influenced by superheating (Li et al. 2015, Wang et al. 2003). The underlying reason can be attributed to the existence of two temperatures, usually denoted by the dissolution temperature T_d and the branching temperature T_b (Li et al. 2015, I.G. Brodova 2002). At the temperature below T_d, the Al and Si-rich particles which have been inherited from the solid AlSi10Mg alloy exist in the liquid phase. Once the temperature exceeds T_d, these particles begin to be melted. When the temperature is over T_b, molten Al and Si can be considered to mix homogenously (Li et al. 2015, I.G. Brodova 2002).

According to previous studies, T_d and T_b of AlSi10Mg alloy should be around 1020 ± 130 °C and 1170 ± 30 °C, respectively (Li et al. 2015, Calvo-Dahlborg et al. 2013), which are much higher than the eutectic temperature of Al-Si alloys (577 °C). During the direct laser AM process, the temperature of a large part of the melt track exceeds T_d but does not reach T_b (Li et al. 2015, I.G. Brodova 2002). Hence, a large part of the AlSi10Mg alloy melt track undergoes a superheating condition, which will lead to an inhomogeneous microstructure of the direct laser AM processed AlSi10Mg alloy. Therefore, an inhomogeneous Al-rich and Si-rich microstructure is expected, which is helpful to form heterogeneous deformation features. This peculiar process from the direct laser AM, results in a microstructure which works in competition during the deformation.

5.3.3 Final remarks

SEM images in Figure 72 to Figure 82 show the fracture surfaces of microsamples oriented along the x, y and z directions on the additive manufactured part. Inspection of these images highlights three major features which are present for the orientations. Firstly, the fracture surfaces are covered in small dimples resulting from the ductile fracture process. The nominal void sizes are presented in Figure 78 b) and Figure 81 b). It shows that the ductile facture process was active but the small dimples formed did not grow during this process, which are indicative of moderate strains to failure as observed in the stress-strain responses. Secondly, the fracture surfaces express river like patterns that rise out of plane. These river like patterns are attributed to deformation manifesting itself in the boundaries of the melt pools resulting in step cleavage. These step cleavage features are a brittle response and would have been the mechanism of separation precluding extensive plastic deformation. These observations conclude that the AM manufactured materials have a mixed mode deformation.

Thirdly, the microsamples examined express direct processing defects on the fracture surface. The material volume sampled by the microsamples is relatively small compared to a work part. The observations of defects on the microsamples is telltale that the as-fabricated material has wide spread defects.

Collectively, this characterization of the material provides guidance on a fruitful path for improvement. By working to eliminate the direct defects, i.e. inconsistent solidification, etc.,

and improving melt pool boundary strength/robustness, these materials show potential to have increased toughness.

6 Conclusions and Future Work

6.1 Conclusions

In this work, the mechanical behavior of an AlSi10Mg aluminum alloy part produced using direct metal laser sintering (DMLS) is investigated and characterized along the part, for three different orientations: x, y and z (Figure 53). The results show that mechanical properties values varied along the part and for the different orientations studied.

For each orientation studied, the Young's modulus presents a relatively high variability along the part, suggesting the different prevalence of grains with a specific crystallographic orientation for each microsample. Young's modulus values vary from 36 GPa to 122 GPa for the x direction oriented microsamples, from 34 GPa to 123 GPa on the y direction and from 45 GPa to 122 GPa on the z direction. Furthermore, similar variations and range of values of this mechanical property along the part are found when comparing the three different orientations.

Yield strength and ultimate tensile strength (UTS) show variations along the part, for a given orientation. These variations can be justified by local slightly different microstructures formed along a specific orientation, resulting from the AM process.

As opposed to the referred in literature, values of yield strength and UTS have shown measurable differences for the x and y orientations, i.e. directions parallel to the powder deposition plane. Comparing these two orientations, yield strength differences showed to be higher than UTS differences. Yield strength as well as UTS values are higher for the y orientation. For a finite number of layers of the AM part, the rotation of the scanning path by 67 degrees for consecutive layers and the melt pool overlaps is not sufficient to generate an isotropic microstructure along the powder deposition plane. If not taken into consideration in structural design, the wrong assumptions can be made specially for thin features with the smallest dimension parallel to the build direction.

When comparing these mechanical properties values between the powder deposition plane directions and the build direction, yield strength and ultimate tensile strength (UTS) values also showed to be different. Yield strength showed to be lower for the build direction and UTS higher. The microstructural anisotropy introduced by means of the layer-by-layer approach of the additive manufacturing process justifies these mechanical properties variations. Tensile characteristics of the material along the powder deposition plane directions are dictated mainly by the very fine microstructure of melt pool cores. However, tensile characteristics of the

material along the build direction are dictated mainly by the coarser and elongated grains of the melt pool boundaries and overlaps. Therefore, higher yield strength values are associated to the powder deposition plane orientations, but lower ultimate tensile strength (UTS). Furthermore, strain to failure have shown to be higher for the powder deposition plane directions.

The mechanical properties values obtained do not match the ones reported in literature, obtained using standard large sized samples for tensile testing. The use of microsamples allowed to explore the material inhomogeneities and understand the influence of the AM process parameters on the additive manufactured part mechanical properties. This know-how is essential to fill the knowledge gap existent in literature about the mechanical properties variation in an additive manufactured part.

A fractographic analysis to the fracture surface of the tested microsamples using scanning electron microscopy (SEM) showed that the AM manufactured materials have a mixed mode deformation, while necking was not evident. The existent small dimples indicate that the ductile fracture process was active, but their overall size indicates that they did not grow during this process resulting in moderate strains to failure. On the contrary, step cleavage features are a brittle response and would have been the mechanism of separation preventing for extensive plastic deformation to occur.

Microsamples fracture angles showed that the samples harvested from the x and y orientations and that the two mimic each other. The deviation from 45 degrees with the tensile axis is attributed to microstructural texturing that results from the AM processing. Microsamples oriented along the z direction present angle variations and out of plane features that are attributed to the tensioned processed material layers. The shape of these layers expresses themselves on the materials fracture surface.

The SEM images of the fracture surfaces also showed the presence of processing defects, suggesting localized lack of overlap between melt pools. Due to the small volume of material sampled by microsamples, the observations of defects on the microsamples is telltale that the as-fabricated material has wide spread defects.

Collectively, this characterization of the material provides guidance on a fruitful path for improvement. By working to eliminate the direct defects, i.e. inconsistent solidification, etc., and improving melt pool boundary strength/robustness, these materials show potential to have increased toughness.

6.2 Future research

To complement the present work on studying the orientation and location dependency of mechanical properties on an AlSi10Mg aluminum alloy part produced using direct metal laser sintering (DMLS), the following studies should be done:

- Analyze cross-sectional and longitudinal, i.e. over the microsample gage length, microstructures of the microsamples tested, along the part and for each of the three orientations.

Moreover, the study on the mechanical properties variation on an additive manufactured part using a microsample approach could be expanded:

- As in typical structural applications, the material from certain sections of a part is solicited along directions other than the horizontal and vertical directions, i.e. powder deposition plane and build direction respectively. A study to understand how the mechanical properties of an additive manufactured part vary for different orientations other than along the powder deposition plane and build direction could be made, using a microsample approach;
- Different additive manufacturing technologies using different scanning strategies and processing parameters could also be investigated.

References

A. Bogner, P.-H. Jouneau, G. Thollet, D. Basset, C. Gauthier. 2006. "A history of scanning electron microscopy developments: Towards ‘‘wet-STEM’’ imaging."

Amanda J. Sterling, Brian Torries, Nima Shamsaei, Scott M. Thompson, Denver W. Seely. 2015. "Fatigue behavior and failure mechanisms of direct laser deposited Ti–6Al–4V."

Ashby, Michael. 2015. *Materials and Sustainable Development*. 1st Edition ed.

ASTM International. 100 Barr Harbour Dr., PO Box C700 West Conshohocken Pennsylvania 19428-2959, United States. "Standard Test Methods for Tension Testing of Metallic Materials. Designation: E8/E8M – 09."

Bartłomiej Wysocki, Piotr Maj, Agnieszka Krawczy´nska, Krzysztof Ro˙zniatowski, Joanna Zdunek, Krzysztof Jan Kurzydłowski, Wojciech´Swi¸eszkowski. 2016. "Microstructure and mechanical properties investigation of CPtitanium processed by selective laser melting (SLM)."

Bing Pan, Kemao Qian, Huimin Xie and Anand Asundi. 2009. "Two-dimensional digital image correlation for in-plane displacement and strain measurement: a review."

Calvo-Dahlborg, M., P. S. Popel, M. J. Kramer, M. Besser, J. R. Morris, and U. Dahlborg. 2013. "Superheat-dependent microstructure of molten Al–Si alloys of different compositions studied by small angle neutron scattering." *Journal of Alloys and Compounds* 550 (Supplement C):9-22. doi: https://doi.org/10.1016/j.jallcom.2012.09.086.

Cheng, Christopher Lee. 2008. "Mechanical and Microstructural Characterization of Copper Microsamples After Cold Drawing." Master of Science in Mechanical Engineering, University of Maryland, Baltimore County.

D. A. LaVan and W. N. Sharpe, Jr. 1999. "Tensile Testing of Microsamples."

D. Manfredi, F. Calignano, E. P. Ambrosio, M.Krishnan, R. Canali, S. Biamino, M. Pavese, E. Atzeni, L. Iuliano, P. Fino, C. Badini. 2013. "Direct Metal Laser Sintering: an additive manufacturing technology ready to produce lightweight structural parts for robotic applications."

D.S. Gianola and W.N. Sharpe, Jr. 2004. "Techniques for testing thin films in tension."

de Assumpção Pereira-da-Silva, Marcelo, and Fabio A. Ferri. 2017. "1 - Scanning Electron Microscopy A2 - Róz, Alessandra L. Da." In *Nanocharacterization Techniques*, edited by Marystela Ferreira, Fabio de Lima Leite and Osvaldo N. Oliveira, 1-35. William Andrew Publishing.

Diego Manfredi, Flaviana Calignano, Manickavasagam Krishnan, Riccardo Canali, Elisa Paola Ambrosio and Eleonora Atzeni. 2013. "From Powders to Dense Metal Parts: Characterization of a Commercial AlSiMg Alloy Processed through Direct Metal Laser Sintering."

E. Atzeni, M. Barletta, F. Calignano, L. Iuliano, G. Rubino, V. Tagliaferri. 2016. "Abrasive Fluidized Bed (AFB) finishing of AlSi10Mg substrates manufactured by Direct Metal Laser Sintering (DMLS)."

E. Balducci, L. Ceschini, S. Messieri, S. Wenner, R. Holmestad. 2017. "Thermal stability of the lightweight 2099 Al-Cu-Li alloy: Tensile tests and microstructural investigations after overaging."

Flaviana Calignano, Diego Manfredi, Elisa Paola Amb rosio, Sara Biamino, Mariangela Lomb ardi, Eleonora Atzeni, Alessandro Salmi, Paolo Minetola, Luca Iuliano, and Paolo Fino. 2017. "Overview on Additive Manufacturing Technologies."

Fonseca, Iván Darío Romero. 2014. "Correction of the post – necking true stress – strain data using instrumented nanoindentation." University of North Carolina at Charlotte.

Frazier, William E. 2014. "Metal Additive Manufacturing: A Review." *Journal of Materials Engineering and Performance*.

Gebhardt, Andreas, and Jan-Steffen Hötter. 2016. "4 - Rapid Prototyping." In *Additive Manufacturing*, 291-352. Hanser.

GmbH, EOS. 2010. Technical Description EOSINT M 280.

Groover, Mikell P. 2007. *Fundamentals of Modern Manufacturing - Materials, Processes and Systems*. Third Edition ed.

Haijun Gong, Khalid Rafi, Hengfeng Gu, Thomas Starr, Brent Stucker. 2014. "Analysis of defect generation in Ti–6Al–4V parts made using powder bed fusion additive manufacturing processes."

Herderick, E. 2011. "Additive Manufacturing of Metals: A Review."

Hernandez, Kaufui V.Wong and Aldo. 2012. "A Review of Additive Manufacturing."

I.G. Brodova, P.S. Popel, G.I. Eskin. 2002. *Liquid Metal Processing: Application to Aluminium Alloy Production*.

Jorge Rodrigues, Paulo Martins. 2005. *Tecnologia Mecânica - Tecnologia da Deformação Plástica*. Vol. I - Fundamentos Teóricos.

Joseph Goldstein, Dale E. Newbury, Patrick Echlin, David C. Joy, Alton D. Romig Jr., Charles E. Lyman, Charles Fiori, Eric Lifshin. 2012. *Scanning Electron Microscopy and X-Ray Microanalysis: A Text for Biologists, Materials Scientists, and Geologists*: Springer Science & Business Media.

K.J. Hemker and W.N. Sharpe, Jr. 2007. "Microscale Characterization of Mechanical Properties."

Lawrence E. Murr, Edwin Martinez, Krista N. Amato, Sara M. Gaytan, Jennifer Hernandez, Diana A. Ramirez, Patrick W. Shindo, Frank Medina, Ryan B. Wicker. 2012. "Fabrication of Metal and Alloy Components by Additive Manufacturing: Examples of 3D Materials Science."

Li, X. P., X. J. Wang, M. Saunders, A. Suvorova, L. C. Zhang, Y. J. Liu, M. H. Fang, Z. H. Huang, and T. B. Sercombe. 2015. "A selective laser melting and solution heat treatment refined Al–12Si alloy with a controllable ultrafine eutectic microstructure and 25% tensile ductility." *Acta Materialia* 95 (Supplement C):74-82. doi: https://doi.org/10.1016/j.actamat.2015.05.017.

M. Fera, F. Fruggiero, A. Lambiase and R. Macchiaroli. 2016. "State of the art of additive manufacturing: Review for tolerances, mechanical resistance and production costs."

M. W. Khaing, J. Y. H. Fuh, L. Lu. 2001. "Direct metal laser sintering for rapid tooling: processing and characterisation of EOS parts." *Journal of Materials Processing Technology*.

M. Zupan, M. J. Hayden, C. J. Boehlert and K. J. Hemker. 2001. "Development of High-temperature Microsample Testing."

Masuzawa, T. 2000. "State of the Art of Micromachining."

Ming Tang, P. Chris Pistorius. 2016. "Oxides, porosity and fatigue performance of AlSi10Mg parts produced by selective laser melting."

Mohammad, Mohammad Yeakub Ali & Ammar Sami. 2008. "Experimental Study of Conventional Wire Electrical Discharge Machining for Microfabrication."

Nannan GUO, Ming C. LEU. 2013. "Additive manufacturing: technology, applications and research needs."

Nesma T. Aboulkhair, Nicola M. Everitt, Ian Ashcroft, Chris Tuck. 2014. "Reducing porosity in AlSi10Mg parts processed by selective laser melting."

Nickels, Liz. 2015. "AM and aerospace: an ideal combination."

Nimer, Salahudin M. 2011. "Local Property Characterization of Friction Stir Welded Titanium 5111." Master of Science in Mechanical Engineering, University of Maryland, Baltimore County.

Nimer, Salahudin M. 2016. "Microscale mechanical experiments at elevated temperatures: System development and material characterization." Doctor of Philosophy in Mechanical Engineering, University of Maryland, Baltimore County.

R. E. Smallman, R. J. Bishop. 1999. *Modern Physical Metallurgy & Materials Engineering*. Sixth edition ed.

Rafal M. Molak, Krystian Paradowski, Tomasz Brynk, Lukasz Ciupinski, Zbigniew Pakiela, Krzysztof J. Kurzydlowski. 2008. "Measurement of mechanical properties in a 316L stainless steel welded joint." *International Journal of Pressure Vessels and Piping*.

Reichelt, Rudolf. 2007. "Scanning Electron Microscopy." In *Science of Microscopy*, edited by Peter W. Hawkes and John C. H. Spence, 133-272. New York, NY: Springer New York.

Rui Campos Guimarães, José A. Sarsfield Cabral. *Estatística, 2.ª edição*.

Seifi, John J. Lewandowski and Mohsen. 2016. "Metal Additive Manufacturing: A Review of Mechanical Properties."

Silva, Lucas Filipe Martins da. 2012 *Comportamento mecânico dos materiais*. Edited by Publindústria.

Sofiane Guessasma, Weihong Zhang, Jihong Zhu, Sofiane Belhabib, and Hedi Nouri. 2015. "Challenges of additive manufacturing technologies from an optimisation perspective."

Systems, EOS GmbH - Electro Optical. 2014. EOS Aluminium AlSi10Mg - material data sheet.

Thijs, Lore, Karolien Kempen, Jean-Pierre Kruth, and Jan Van Humbeeck. 2013. "Fine-structured aluminium products with controllable texture by selective laser melting of pre-alloyed AlSi10Mg powder." *Acta Materialia* 61 (5):1809-1819. doi: https://doi.org/10.1016/j.actamat.2012.11.052.

Wang, Jun, Shuxian He, Baode Sun, Qixin Guo, and Mitsuhiro Nishio. 2003. "Grain refinement of Al–Si alloy (A356) by melt thermal treatment." *Journal of Materials Processing Technology* 141 (1):29-34. doi: https://doi.org/10.1016/S0924-0136(02)01007-5.

Wei Pei, Wei Zhengying, Chen Zhen, Du Jun, He Yuyang, Li Junfeng, Zhou Yatong. 2017. "The AlSi10Mg samples produced by selective laser melting: single track, densification, microstructure and mechanical behavior."

Wilfrid J. Dixon, Frank J. Massey. 1950. *Introduction to Statistical Analysis*. Edited by INC. McGRAW-HILL BOOK COMPANY.

William D. Callister, Jr. 2001. *Fundamentals of Materials Science and Engineering*. Fifth edition ed.

Y.M. Wang, K. Wang, D. Pan, K. Lu, K.J. Hemker, E. Ma. 2003. "Microsample tensile testing of nanocrystalline copper."

Yan, Chunze, Liang Hao, Ahmed Hussein, Philippe Young, Juntong Huang, and Wei Zhu. 2015. "Microstructure and mechanical properties of aluminium alloy cellular lattice structures manufactured by direct metal laser sintering." *Materials Science and Engineering: A* 628 (Supplement C):238-246. doi: https://doi.org/10.1016/j.msea.2015.01.063.